

Final Report for Period: 7/1/2002 – 6/30/2007

Submitted on: 09/28/2007

Principal Investigator: Moloney, Jerome

Award ID: F49620-02-1-0380

Organization: University of Arizona

Title: “Novel Designs and Coupling Schemes for Affordable High Energy Laser Modules”

1.	Executive Summary	1
2.	List of Participants	6
3.	List of Publications	7
4.	List of Inventions	20
5.	Technical Report: Fiber Project.....	21
	5.1. Chip-Scale Cladding-Pumped Fiber Lasers Utilizing Microstructured Fibers.....	21
	5.2. Watt-level Single-Frequency Fiber Lasers	25
	5.3 Spin-off Compact Phosphate Fiber Laser Development	31
	5.4. Phase Locking in Monolithic Multicore Fiber Laser.....	38
	5.5. UV-Written Bragg Gratings in Phosphate Glass Fiber.....	42
	5.6 Tapered fiber bundles for combining pump lasers used in fiber lasers/amplifiers	43
6.	Technical Report: VECSEL Project	52
	6.1 First Principles Quantum Design Approach for Semiconductor Epitaxial Growth.....	52
	6.2 High-Power High-Brightness VECSELS.....	52
	6.2. Tunable High-Power Linearly Polarized VECSELS with a Narrow Linewidth	56
	6.3. Tunable Watt-Level Blue-Green VECSEL	59
	6.4. Spectral Beam Combining of VECSELS	61
	6.5. MultiChip VECSELS: A Coherent Power Scaling Scheme.....	62
7.	MIT Final Report 1	64
	7.1 Introduction.....	64
	7.2 Fiber Laser Structure.....	64
	7.3 Optical Properties.....	65
	7.4 Conclusions.....	68
8.	MIT Final Report 2	70

1. Executive Summary

This report details technical achievements of this basic research multidisciplinary effort entitled “Affordable High Energy Lasers”. The body of results reported is substantial and the report is partitioned into three main sections. The first details technical achievements under the compact phosphate fiber project at the University of Arizona. The second highlights key results under a smaller level seed project on semiconductor optically pumped surface emitting lasers or VECSELS (vertical external cavity surface emitting lasers). Finally, work carried out under a subcontract to the Massachusetts Institute of Technology on novel sideways lasing photonic bandgap fibers and photonic bandgap calculations are appended as separate reports at the end of the document.

An overriding theme of the entire project was the development and use of sophisticated theoretical and simulation capabilities to drive the design, testing and implementation of the various experimental demonstrations. The impact of such an approach was greatest in the VECSEL project where a novel

quantum semiconductor epi design approach was used to fast-track to optimized VECSEL sub-cavity structures. The remainder of this technical summary highlights the main achievements of the project that are described more fully in the following technical sections.

In a comprehensive effort we developed extremely compact, high-power fiber lasers that can be utilized as building blocks for scalable multi-kW laser systems. In our approach we vertically integrated fabrication, testing, and optimization of all components necessary for manufacturing of fiber laser units including highly doped specialty glasses, fiber preforms, fiber drawing techniques, fiber Bragg gratings, fiber facet coatings, and fusion splicing of fiber components.

Our efforts focused on fiber lasers that emit at the eye-safe wavelength around 1550 nm. We developed phosphate glasses that have been co-doped with high concentrations of Yb and Er ions and optimized for efficient pump absorption and laser emission. In addition, compatible photosensitive phosphate glass has been developed that enabled the fabrication of the first UV written fiber Bragg gratings in any phosphate fiber and eliminated the need for unstable and unreliable splices between silica and phosphate fiber within the fiber laser cavity.

Step-index and microstructured fibers with large active core areas have been designed and fabricated. Furthermore, fibers integrating up to 36 active cores have been drawn and utilized to assemble extremely compact multi-core lasers. Both approaches are complementary in order to push the limits of achievable active core area the crucial factor that determines both the efficiency of multimode pump light absorption and the maximum output power per unit of fiber length.

In the course of this project we demonstrated record-breaking single mode fiber lasers with continuous wave output powers beyond 1.3 W per cm of active fiber length. This achievement was a result of several loops of materials and device improvements that have been documented in a series of journal publications during the project. The most advanced device used 3.5 cm of active microstructured fiber and generated continuous output powers of 4.7 W.

The approach of developing rigid and short fiber laser units also enabled us to utilize the large wavelength spacing between longitudinal modes to build single frequency fiber lasers with integrated narrowband fiber Bragg gratings. Building the world's first cladding pumped single frequency fiber lasers we were able to increase the output power of single frequency fiber lasers by more than an order of magnitude to levels of about 2 W. These single frequency lasers can be combined coherently and are suitable building blocks for scalable, very high power laser systems.

In an effort to develop fully-integrated, rugged and compact fiber-laser devices, we have devised a side-pumping scheme for optically pumping short fibers with high concentration of doping. This scalable pumping scheme allows for pumping a single active fiber with multiple (up to twelve) independent medium-power pump laser sources. We have extensively used side-pumped heavily doped phosphate-glass fibers in five major application areas:

- Development of eye-safe Watts-level single-frequency CW fiber-laser oscillators at 1.5 μ m
- Demonstration of Watts-level CW fiber lasers at 1 μ m based on gain-guiding Ytterbium-doped fibers with extremely high concentration of doping of up to 20%
- Development of high-power short-cavity modelocked fiber-laser oscillators at 1.5 μ m
- Distortion-free amplification of ultrashort pulses to tens of kilowatts of peak power and nonlinear frequency conversion of these picosecond sources into blue-green
- Generation of high-energy pulses in short phosphate-glass fibers (Over 0.2mJ pulse energy with nanosecond pulses demonstrated, can be scaled to the multi-mJ level)

The major accomplishments in these areas are summarized below, and more detailed description is given in the Technical Report section.

Our side-pumped fiber-laser devices are fully spliced and fiber pigtailed. They have excellent polarization extinction ratios. These devices can be straightforwardly packaged, and we welcome requests for delivery of the prototypes of these devices to interested parties for the purposes of continuing collaborative research.

Fiber-laser devices demonstrated in the course of this MRI clearly demonstrate the unique capabilities of short phosphate fibers in generation and amplification of short and ultrashort optical pulses. These fibers hold promise of finally bringing the ultrafast-laser technology from a research laboratory to practice. Potential applications that can be beneficial to DOD include directed energy, free-space OCOMM, and LIDAR. It is unfortunate that lack of funding can delay or even terminate a further development of this technology with the end of this MRI program.

CW single-frequency fiber-laser oscillators at 1.5 μ m: It is known that the output power of a single-frequency laser oscillator with a standing-wave laser cavity is limited by the spatial hole-burning effect in the active medium. This limitation is severe, and in the case of a fiber laser with narrowest available fiber-Bragg grating reflectors, it restricts the cavity length of a robustly single-frequency laser oscillator by ~ 3 to 5cm. The two known solutions for the spatial hole-burning problem are by using ring and twisted-mode laser cavities. We have used both approaches, and demonstrated 1W and 2W of average output power at 1.5 μ m, using ring-cavity and twisted-mode cavity fiber-laser designs, respectively. The 2W result is the highest output power among all single-frequency fiber-laser oscillators demonstrated previously, and it beats the widely publicized DFB fiber laser by two orders of magnitude.

Gain-guided Yb-doped fiber lasers at 1 μ m: Since the solubility of Ytterbium oxide in the phosphate glass host is by an order of magnitude higher than that for Erbium oxide, massive doping concentrations of Yb₂O₃ of up to 20% and beyond are attainable with these fibers. We have investigated the feasibility of using these heavily Ytterbium-doped fibers for construction of compact fiber-laser sources at 1 μ m wavelength. In particular, we have found that these fibers, if pumped with light at 975nm wavelength, can relatively straightforwardly be operated in the gain-guiding mode. Thus a substantial power scaling without sacrificing the beam-quality performance must be possible with these fibers, by increasing the core size of the fiber.

Modelocked fiber-laser oscillators with high pulse-repetition rates: The fundamental pulse repetition rate of a modelocked fiber-laser oscillator is inversely proportional to the cavity length of the oscillator. Thus using short and highly doped phosphate fibers as gain elements of a modelocked laser oscillator allows for operation at high repetition rates, with high average power due to the high concentration of doping. The high pulse repetition rates are advantageous in high data-rate optical communications and in the frequency metrology applications. Using only 1cm-long phosphate-fiber cavity and a carbon nanotube-based saturable absorber, we have demonstrated a fiber-laser oscillator passively modelocked at the fundamental repetition rate of 10GHz. With more conventional semiconductor saturable absorber mirror (SESAM), we have demonstrated pulse repetition rates of up to 550MHz, at the average power level of 775mW.

Distortion-free amplification of ultrashort pulses: Amplification of sub-picosecond pulses in doped fibers is limited by the onset of nonlinear effects such as self-phase modulation and Raman scattering. A commonly used way of mitigating the nonlinearities is by using the so-called chirped-pulse amplification (CPA) technique. The CPA requires re-compression of pulses with free-space diffraction gratings, which compromises the main advantages of fiber-based systems such as robustness and ease of alignment.

Heavily doped phosphate fiber is a medium that is uniquely suited for amplification of ultrashort pulses. Amplification of pulses in these fibers, which can be only 10 to 15 centimeters long, occurs so rapidly that no appreciable pulse distortion develops in either spectral or temporal domain. Using this approach, we have demonstrated amplification of picosecond pulses at 1.5 μm to the peak power level of 17 kW. The power density in the fiber core of this amplifier exceeded 20 GW/cm², which is record-high for any ultrafast fiber amplifier reported to-date.

At these power levels, the generated infrared light can be efficiently frequency-converted into the visible and UV in short PPLN crystals operating at room temperature. As an example, we have demonstrated a viable laser transmitter operating in the blue-green transparency window of seawater, by efficient third-harmonic generation of a picosecond fiber-laser system at 1.5 μm .

Generation of high-energy nanosecond pulses in short phosphate-glass fibers: As we have recently demonstrated, short phosphate fibers are capable of efficient energy storage. Amplification of nanosecond pulses at 1.5 μm to 215 μJ energy levels has been demonstrated in 15 cm-long phosphate fiber amplifier with 25 μm core. Due to the extremely short length of the amplifier, the output beam quality was perfect, in spite of the extreme multimode nature of the active fiber. This clearly shows potential for further energy scaling into the multi-mJ domain, by increasing the core size.

Utilizing fibers with multiple active cores, we demonstrated a novel monolithic all fiber scheme to coherently combine the emission from all active cores into a single high power laser beam. This approach can provide a convenient and promising power-scaling solution to compact high-power fiber laser devices. By splitting the gain medium into discrete positions inside the cladding, instead of concentrating all active ions into an oversized core, optical damage and thermal management problems of high power single core lasers can be solved.

The development of technology to fabricate microstructured optical fibers from specialty glasses was amongst the main successes of this research project and the full potential of this technique has yet to be exploited. Besides the demonstrated benefits for cm-sized Watt-level light sources, microstructured fibers will also facilitate improvements in kW-level fiber lasers, pulsed fiber lasers, and amplifiers with high peak powers. Journal publications and numerous invited talks at international conferences are listed below. They reflect the international recognition that our fiber laser research has received.

Tapered fiber bundles: Tapered fiber bundles were used to combine the output power of several semiconductor lasers into a multimode optical fiber for the purpose of pumping fiber lasers and amplifiers. It is generally recognized that the brightness of such combiners does not exceed the brightness of the individual input fibers. We demonstrated that the brightness of the tapered fibers (and fiber bundles) depends on both the taper ratio and the mode-filling properties of the beams launched into the individual fibers. Brightness, therefore, can be increased by selecting sources that fill a small fraction of the input fiber's modal capacity. As proof of concept, we describe measurements on tapered fiber-bundle combiners having a low output étendue. Under low mode-filling conditions per input multimode fiber (i.e., fraction of filled modes ≤ 0.285), we report brightness enhancements of 8.0 dB for 19 \times 1 bundles, 6.7 dB for 7 \times 1 bundles, and 4.0 dB for 3 \times 1 combiners. Our measured coupling efficiency variations of ~1-2% among the various fibers in a given bundle confirm the uniformity and quality of the fabricated devices.

We demonstrated that beam combining with fused and tapered fiber bundles results in brightness increase under restricted-mode launch conditions (mode-filling parameter ~ 0.285) for 3 \times 1, 4 \times 1, 7 \times 1, and 19 \times 1 combiners. The measured values of the coupling efficiency varied about 1-2% among the various fibers in each bundle, thus confirming the high quality of the fabricated devices. To analyze the performance of $N \times 1$ combiners and cascades of such combiners, we devised a simple method employing

a concatenated chain of tapered fibers in which every tapered fiber was fusion-spliced to the next fiber's unaltered facet. Good agreement between the tapered bundle efficiency estimates obtained by this method and the actual (fabricated) combiner efficiencies confirmed the validity of our approach. For cascades of tapered fiber bundles, we achieved brightness enhancement only in the early stages of the cascade. We focused mainly on the dependence of the coupling efficiency on the mode-filling properties of the source. This enabled us to develop practical combiners in the form of fused and tapered fiber bundles and cascades of such bundles.

Quantum design of active semiconductor quantum wells for targeted wavelength emission:

Our theoretical effort in the area of high power, high brightness VECSEL development, focused on two areas: (1) improved understanding of the many-body effects that influence critical semiconductor optical properties and, (2) full 3D modeling of the VECSEL semiconductor sub-cavity and external cavity. Semiconductor wafers for VECSEL devices were designed and optimized prior to growth such that only a single growth cycle was needed after reactor calibration. These grown wafers were then processed and utilized in all subsequent experimental studies documented below.

High power, high brightness VECSEL development: In a comprehensive effort we developed very compact, high-power high-brightness tunable vertical-external-cavity surface-emitting lasers (VECSELs) that can be utilized as building blocks for scalable multi-kW laser systems. In our approach we vertically integrated fabrication, testing, and optimization of all components including semiconductor quantum well gain, distributed Bragg reflector (DBR), microcavity resonances, external cavity design, fabrication of VECSEL chip, low-reflection coating on the chip surface and heat dissipation of the chip.

The semiconductor quantum wells in an optically pumped VECSEL provide the broad band gain for the laser, resulting in a large wavelength tuning range. VECSELs provide wavelength agile laser sources through quantum confinement and a wide choice of constituent group II–VI and III–V material systems. Our research shows that this laser technology potentially provides an innovative approach to low-cost frequency agile lasers engineered for specific applications in the near infrared and visible range (by intracavity nonlinear conversion).

Our efforts focused on InGaAs/GaAs VECSELs emitting around 975 nm. The design of the VECSEL structure is based on the rigorous microscopic quantum design approach and the 3D optical/thermal modeling of the device. The former enables us to precisely determine the gain of the semiconductor quantum well and the gain peak shift as a function of temperature. The latter enabled us to close the design loop and optimize the VECSEL chip prior to wafer growth.

Single-well and double-well VECSEL structures have been designed, grown and fabricated. High-power high-brightness VECSELs were demonstrated and power scaling on single chip VECSEL was studied. Furthermore, the spectral beam combining of VECSELs by using volume Bragg grating and multi-chip VECSEL were investigated. Both approaches are complementary in pushing optically pumped semiconductor laser operation eventually towards kW levels.

In the course of this project we demonstrated tunable high-power (over 10 W) high-brightness VECSELs with a narrow spectral linewidth by employing an intra-cavity birefringent filter. This achievement was a result of several loops of materials and device improvements that have been documented in a series of journal publications during the project. The most advanced device with two VECSEL chips can extend the tunability of the laser to over 30 nm with a reasonably small output variation with the tuned wavelength. This technology opens a new window of opportunity for the application of VECSELs.

Combining intracavity frequency doubling with a high-power tunable VECSEL operating around 976 nm, we first demonstrated a high-power wavelength-tunable blue-green laser operation around 488 nm. This blue-green laser is tremendously useful since it is difficult to generate tunable laser output in this spectral region by other lasers.

The development of technology to design and fabricate VECSEL chips was the main success of this component of the research project. This laser technology is ready to transition into commercial devices. Peer-reviewed journal publications and numerous invited talks at international conferences are listed below. Some of our research work was reported and highlighted by *Photonics Spectra* and *SPIE Newsroom*. They reflect the international recognition that our VECSEL research has received.

2. List of Participants

PI: Jerome V Moloney
Co-PI: Nasser Peyghambarian
Co-PI: Mahmoud Fallahi
Co-PI: Masud Mansuripur

Regular Faculty:

Brio, Moysey
Honkanen, Seppo
Kunyanski, Leonid
Wright Ewan M

Associate Research Professors:

Schülzgen, Axel
Polynkin, Pavel
Kolesik, Miroslav

Assistant Research Professors:

Zakharian, Aramais
Hader, Jorg
Kaneda, Yushi

Consultant:

Koch, S.W

Technical Support:

Temyanko, Valery
Temyanko, Elana
Sabet, Shahriar
Meredith, Gerald R
Whitham, James G

Research Associates:

Qui, Tiequn
Li Li
Andrey V. Kosterin
Dineen, Colm
Kouznetsov, Dmitrii
Fan, Li
Reichelt, Matthias
Panasenko, Dmitriy Y
Zhang, Hongxi

Graduate Students :

Suzuki, Shigeru
Polynkin, Alexandre
Zhu, Xiushan
Yong Xie
Tao Liu
Hongxi Zhang
Khanh Q. Kieu
Gundu, Krishna Mohan
Kano, Patrick
Katona, Gregory A
Kulkarni, Prajit
Li, Hongbo Bo
Matus, Marcelo A
Xie, Yong
Suzuki, Shigeru
Bedford, Robert G
Hessenius, Chris A
Hsu, Ta-Chen
Liu, Tao
Miller, Darren A
Madasamy, Pratheepan
Merzylak, Yegegeni A
Peng, Xiang
Song, Feng
Thekkiniathu, Sindhu G
Wu, Jianfeng
Zhu, Xiushan
Palaria, Amritanshu
Schillgalies, Marc O
Udovich, Joshua A

3. List of Publications

Peer-Reviewed Journal Publications

1. J.V. Moloney, J. Hader, and S.W. Koch, "Laser and amplifier applications", Laser & Photon. Rev. Vol. 1, pp. 24-43 (2007).

2. Joerg Hader, Jerome V. Moloney, Angela Thranhardt, and Stephan W. Koch, “ Nitride Semiconductor Devices: Principles and Simulation” ed. J. Piprek, Wiley-VCH Verlag, (2007).
3. Li Fan, Mahmoud- Fallahi, Jorg Hader, Aramais R. Zakharian, Jerome V.Moloney, Wolfgang Stolz, Stephan W. Koch, James T. Murray and Robert Bedford“, Linearly polarized dual-wavelength vertical-external-cavity surface-emitting laser”, *Appl. Phys. Lett.*, **90**, 181124 (2007).
4. Li Fan, Mahmoud Fallahi, Aramais R. Zakharian, Jorg Hader, Jerome V.Moloney, Robert Bedford, James T. Murray, Wolfgang Stolz, and Stephan W. Koch, “Enhanced tunability of a two-chip vertical-external-cavity surface-emitting laser”, *IEEE Photon. Techn. Lett.*, **19**, 544 (2007).
5. P. Polynkin, N. Peyghambarian, J. Moloney, “Efficient energy storage in large-mode-area, heavily Er:Yb co-doped phosphate-glass fibers”, submitted to *Optics Letters* (August 2007).
6. P. Polynkin, V. Temyanko, J. Moloney, N. Peyghambarian, “Dramatic change of guiding properties in heavily Yb-doped, soft-glass active fibers caused by optical pumping”, *Applied Physics Letters*, **90**, 241106 (2007).
7. P. Polynkin, R. Roussev, M. Fejer, N. Peyghambarian, J. Moloney, “Laser transmitter for undersea communications using third-harmonic generation of fiber-laser system at 1.5 μ m”, *IEEE Photonics Technology Letters*, **19**, 1328 (2007).
8. X. Zhu, A. Schülzgen, L. Li, H. Li, V. L. Temyanko, J. V. Moloney, and N. Peyghambarian, "Birefringent In-Phase Supermode Operation of a Multicore Microstructured Fiber Laser", *Optics Express* **15**, 10340 (2007).
9. H. Li, M. Brio, L. Li, A. Schülzgen, N. Peyghambarian, and J. V. Moloney, “Study of Multimode Interference in Circular Step-Index Fibers Studied with the Mode Expansion Approach”, *Journal of Optical Society of America B*, **24**, 2707 (2007).
10. L. Li, A. Schülzgen, H. Li, V. L. Temyanko, J. V. Moloney, and N. Peyghambarian, "Phase-Locked Multicore All-Fiber Lasers: Modeling and Experimental Investigation", *JOSA B* **24**, 1721 (2007).
11. H. Li, A. Mafi, A., A. Schülzgen, L. Li, V. Temyanko, N. Peyghambarian, J. Moloney, "Analysis and Design of Photonic Crystal Fibers Based on an Improved Effective-Index Method", *Journal of Lightwave Technology*, Vol. 25, 1224-1230, 2007.
12. Bueckers, G. Blume, A. Thraenhardt, C. Schlichenmaier, P.J. Klar, G. Weiser, S.W. Koch, J. Hader, JV Moloney, T. J. C. Hosea, S. J. Sweeney, S. R. Johnson, Y-H Zhang, “Microscopic electroabsorption line shape analysis for Ga(AsSb)/GaAs heterostructures”, *Journal of Applied Physics* **101** (3), 033118, Feb 2007.
13. K.S. Lee, C.S. Kim, R.K. Kim, G. Patterson, M. Kolesik, J.V. Moloney, N. Peyghambarian, “Dual-wavelength external cavity laser with a sampled grating formed in a silica PLC waveguide for terahertz beat signal generation” *Applied Physics B* (2007) Lasers and Optics
14. Yushi Kaneda, Li Fan, Ta-Chen Hsu, Nasser Peyghambarian, Mahmoud Fallahi, Aramais

- R.Zakharian, Jorg Hader, Jerome V.Moloney, Wolfgang Stolz, Stephan W. Koch, Robert Bedford, Armen Seviaan and Leonid Glebov “High Brightness Spectral Beam Combination of High Power Vertical External Cavity Surface Emitting Lasers”,*IEEE Photon. Techn. Lett.*, **18**, 1795 (2006).
15. P. Polynkin, A. Polynkin, D. Panasenko, N. Peyghambarian, J. Moloney, “All-fiber picosecond laser system at 1.5 μ m based on amplification in short and heavily doped phosphate-glass fiber”, *IEEE Photonics Technology Letters*, **18**, 2194 (2006)
 16. P. Polynkin, A. Polynkin, D. Panasenko, N. Peyghambarian, M. Mansuripur, J. Moloney, “All-fiber passively mode-locked laser oscillator at 1.5 μ m with Watts-level average output power and high repetition rate”, *Optics Letters*, **31**, 592 (2006).
 17. A. Polynkin, P. Polynkin, D. Panasenko, M. Mansuripur, J. Moloney, N. Peyghambarian, “Short cavity passively mode-locked picosecond Er/Yb co-doped fibre laser oscillator with high average power”, *Electronics Letters*, **42**, 41 (2006).
 18. D. Panasenko, P. Polynkin, A. Polynkin, J. Moloney, M. Mansuripur, N. Peyghambarian, “Er/Yb femtosecond ring fiber oscillator with 1.1W average power and GHz repetition rates”, *IEEE Photonics Technology Letters*, **18**, 853 (2006).
 19. A. Thranhardt, C. Buckers, C. Schlichenmaier, I. Kuznetsova, S. W. Koch, J. Hader, J. V. Moloney, “Microscopic simulation of semiconductor lasers at telecommunication wavelengths”, *Opt. Quant. El.* **38**, 1005 (2006).
 20. Krishna Mohan Gundu, Miroslav Kolesik, Jerome V. Moloney, “Mode shaping in multi-core fibers”, *Optical Society of America*, 2006.
 21. Thranhardt A, Meier T, Reichelt M, Schlichenmaier C, Pasenow B, Kuznetsova I, Becker S, Stroucken T, Hader J, Zakharian AR, Moloney JV, Chow WW, Koch SW, “Microscopic modeling of the optical properties of semiconductor nanostructures”
JOURNAL OF NON-CRYSTALLINE SOLIDS 352 (23-25): 2480-2483 JUL 15 2006.
 22. Mahmoud Fallahi, Jerome V. Moloney, Li Fan, “High Power Vertical-External-Cavity Surface Emitting Laser and Their Applications”, *SPIE* Vol. 6127 61270C-1.
 23. J. Hader, J. V. Moloney, S.W. Koch, “Influence of internal fields on gain and spontaneous emission in InGaN quantum wells”, *Applied Physics Letters* **89**, 171120 (2006).
 24. A.Thraenhardt, S.W.Koch, J.Hader, J.V.Moloney, “Carrier dynamics in quantum well lasers”, *Opt.Quant.El.*, **38**, 361 (2006).
 25. H. Yoda, P. Polynkin, M. Mansuripur, “Beam quality factor of higher order modes in a step-index fiber”, *IEEE Journal of Lightwave Technology*, **23**, 1350 (2006).
 26. S. Suzuki, A. Schülzgen, S. Sabet, J. V. Moloney, and N. Peyghambarian, “Photosensitivity of Ge-Doped Phosphate Glass to 244 nm Irradiation”, *Appl. Phys. Lett.* **89**, 171913 (2006).
 27. J. Albert, A. Schülzgen, V. L. Temyanko, S. Honkanen, and N. Peyghambarian, “Strong Bragg gratings in Phosphate Glass Single Mode Fiber”, *Appl. Phys. Lett.* **89**, 101127 (2006).

28. L. Li, A. Schülzgen, S. Chen, V. L. Temyanko, J. V. Moloney, and N. Peyghambarian, "Phase Locking and In-Phase Supermode Selection in Monolithic Multicore Fiber Lasers", *Opt. Lett.* **31**, 2577 (2006).
29. L. Li, A. Schülzgen, V. L. Temyanko, M. M. Morrell, S. Sabet, H. Li, J. V. Moloney, and N. Peyghambarian, "Ultra-Compact Cladding-Pumped 35-mm-Short Fiber Laser with 4.7-W Single-Mode Output Power", *Appl. Phys. Lett.* **88**, 161106 (2006).
30. A. Schülzgen, L. Li, V. L. Temyanko, S. Suzuki, J. V. Moloney, and N. Peyghambarian "Single-Frequency Fiber Oscillator with Watt-Level Output Power Using Photonic Crystal Phosphate Glass Fiber", *Optics Express* **14**, 7087 (2006).
31. Jorg Hader, Jerome V.Moloney, Mahmoud Fallahi, Li Fan, and Stephan W. Koch "Closed-loop design of a semiconductor laser", *Opt. Lett.*, **31**, 3300 (2006).
32. Li Fan, Mahmoud Fallahi, Jorg Hader, Aramais R. Zakharian, Jerome V.Moloney, James T. Murray, Robert Bedford, Wolfgang Stolz, and Stephan W. Koch, "Multi-chip vertical-external-cavity surface-emitting laser: a coherent power scaling scheme", *Opt. Lett.*, **31**, 3612 (2006).
33. Li Fan, Ta-Chen Hsu, Mahmoud Fallahi, James T. Murray, Robert Bedford, Yushi Kaneda, Aramais R.Zakharian, Jorg Hader, Jerome V.Moloney, Wolfgang Stolz, and Stephan W. Koch, "Tunable watt-level blue-green vertical-external-cavity surface-emitting lasers by intracavity frequency doubling", *Appl. Phys. Lett.*, **88**, 251117 (2006).
34. Li Fan, Mahmoud Fallahi, James T. Murray, Robert Bedford, Yushi Kaneda, Aramais R. Zakharian, Jorg Hader, Jerome V.Moloney, Wolfgang Stolz, and Stephan W. Koch, "Tunable high-power high-brightness linearly polarized vertical-external-cavity surface-emitting lasers", *Appl. Phys. Lett.*, **88**, 021105 (2006).
35. Aramais R. Zakharian, Jorg Hader, Jerome V.Moloney, and Stephan W. Koch , "VECSEL threshold and output power-shutoff dependence on the carrier recombination rates", *IEEE Photon. Techn. Lett.*, **17**, 2511 (2005).
36. Li Fan, Jorg Hader, Marc Schillgalies, Mahmoud Fallahi, Aramais R. Zakharian, Jerome V.Moloney, Robert Bedford, James T. Murray, Stephan W. Koch and Wolfgang Stolz "High-Power Optically Pumped VECSEL Using a Double-Well Resonant Periodic Gain Structure", *IEEE Photon. Techn. Lett.*, **17**, 1764 (2005).
37. L. Fan, M. Fallahi, J. Harder, A. R. Zakharian, M. Kolesik, J. V. Moloney, T. Qui, A. Schülzgen, N. Peyghambarian, W. Stolz, S. W. Koch, and J. T. Murray "Over 3 W High-Efficiency Vertical-External-Cavity Surface-Emitting Lasers and Application as Efficient Fiber Laser Pump Sources", *Appl. Phys. Lett.*, **86**, 211116 (2005).
38. P. Polynkin, A. Polynkin, M. Mansuripur, J. Moloney, N. Peyghambarian, "Single-frequency fiber laser oscillator with watts-level output power at 1.5 μ m by use of a twisted-mode technique", *Optics Letters*, **30**, 2745 (2005).
39. A. Polynkin, P. Polynkin, M. Mansuripur, N. Peyghambarian, "Single-frequency fiber ring laser with 1W output power at 1.5 μ m", *Optics Express*, **13**, 3179 (2005).

40. A. Polynkin, P. Polynkin, A. Schülzgen, M. Mansuripur, N. Peyghambarian, "Watts-level, short, all-fiber laser at 1.5 μ m with a large core and diffraction-limited output via intracavity spatial-mode filtering", *Optics Letters*, **30**, 403 (2005).
41. L. Li, A. Schülzgen, V. L. Temyanko, S. Sabet, M. M. Morrell, H. Li, A. Mafi, J. V. Moloney, and N. Peyghambarian, "Investigation of Modal Properties of Microstructured Optical Fibers with Large Depressed-Index Cores" *Opt. Lett.* **30**, 3275 (2005).
42. T. Qiu, A. Schülzgen, L. Li, A. Polynkin, V. L. Temyanko, J. V. Moloney, and N. Peyghambarian, "Generation of Watt-Level Single Longitudinal Mode Output from Cladding Pumped Short Fiber Lasers" *Opt. Lett.* **30**, 2748 (2005).
43. L. Fan, M. Fallahi, J. Harder, A. R. Zakharian, M. Kolesik, J. V. Moloney, T. Qui, A. Schülzgen, N. Peyghambarian, W. Stolz, S. W. Koch, and J. T. Murray, "Over 3 W High-Efficiency Vertical-External-Cavity Surface-Emitting Lasers and Application as Efficient Fiber Laser Pump Sources", *Appl. Phys. Lett.* **86**, 211116, (2005).
44. L. Li, A. Schülzgen, V. L. Temyanko, T. Qiu, M. M. Morrell, Q. Wang, A. Mafi, J. V. Moloney, and N. Peyghambarian, "Short-Length Microstructured Phosphate Glass Fiber Lasers with Large Mode Areas", *Opt. Lett.* **30**, 1141 (2005).
45. L. Li, H. Li, T. Qiu, V. L. Temyanko, M. M. Morrell, A. Schülzgen, A. Mafi, J. V. Moloney, and N. Peyghambarian, "3-Dimensional Thermal Analysis and Active Cooling of Short-Length High-Power Fiber Lasers", *Optics Express* **13**, 3420 (2005).
46. A. Polynkin, P. Polynkin, A. Schülzgen, M. Mansuripur, and N. Peyghambarian, "Watts-Level, Short All-Fiber Laser at 1.5 μ m with a Large Core and Diffraction-Limited Output via Intra-Cavity Spatial-Mode Filtering", *Opt. Lett.* **30**, 403 (2005).
47. A. Thranhardt, I. Kuznetsova, C. Schlichenmaier, S.W. Koch, L. Shterengas, G. Belenky, J.Y. Yeh, L.J. Mawst, N. Tansu, J. Hader, J.V. Moloney, and W.W. Chow, " Nitrogen incorporation effects on gain properties of GaInNAs lasers: Experiment and theory," *Appl. Phys. Lett.* **86**, 201117 (2005).
48. C. Schlichenmaier, H. Gruning, A. Thranhardt, P.J. Klar, B. Kunert, K. Volz, W. Stolz, W. Heimbrod, T. Meier, S.W. Koch, J. Hader, and J.V. Moloney, " Type I-type II transition in InGaAs-GaNAs heterostructures", *Appl. Phys. Lett.* **86**, 081903 (2005).
49. J. Hader, J.V. Moloney, and S.W. Koch, " Supression of carrier recombination in semiconductor lasers by phase-space filling", *Appl. Phys. Lett.* **87**, 201112 (2005).
50. A.R. Zakharian, J. Hader, J.V. Moloney, and S.W. Koch, " VECSEL threshold and output power-shutoff dependence on the carrier recombination rates", *IEEE Photon. Technol. Lett.* **17**, 2511-2513 (2005).
51. S.W. Koch, J. Hader, A. Thranhardt, and J. V. Moloney, "Gain and Absorption: Many-Body Effects" *Optoelectronic Devices Advanced Simulation and Analysis*, ISBN #0-387-22659-1 2005 Springer Science & Business Media, Inc.
52. B. Grote, E.K. Heller, R. Scarmozzino, J. Hader, J.V. Moloney and S.W. Koch, "Quantum Well Laser Diodes: Temperature and Many-Body Effects", *Optoelectronic Devices Advanced*

Simulation and Analysis, ISBN #0-387-22659-1 2005 Springer Science & Business Media, Inc.

53. J. Hader, J.V. Moloney, and S.W. Koch, " Microscopic evaluation of spontaneous emission- and Auger-processes in semiconductor lasers", *IEEE J. Quantum Electron.* 41, 1217-1226 (2005).
54. B. Schlichenmaier, A.Thranhardt, T.Meier, S.W. Koch, W.W. Chow, J.Hader, J.V.Moloney, "Gain and carrier losses of (GaIn)(NAs) heterostructures in the 1300--1500nm range", *Appl. Phys. Lett.*, 87, 261109, 20.
55. Bernhard Pasenow, Matthias Reichelt, Tineke Stroucken, Torsten Meier, Stephan W. Koch, Aramis R. Zakharian, Jerome V. Moloney, " Enhanced light-matter interaction in semiconductor heterostructures embedded in one-dimensional photonic crystals" *JOSA B*, Volume 22, Issue 9, September 2005, 2039-2048.
56. Pavel Polynkin, Alexander Polynkin, Masud Mansuripur, Jerome Moloney, Nasser Peyghambarian, "Compact Single-Frequency Fiber Laser Oscillator Emits Watts-level Output Power at 1.5 μm ", *OPN*, December 2005.
57. Kano, P., M. Brio, and J. Moloney, "Application of Weeks method for the numerical inversion of the Laplace transform to the matrix exponential", *Communications in mathematical sciences*, vol. 3, no. 3, pp. 335-372, 2005.
58. K.M. Gundu, M. Brio, J. V. Moloney, " A mixed high-order vector finite element method for waveguides: convergence and spurious mode studies", *International Journal of Numerical Modelling: Electronic Networks, Devices and Fields* Volume 18, Issue 5 2005 (p 351-364).
59. T. Qiu, L. Li, A. Schülzgen, V. L. Temyanko, T. Luo, S. Jiang, A. Mafi, J. V. Moloney, and N. Peyghambarian, "Generation of 9.3-W Multimode and 4-W Singlemode Output from 7-cm Short Fiber Lasers", *IEEE Photonics Techn. Lett.* **16**, 2592 (2004).
60. A. Mafi, J. V. Moloney, D. Kouznetsov, A. Schülzgen, S. Jiang, T. Luo, and N. Peyghambarian, "A Large-Core, High Power, Single-Mode Photonic Crystal Fiber Laser", *IEEE Photonics Techn. Lett.* **16**, 2592 (2004).
61. L. Li, M. M. Morrell, T. Qiu, V. L. Temyanko, A. Schülzgen, A. Mafi, D. Kouznetsov, J. V. Moloney, T. Luo, S. Jiang, and N. Peyghambarian, "Short Cladding-Pumped Er/Yb Phosphate Fiber Laser with 1.5 W Output Power", *Appl. Phys. Lett.* **85**, 2721 (2004).
62. A. Kosterin, V. Temyanko, M. Fallahi, and M. Mansuripur, "Tapered fiber bundles for combining high-power diode lasers," *Applied Optics* **43**, 3893 (2004).
63. A. Kosterin, J. K. Erwin, M. Fallahi, and M. Mansuripur, "Heat and temperature distribution in a cladding pumped, Er:Yb co-doped phosphate fiber," *Review of Scientific instruments* **75**, 5166 (2004)
64. P. Polynkin, V. Temyanko, M. Mansuripur, N. Peyghambarian, "Efficient and scalable side pumping scheme for short high-power optical fiber lasers and amplifiers", *IEEE Photonics Technology Letters*, **16**, 2024 (2004).
65. P. Kano, D. Kouznetsov, J. V. Moloney and M. Brio, "Slab delivery of incoherent pump light to double-clad fiber amplifiers: Numerical simulations", *EE J. Quantum Electronics*, 40, pp 1301-

1305, 2004.

66. Arash Mafi and Jerome V. Moloney. "Phase locking in a passive multicore photonic crystal fiber", *JOSA B*. Volume 21, Issue 5, pp 897-902, May 2004.
67. A. Thranhardt, S. Becker, C. Schlichenmaier, I. Kuznetsova, T. Meier, S.W. Koch, J. Hader, J.V. Moloney, and W.W. Chow, " Nonequilibrium gain in optically pumped GaInNAs laser structures", *Appl. Phys. Lett.* 85, 5526-5528 (2004).
68. T. Qiu, L. Li, A. Schulzgen, V.L. Temyanko, T. Luo, S. Jiang, A. Mafi, J.V. Moloney, and N. Peyghambarian, "Generation of 9.3-W Multimode and 4-W Single-Mode Output from 7-cm Short Fiber Lasers", *IEEE Photonics Techn. Lett* 16, 2592, 2004.
69. M. Matus, M.Kolesik, J.V.Moloney, M.Hofmann, S.W.Koch, "Dynamics of two-color laser systems with spectrally filtered feedback", *JOSA B*, Vol 21, Issue 10, pp **1758** ,October 2004.
70. Li Fan, Mac Schillgalies, Mahmoud Fallahi, Thomas R. Nelson, Jr., James E. Ehret, Donald L. Agresta, Jerome Moloney, Jorg Hader, Aramais Zakharian, "Heat Dissipation for High Power Optically Pumped Semiconductor Vertical External Cavity Surface Emitting Lasers", *IEEE*, 2003.
71. A. R. Zakharian, J. Hader, J. V. Moloney, S. W. Koch, P. Brick, and S. Lutgen, "Experimental and theoretical analysis of optically pumped semiconductor disk lasers", *Appl. Phys. Lett.*, **83**, 1313 (2003).

Publicity Articles

1. P. Polynkin, A. Polynkin, D. Panasenko, N. Peyghambarian, J. Moloney, "Generating Ultrafast Pulses by Direct Amplification in Short, Heavily Doped Phosphate-Glass Fiber", in "Optics in 2006" issue of *Optics and Photonics News*, p. 49 (December 2006).
2. P. Polynkin, A. Polynkin, M. Mansuripur, J. Moloney, N. Peyghambarian, "Compact single-frequency fiber laser oscillator emits Watts-level output power at 1.5 μ m", in "Optics in 2005" issue of *Optics and Photonics News*, p. 27 (December 2005).
3. N. Peyghambarian, T. Qiu, P. Polynkin, A. Schulzgen, Li Li, V. Temyanko, M. Mansuripur, J. Moloney, "Short fiber lasers produce record power/length of 1.33 W/cm", in "Optics in 2004" issue of *Optics and Photonics News*, p. 41 (December 2004).
4. H. Li, A. Mafi, A. Schülzgen, L. Li, V. L. Temyanko, N. Peyghambarian, and J. V. Moloney, J "Efficient side-pumping scheme excites short fiber lasers", *Photonics Spectra*, **38**, 116 (2004).
5. Li Fan, Mahmoud Fallahi, Jorg Hader, Aramais R. Zakharian, Jerome V.Moloney, James T. Murray, Robert Bedford, Wolfgang Stolz, and Stephan W. Koch, "Multi-chip vertical-external-cavity surface-emitting laser: a coherent power scaling scheme", *Opt. Lett.*, **31**, 3612 (2006).
(This paper was highlighted by *Photonics Spectra* (February 2007, p.22 and SPIE Newsroom (DOI: 10.1117/2.1200704.0631)

6. Li Fan, Ta-Chen Hsu, Mahmoud Fallahi, James T. Murray, Robert Bedford, Yushi Kaneda, Aramais R. Zakharian, Jorg Hader, Jerome V. Moloney, Wolfgang Stolz, and Stephan W. Koch, "Tunable watt-level blue-green vertical-external-cavity surface-emitting lasers by intracavity frequency doubling", *Appl. Phys. Lett.*, **88**, 251117 (2006).
(This paper was highlighted by *Photonics Spectra* (September 2006, p.93).)
7. Li Fan, Mahmoud Fallahi, James T. Murray, Robert Bedford, Yushi Kaneda, Aramais R. Zakharian, Jorg Hader, Jerome V. Moloney, Wolfgang Stolz, and Stephan W. Koch, "Turnable high-power high-brightness linearly polarized vertical-external-cavity surface-emitting lasers", *Appl. Phys. Lett.*, **88**, 021105 (2006).
(This paper was highlighted by *Photonics Spectra* (March 2006, p24).)
8. Jorg Hader, Jerome V. Moloney, Mahmoud Fallahi, Li Fan, and Stephan W. Koch "Closed-loop design of a semiconductor laser", *Opt. Lett.*, **31**, 3300 (2006).
(This paper was reported by SPIE Newsroom (DOI: 10.1117/2.1200702.0536).)

Conference Proceedings and Talks

1. L. Li, A. Schülzgen, V. L. Temyanko, H. Li, J. V. Moloney, and N. Peyghambarian, "An All-Fiber Approach for In-Phase Supermode Phase-Locked Operation of Multicore Fiber Lasers", *Proceedings SPIE* **6453**, 64531K-1 (2007).
2. S. W. Koch, M. Kira, M. R. Hofmann, J. V. Moloney, Li Fan, and Mahmoud Fallahi, "Generation of terahertz radiation using semiconductor heterostructures", *Proceedings of SPIE* **6468**, Physics and simulation of optoelectronic Devices XV, 6448-61 (2007), San Jose, California, USA.
3. J. V. Moloney, J. Hader, Li Fan, M. Fallahi, and S. W. Koch, "Closed-loop design of a semiconductor laser" (invited paper). *Proceedings of SPIE* **6475**, Integrated Optics: Devices, Materials, and Technologies XI, 6475, 64750M (2007), San Jose, California, USA.
4. J. V. Moloney, J. Hader, Li Fan, M. Fallahi, and S. W. Koch, "Closed-loop design of a semiconductor laser", *invited talk at Photonics West 2007*, San Jose, California, USA, 2007.
5. S. W. Koch, M. Kira, M. R. Hofmann, J. V. Moloney, Li Fan, and Mahmoud Fallahi, "Generation of terahertz radiation using semiconductor heterostructures", *Physics and simulation of optoelectronic Devices XV, Photonics West 2007*, San Jose, California, USA (2007).
6. P. Polynkin, R. Roussev, M. Fejer, N. Peyghambarian, J. Moloney, "Laser transmitter at 518nm for optical undersea communications using efficient nonlinear conversion of a picosecond fiber-laser system at 1.5 μ m", *Frontiers in Optics and Laser Science, OSA 91st Annual Meeting*, San Jose, CA, September 2007, paper FWB6
7. S. Yamashita, T. Yoshida, S. Set, P. Polynkin, N. Peyghambarian, "Passively Mode-Locked Short-Cavity 10GHz Er:Yb-codoped Phosphate-Fiber Laser using Carbon Nanotubes", *SPIE Photonics West 2007*, San Jose, CA, January 2007, paper 6453-72
8. L. Fan, M. Fallahi, James T. Murray, J. Hader, A.R. Zakharian, J. V. Moloney, R. Bedford, S.W. Koch and W. Stolz, "Tunable high-power blue-green laser based on intracavity frequency

- doubling of a diode-pumped tunable vertical-external-cavity surface-emitting lasers”, *OSA Advanced Solid State Photonics*, Vancouver, Canada, 2007.
9. A. Schülzgen, "Single-Frequency Photonic Crystal and Multicore Fiber Lasers”, *invited talk at Photonics North 2007*, Ottawa (CANADA) 2007.
 10. P. Polynkin, R. Roussev, M. Fejer, N. Peyghambarian, J. Moloney, “Dual-band laser transmitter for above- and under-water communications using third-harmonic generation of fiber-laser system at 1.5 μm ”, *OSA meeting on Nonlinear Photonics*, Quebec City, Canada, September 2007, paper NTuA5
 11. A. Schülzgen, J. M. Auxier, S. Honkanen, L. Li, V. L. Temyanko, S. H. Chen, S. Suzuki, M. M. Morrell, S. Sabet, S. Sen, N. F. Borrelli, and N. Peyghambarian, "Active Micro- and Nano-Structured Glass Fiber and Waveguide Devices”, *proceedings SPIE 6183*, 618306 (2006).
 12. N. Peyghambarian, M. Fallahi, H. Li, L. Li, A. Mafi, M. Mansuripur, J. V. Moloney, R. A. Norwood, D. Panasenکو, A. Polynkin, P. Polynkin, T. Qiu, A. Schülzgen, V. L. Temyanko, J. Wu, S. Jiang, Chavez, J. Geng, and Ch. Spiegelberg, "Microstructured and Multicore Fibers and Fiber Lasers”, *Optical Fiber Communication Conference and National Fiber Optic Engineers Conference, Technical Digest, OFC/NFOEC*, 3 (2006).
 13. M. Fallahi, L. Fan, T-C. Hsu, Y. Kaneda, A. R. Zakharian, J. Hader, J. V. Moloney, J. T. Murray, R. Bedford, W. Stolz, and S. W. Koch, “Tunable high-power high-brightness diode-pumped VECSELs and their applications”, *The 19th Solid State and Diode Laser Technology Review (SSDLTR)*, Albuquerque, New Mexico, 13-15 June 2006.
 14. Mahmoud Fallahi, Jerome V. Moloney and Li Fan “High Power Vertical-External-cavity Surface-Emitting Lasers and Their Applications” (*Invited paper*). *Proceedings of SPIE 6127, Quantum Sensing and Nanophotonic Devices III*, pp.6127C (2006), San Jose, California, USA.
 15. Mahmoud Fallahi, Jerome V. Moloney and Li Fan, “High Power Vertical-External-Cavity Surface- Emitting Lasers and Their Applications”, *invited talk at Photonics West 2006*, San Jose, California, USA, 2006.
 16. A. Schülzgen, N. Peyghambarian, M. Fallahi, H. Li, L. Li, A. Mafi, M. Mansuripur, J. V. Moloney, R. A. Norwood, D. Panasenکو, A. Polynkin, P. Polynkin, T. Qiu, V. L. Temyanko, J. Wu, S. Jiang, Chavez, J. Geng, and Ch. Spiegelberg, "Microstructured and Multicore Fibers and Fiber Lasers”, *invited talk at the Optical Fiber Communication Conference, OFC 2006*, Anaheim (USA) 2006.
 17. A. Polynkin, P. Polynkin, D. Panasenکو, M. Mansuripur, J. Moloney, N. Peyghambarian, “All-fiber source of high-power picosecond pulses at 1.5 μm using heavily-doped phosphate-fiber amplifier”, *CLEO 2006, (paper, CThJ2)*, Long Beach, CA, May 2006.
 18. P. Polynkin, A. Polynkin, D. Panasenکو, M. Mansuripur, J. Moloney, N. Peyghambarian, “Picosecond fiber laser oscillator at 1.5 μm with 2.3W average power and 160MHz repetition rate”, *Photonics West 2006, (paper 6102-41)* San Jose, CA, January 2006.

19. D. Panasenکو, P. Polynkin, A. Polynkin, J. Moloney, M. Mansuripur, N. Peyghambarian, "High average power harmonically mode locked femtosecond ring laser based on phosphate glass fiber", OFC 2006, (*paper OThJ6*) Anaheim, CA, March 2006.
20. N. Peyghambarian, L. Li, A. Schülzgen, V. L. Temyanko, J. V. Moloney, and H. Li, "Ultra-Compact High Power Fiber Lasers with Phosphate Microstructured Optical Fibers", *Solid State & Diode Laser Technology Review 2006*, Albuquerque, NM (USA) 2006.
21. P. Polynkin, A. Polynkin, D. Panasenکو, M. Mansuripur, N. Peyghambarian, J. Moloney, "Development of Watts-level sources of ultra-short pulses at 1.5 μ m using heavily-doped Phosphate glass fibers", 19th Solid State and Diode Laser Review (SSDLTR), Albuquerque, New Mexico, June 2006, paper FIBER1-5
22. A. Schülzgen, "Compact, High-Power, Photonic Crystal Fiber Lasers", *invited talk at International Conference on High Power Laser Beams (HPLB-2006)*, Nizhny Novgorod (RUSSIA) 2006.
23. N. Peyghambarian, A. Schülzgen, L. Li, V. L. Temyanko, J. V. Moloney, and H. Li, "Fiber Lasers with Phosphate Photonic Crystal and Multicore Fibers", *invited talk at the Summer Topicals 2006, IEEE Lasers & Electro-Optics Society*, Quebec City (CANADA) 2006.
24. A. Schülzgen, "Active Micro- and Nano-Structured Glass Fiber and Waveguide Devices", *invited talk at Photonics Europe 2006, Strasbourg (FRANCE) 2006*.
25. J. Hader J. V. Moloney, S. W. Koch, L. Fan and M. Fallahi, "Carrier recombination in semiconductor lasers: Beyond the ABC", *The 6th Numerical Simulation of Optoelectronic Devices (NUSOD) Conference*, Singapore 11-14 Sept. 2006.
26. P. Polynkin, A. Polynkin, D. Panasenکو, M. Mansuripur, J. Moloney, N. Peyghambarian, "All-fiber source of high-power picosecond pulses at 1.5 μ m using short and heavily doped phosphate-fiber amplifier", *OSA topical meeting on optical amplifiers and their applications (OAA 2006)*, Whistler, Canada, June 2006, paper OMC4
27. A. Chavez-Pirson, W. Tian, S. Jiang, G. Katona, J. Lee, A. Schülzgen, and N. Peyghambarian, "Sub-Picosecond Pulse Amplification in a Short Length, Highly Doped Erbium/Ytterbium Phosphate Fiber Amplifier", *OSA Topical Meeting: Optical Amplifiers and Their Applications (OAA)*, Whistler (CANADA) 2006.
28. R. G. Bedford, M. Kolesik, J. L. A. Chilla, M. k. Reed, T. R. Nelson and J. V. Moloney , "Power-limit mechanisms in VECSELS", *Proceedings of SPIE* **5814**,199-208, 2005.
29. N. Peyghambarian, A. Schulzgen, M. Mansuripur, J.V. Moloney, T. Qiu, Y. Kaneda, P. Polynkin, L. Li, J. Wu, A. Polynkin, V.L. Temyanko, A. Mafi, S. Jiang, Ch. Spiegelberg, A. Chavez, J. Geng, and T. Luo, "Chip Scale, High Power Microstructure Fiber Laser" *MRS Proceedings* Vol. 883, FF2.1 (MRS Spring Meeting) (2005).
30. N. Peyghambarian, A. Schülzgen, L. Li, V. L. Temyanko, P. Polynkin, A. Polynkin, D. Panasenکو, M. Mansuripur, A. Mafi, and J. V. Moloney, "Microstructured Fiber Laser", *Proceedings Annual Meeting IEEE-LEOS 2005*, 432 (2005).
31. T. Qiu, A. Schülzgen, A. Mafi, L. Li, J. Wu, V. L. Temyanko, A. Mafi, J. V. Moloney, and N. Peyghambarian, "Experiments and Modeling of High Power Er-Yb Doped Short Fiber

- Laser”, *Optical Fiber Communication Conference, Technical Digest, OFC/NFOEC, Vol. 2, 3* (2005).
32. N. Peyghambarian, A. Schülzgen, M. Mansuripur, J. V. Moloney, T. Qiu, Y. Kaneda, P. Polynkin, L. Li, J. Wu, A. Polynkin, V. L. Temyanko, A. Mafi, S. Jiang, Ch. Spiegelberg, A. Chavez, J. Geng, and T. Luo, "Chip-Scale, High Power Microstructure Fiber Laser”, *MRS Proceedings Vol. 883*, FF2.1 (MRS Spring Meeting) 2005.
 33. A. M. Abdi, S. Suzuki, A. Schülzgen, and A. R. Kost "Fiber Bragg Grating Array Calibration”, *Proceedings SPIE 5765*, 552 (2005).
 34. J. Wu, S. Jiang, T. Qiu, M. M. Morrell, A. Schülzgen, and N. Peyghambarian, "Tm³⁺ Doped Tellurite Glass Microsphere Laser”, *Proceedings SPIE 5723*, 21 (2005).
 35. J. Wu, S. Jiang, T. Qiu, M. M. Morrell, A. Schülzgen, and N. Peyghambarian, "Cross-Relaxation Energy Transfer in Tm³⁺ Doped Tellurite Glass”, *Proceedings SPIE 5723*, 152 (2005).
 36. J. M. Auxier, A. Schülzgen, M. M. Morrell, B. R. West, S. Honkanen, S. Sen, N. F. Borrelli, and N. Peyghambarian, "Quantum Dots for Fiber Laser Sources”, *Proceedings SPIE 5709*, 249 (2005).
 37. N. Peyghambarian, A. Schülzgen, M. Mansuripur, J. V. Moloney, T. Qiu, Y. Kaneda, P. Polynkin, L. Li, J. Wu, A. Polynkin, V. L. Temyanko, Mafi, S. Jiang, Ch. Spiegelberg, A. Chavez, J. Geng, and T. Luo, "Chip-Scale, High Power Microstructure Fiber Laser”, *invited talk at the MRS Spring Meeting 2005*, San Francisco, CA (USA) 2005.
 38. L. Li, A. Schülzgen, V. L. Temyanko, M. M. Morrell, S. Sabet, H. Li, J. V. Moloney, and N. Peyghambarian, "High-Power Short-Length Microstructured Phosphate Fiber Laser with Large Mode Areas”, *Frontiers in Optics 2005/Laser Science-XXI, 89th Annual Meeting of the Optical Society of America*, Tucson (USA) 2005.
 39. M. A. Leigh, A. Schülzgen, S. Honkanen, M. M. Morrell, and N. Peyghambarian, "Writing Annular Waveguides in Co-Doped Phosphate Glass using Ultrafast Pulses”, *Frontiers in Optics 2005/Laser Science-XXI, 89th Annual Meeting of the Optical Society of America*, Tucson, AZ (USA) 2005.
 40. H. Gan, R. A. Norwood, L. Li, J. Wu, A. Schülzgen, A. Fardad, C. De Silva, Z. Zheng, N. Peyghambarian, "Lanthanide nanoparticle doped low-loss sol-gel amplifier materials”, *SPIE's 50th Annual Meeting*, San Diego, CA (USA) 2005.
 41. L. Li, A. Schülzgen, V. L. Temyanko, T. Qui, A. Mafi, J. V. Moloney, and N. Peyghambarian, "Microstructured Phosphate Glass Fiber Lasers with Large Mode Areas”, *Optical Fiber Communication Conference OFC 2005*, Anaheim, CA (USA) 2005.
 42. T. Qiu, A. Schülzgen, A. Mafi, L. Li, J. Wu, V. L. Temyanko, J. V. Moloney, and N. Peyghambarian, "Experiments and Modeling of High Power Doped Er-Yb Doped Short Fiber Lasers”, *Optical Fiber Communication Conference OFC 2005*, Anaheim (USA) 2005.
 43. A. M. Abdi, S. Suzuki, A. Schülzgen, and A. R. Kost, "Fiber Bragg Grating Array Calibration” *12th SPIE Annual Symposium on Smart Structures and Materials*, San Diego, CA (USA) 2005.

44. J. Wu, S. Jiang, T. Qui, M. M. Morrell, A. Schülzgen, and N. Peyghambarian, "Cross-Relaxation Energy Transfer in Tm^{3+} Doped Tellurite Glass", *Photonics West '05, San Jose (USA) 2005*.
45. J. Wu, J. Jiang, T. Qui, M. M. Morrell, A. Schülzgen, and N. Peyghambarian "Tm³⁺ Doped Tellurite Glass Microsphere Laser", *Photonics West '05, San Jose, CA (USA) 2005*.
46. P. Polynkin, A. Polynkin, D. Panasenko, N. Peyghambarian, M. Mansuripur, and J. Moloney, "Watts-level, all-fiber laser at 1.5 μ m modelocked with a saturable semiconductor absorber", *Frontiers in Optics/Laser Science XXI OSA meeting, Tucson, AZ, October 2005, paper JTUC45*
47. P. Polynkin, A. Polynkin, M. Mansuripur, N. Peyghambarian, "Single-Frequency, Linearly Polarized Fiber Laser with 1.9W Output Power at 1.5 μ m Using Twisted-Mode Technique", *CLEO 2005, (Postdeadline paper CPDB11), Baltimore, MD, May 2005*.
48. N. Peyghambarian, A. Schülzgen, L. Li, V. L. Temyanko, P. Polynkin, A. Polynkin, D. Panasenko, M. Mansuripur, A. Mafi, J. V. Moloney, "Microstructured Fiber Laser", *invited Talk at the 18th Annual Meeting of the IEEE Lasers & Electro-Optics Society, LEOS 2005, Sydney (AUSTRALIA) 2005*.
49. N. Peyghambarian, A. Schülzgen, T. Qiu, L. Li, V. L. Temyanko, P. Polynkin, M. Mansuripur, A. Mafi, and J. V. Moloney, "Recent Advances Towards 1 W/cm Single Mode Fiber Lasers", *Proceedings Annual Meeting IEEE-LEOS 2004, Vol. 2, 869 (2004)*.
50. T. Qui, L. Li, V. L. Temyanko, J. Wu, A. Schülzgen, N. Peyghambarian, T. Luo, S. Jiang, A. Mafi, D. Kouznetsov, and J. V. Moloney, "Generation of High Power 1535 nm Light from a Short Cavity Cladding Pumped Er:Yb Phosphate Fiber Laser", *Proceedings CLEO '04 (CMS5), San Francisco (USA) 2004*.
51. N. Peyghambarian, A. Schülzgen, T. Qiu, L. Li, V. L. Temyanko, M. M. Morrell, J. V. Moloney, A. Mafi, D. Kouznetsov, P. Kano, S. Jiang, and T. Luo, "High Power Doped Phosphate Glass Fiber Laser Development", *SSDLTR 2004 Technical Digest, P-30 (2004)*.
52. N. Peyghambarian, T. Qui, L. Li, V. L. Temyanko, A. Schülzgen, A. Mafi, and J. V. Moloney, "Few Centimeter Single Mode Fiber Lasers Generating Several Watts Output Power at 1535 nm" *International Conference on Nonlinear Optics: Materials, Fundamentals and Applications, Waikoloa (USA) 2004*.
53. N. Peyghambarian, A. Schülzgen, T. Qiu, L. Li, A. Schülzgen, V. L. Temyanko, M. M. Morrell, J. V. Moloney, A. Mafi, D. Kouznetsov, P. Kano, S. Jiang, and T. Luo, "High Power Doped Phosphate Glass Fiber Laser Development", *Solid State & Diode Laser Technology Review 2004, Albuquerque, NM (USA) 2004*.
54. T. Qui, L. Li, V. L. Temyanko, J. Wu, A. Schülzgen, N. Peyghambarian, T. Luo, S. Jiang, A. Mafi, D. Kouznetsov, and J. V. Moloney, "Generation of High Power 1535 nm Light from a Short Cavity Cladding Pumped Er:Yb Phosphate Fiber Laser", *CLEO '04, San Francisco (USA) 2004*.

55. A. Schülzgen, "Fiber Lasers – High Brightness Coherent Light Sources", *Annual Photonic and Imaging Initiatives Workshop*, Tucson, AZ (USA) 2004.
56. N. Peyghambarian, A. Schülzgen, T. Qiu, L. Li, V. Temyanko, P. Polynkin, M. Mansuripur, A. Mafi, and J. V. Moloney, "Recent Advances Towards 1 W/cm Single Mode Fiber Lasers", *invited talk at the 17th Annual Meeting of the IEEE Lasers & Electro-Optics Society - LEOS 2004*, Rio Grande (PUERTO RICO) 2004.
57. J. V. Moloney, D. Kouznetsov, A. Mafi, A. Schülzgen, M. Mansuripur, M. Fallahi, and N. Peyghambarian, "Novel Designs for Double-Clad and Photonic Crystal Highly-Doped Fiber Amplifiers and Lasers", *SSDLTR 2003 Technical Digest, Fiber-4* (2003).
58. Li Fan, Schillgalies, M., Fallahi, M., Nelson, T. R. Jr., Ehret, J. E., Agresta, D. L., Moloney, J., Hader, J., Zakharian, A., "Heat dissipation for high power optically pumped semiconductor vertical external cavity surface emitting lasers", *The 16th Annual Meeting of the IEEE*, Vol. 1, pp79-80, *IEEE-LEOS 2003*, October, 2003.
59. Aramais Zakharian, J. Hader, Jerome V. Moloney, Li Fan, Robert Bedford and M. Fallahi and S.W. Koch "High brightness vertical external cavity surface emitting lasers", *IEEE-LEOS 2003*, October, 2003. *The 16th Annual Meeting of the IEEE*, Vol. 2, pp509-510.
60. A. R. Zakharian, J. Hader, J. V. Moloney, S. W. Koch, S. Llutgen, P. Brick, T. Albrecht, S. Grotsch, J. Luft and W. Spath, "Modeling and experimental result analysis for high-power VECSELS", *Proceeding of SPIE*, 4993, 104 (2003).
61. J. V. Moloney, D. Kouznetsov, A. Mafi, A. Schülzgen, M. Mansuripur, M. Fallahi, and N. Peyghambarian, "Novel Designs for Double-Clad and Photonic Crystal Highly-Doped Fiber Amplifiers and Lasers", *invited talk at Solid State & Diode Laser Technology Review 2003*, Albuquerque, NM (USA) 2003.
62. L. Li, V. L. Temyanko, M. M. Morrell, M. Mansuripur, A. Schülzgen, N. Peyghambarian, D. Kouznetsov, J. V. Moloney, T. Luo, S. Jiang, "Compact Cladding Pumped Fiber Laser at Telecom Wavelength", *Laser Science-XIX, 87th Annual Meeting of the Optical Society of America*, Tucson, AZ (USA) 2003.
63. L. Fan, Schillgalies, M., Fallahi, M., Nelson, T. R. Jr., Ehret, J. E., Agresta, D. L., Moloney, J., Hader, J., Zakharian, A. "Heat dissipation for high power optically pumped semiconductor vertical external cavity surface emitting lasers", *The 16th Annual Meeting of the IEEE, IEEE-LEOS 2003*, Tucson, AZ, (USA) 2003.
64. Aramais Zakharian, J. Hader, Jerome V. Moloney, Li Fan, Robert Bedford and M. Fallahi and S.W. Koch, "High brightness vertical external cavity surface emitting lasers", *The 16th Annual Meeting of the IEEE, IEEE-LEOS 2003*, Tucson, USA 2003.
65. A. R. Zakharian, J. Hader, J. V. Moloney, S. W. Koch, S. Llutgen, P. Brick, T. Albrecht, S. Grotsch, J. Luft and W. Spath, "Modeling and experimental result analysis for high-power VECSELS", *High-Power Fiber and Semiconductor Lasers, Photonics West 2003*, San Jose, CA, USA (2003).

4. List of Inventions

US Patent Applications:

US patent PCT/US2005/016923; filed on May 3, 2006:
“Microstructured optical fibers and manufacturing methods thereof”
Inventors: N. Peyghambarian, A. Schülzgen, V. Temyanko

M.I.T. Case No. 12066
Patent Cooperation Treaty Serial No. US07/001704, Filed January 19, 2007
"Surface-Emitting Fiber Laser"
Inventors: Yoel Fink, John D. Joannopoulos, Ken Kuriki, Nicholas D. Orf and Ofer Shapira

Inventions with Provisional Patent Applications:

UA05-104 (2007)
“Continuously tunable high power (multi-watts) high brightness linearly polarized vertical external cavity surface emitting lasers”
Inventors: L. Fan, M. Fallahi, J. Moloney

UA08-014 (2007)
“Beam combination of high-power lasers using temporal pulse stacking”
Inventor: P. Polynkin

UA07-072 (2007):
“Laser transmitter for optical undersea communications, using nonlinear conversion of a modelocked fiber-laser system with pulse picking”
Inventors: P. Polynkin, J. Moloney, N. Peyghambarian

UA07-088 (2007):
“Distributed Feedback Fiber Laser Pumped by Multimode Diode Lasers”
Inventors: N. Peyghambarian, A. Schülzgen, L. Li, J. Albert

UA06-095 (2006)
“Spliceless Phosphate Glass Fiber Laser and Novel Method of its Fabrication”
Inventors: N. Peyghambarian, A. Schülzgen, S. Honkanen, J. Albert

UA06-059 (2006)
“All-Fiber Mode Selection Technique for Multicore Fiber Laser Devices”
Inventors: N. Peyghambarian, A. Schülzgen, L. Li

UA06-024 (2005)
“Novel Approach for Fabricating All-Fiber Optica...”
Inventors: N. Peyghambarian, A. Schülzgen, V. Temyanko

UA05-020 (2004)
“Novel Approach for Design and Fabrication of Single Mode Microstructured Optical Fibers”

Inventors: N. Peyghambarian, A. Schülzgen, V. Temyanko

UA04-078 (2004)

“Novel Approach for Making Optical Fibers”

Inventors: N. Peyghambarian, A. Schülzgen, V. Temyanko

5. Technical Report: Fiber Project

5.1. Chip-Scale Cladding-Pumped Fiber Lasers Utilizing Microstructured Fibers

Development of high power fiber lasers has been one a very active research area for the last decade and a half. Regardless of the operating wavelength, cladding-pumped fiber lasers share the common property of being quite long in size. Active fibers as long as several tens of meters are usual and 1 to 2 meters of active fibers are considered as compact size. The long length is required because of the rather low pump absorption coefficient in the cladding pumped scheme. Theoretically, the absorption rate is determined by two main factors: the doping level of the absorbing ions and the ratio of the active core area to the pump-confining cladding area, which is typically much smaller than 0.01 cm^{-1} . Even for Er-Yb co-doped fiber lasers cladding pumped around 975 nm (with greatly enhanced pump absorption due to Yb); active fiber lengths in excess of 1 meter were used to reach Watt-level cw output. To produce Watt-level cw fiber laser cladding-pumped by multimode source while reducing the active fiber length to the centimeter scale, high doping concentration, large core area, and optimized cavity designs are essential. The advantages of such short-length high power fiber laser include the suppression of nonlinear effects such as stimulated Raman and Brillouin scattering, possible single frequency operation, and extremely compact size.

One of the first objectives was the development of phosphate glasses that have been co-doped with high concentrations of Yb and Er ions and optimized for efficient pump absorption and laser emission. Utilizing glasses with a doping levels of $\sim 1 \text{ wt}\%$ Er_2O_3 and $\sim 2 \text{ wt}\%$ Yb_2O_3 , i.e., an Er concentration 5 times as high as that used in a previously reported high-power Er-Yb co-doped fiber lasers, the first Watt-level cm-long fiber laser has been demonstrated in 2004. Glasses, preforms, fibers, and dielectric mirrors have all been fabricated in-house. The lasers performance is shown in figure 1. Up to 1.5 W cw laser output was obtained from an 11 cm long active fiber with properly selected input coupler and output coupler when pumped by a 15 W multimode 975 nm laser. The fiber laser was demonstrated at 1535 nm with a narrow spectrum and a good beam quality of M^2 smaller than 3.

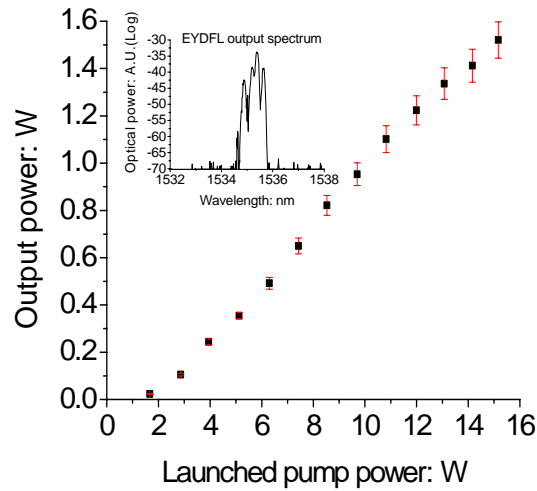


Fig. 1. 11 cm long Er-Yb co-doped fiber laser performance with optimized resonator reflectivity. The inset shows the output spectrum.

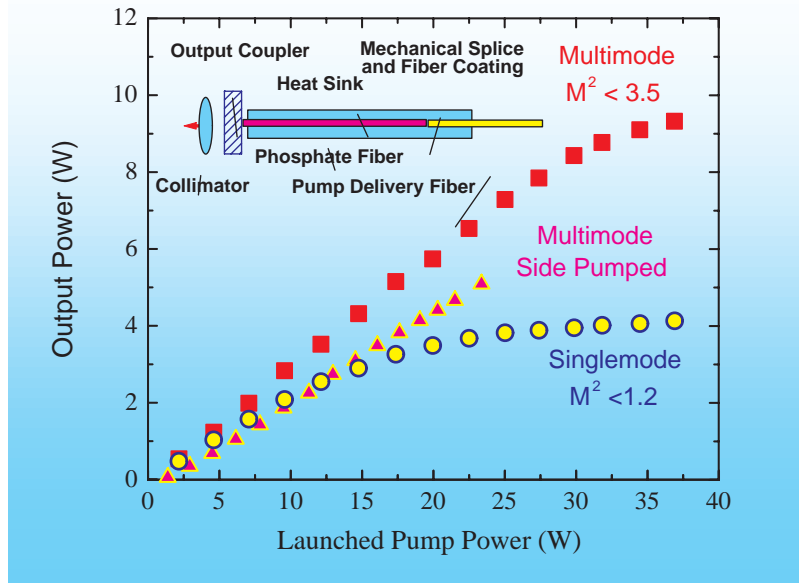


Fig 2. Performance of 7 cm multimode (squares) and single mode (circles) end-pumped fiber lasers, and 12 cm side-pumped multimode fiber laser (triangles). The inset shows the schematic layout of the end-pumped fiber laser.

A few months later, utilizing glasses with even higher doping (8 wt% Yb_2O_3) and active fiber with lower numerical aperture and larger core sizes, we presented new experimental results on even shorter length (7 cm) phosphate fiber lasers shown in figure 2. These lasers generated more than 9.3 W multi-mode and 4.0 W single mode output power. To our knowledge, the power generated per unit fiber length of 1.33W/cm (multi-mode) represented the first record contributed by our group to the fiber laser world.

Microstructured optical fiber (MOF) is well suited for the fabrication of fiber with extremely large mode area that is beyond the limits of conventional step index fiber technology. At the same time, single transverse mode propagation and excellent beam quality can be maintained. To use this concept for our compact fiber lasers we investigated the modal characteristics of MOF whose guiding core consists of one and seven missing air holes using a finite element method. Our systematic and comprehensive study of issues such as the core radius, V number, and core versus cladding refractive indices provided practical design tools that could be directly applied to MOF fiber laser design.

To make practical use of combining the MOF concept with the large doping capabilities in phosphate glasses we developed the technology to fabricate fiber with microstructured fiber cladding from phosphate glasses. To the best of our knowledge we are worldwide the only group that fabricates phosphate glass fiber with micrometer size holes running along the fiber length. Design and realization of one of the first microstructured active phosphate fiber is shown in figure 3. Successively, we fabricated various large core microstructured fibers and compared theoretical predictions with experimentally observed modal structures. In particular, we carried out the first systematic study on how negative core-cladding index difference influences the modal behavior of microstructured optical fiber.

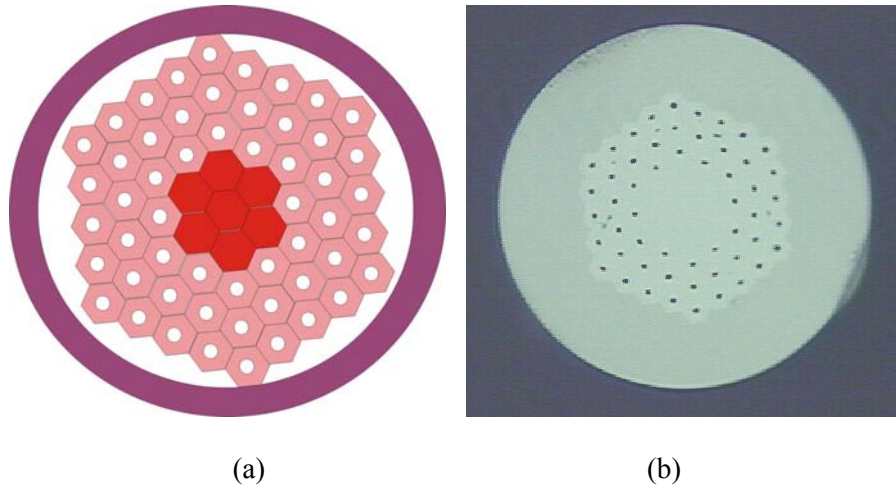


Fig. 3. (a) Illustration of the stacking scheme and (b) microscopic image of one of the first microstructured phosphate fibers with 125 μm outer diameter.

Using such novel design we fabricated a microstructured gain fiber that combined both advantages – large mode area through special fiber design and high Er and Yb doping levels (again, we started doping levels of ~ 1 wt% Er_2O_3 and ~ 2 wt% Yb_2O_3) that are only possible in phosphate glass. Gain fiber with an active core area larger than $500 \mu\text{m}^2$ was first applied to build an ultra compact cladding-pumped fiber laser with more than 3 W single mode output power as shown in figure 4. We demonstrated that while the modal properties change dramatically changing the sizes of the air holes in the cladding (from highly multi-mode to single mode) the fiber laser output power remained almost constant due to the unchanged core material and area.

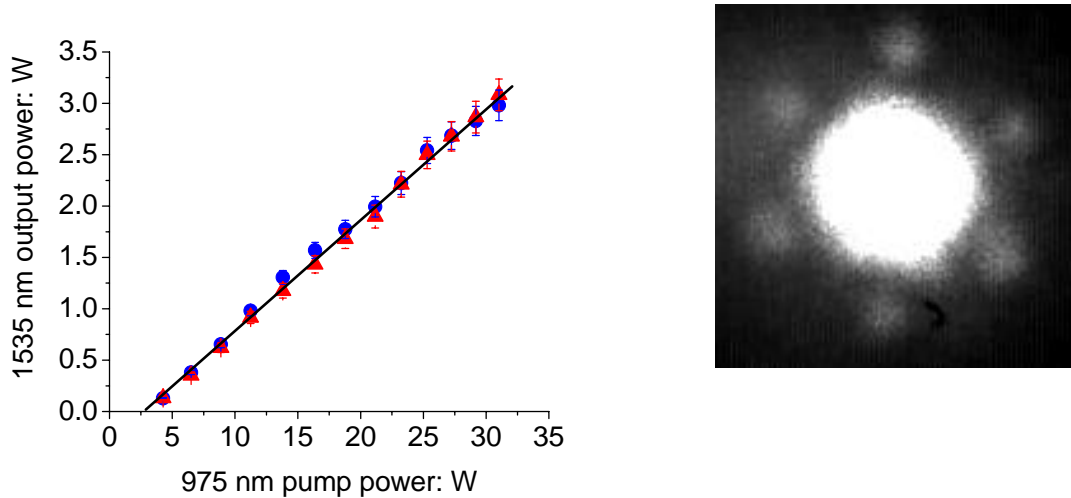


Fig. 4. Signal output vs. pump power of two MOF lasers with different cladding hole diameters but same period. The dots correspond to $d/\Lambda=0.19$ and the triangles represent $d/\Lambda=0.50$. The right picture shows the recorded far field pattern of the single mode laser with $d/\Lambda=0.19$.

Successively we increase the concentration of Yb_2O_3 to 8 wt% in the active core of a microstructured fiber. Although we used an even shorter piece of gain fiber of only 3.5 cm length, 4.7 W of cw fiber laser output could be demonstrated (see figure 5) corresponding to a yield above 1.3 W per cm. Converting multi-mode pump (975 nm) into single-mode signal (1535 nm) a slope efficiency of ~20% with respect to the launched pump could be achieved in this ultra compact fiber laser.

This record-breaking single mode fiber laser with continuous wave output powers beyond 1.3 W per cm of active fiber length was achievement as a result of several loops of materials and device improvements that have been documented in a series of journal publications during the project. This research opened new avenues to develop Watt-level single-frequency light sources at the 1550nm wavelength band.

Microstructured optical fibers are certainly amongst the most active research areas in fiber technology and a lot of challenges remain before the full potential can be exploited. Their design flexibility and multiple promising applications foster rapid progress in fabrication technologies. Besides the demonstrated benefits for cm-sized Watt-level light sources, microstructured fibers will also facilitate improvements in kW-level fiber lasers, pulsed fiber lasers, and amplifiers with high peak powers.

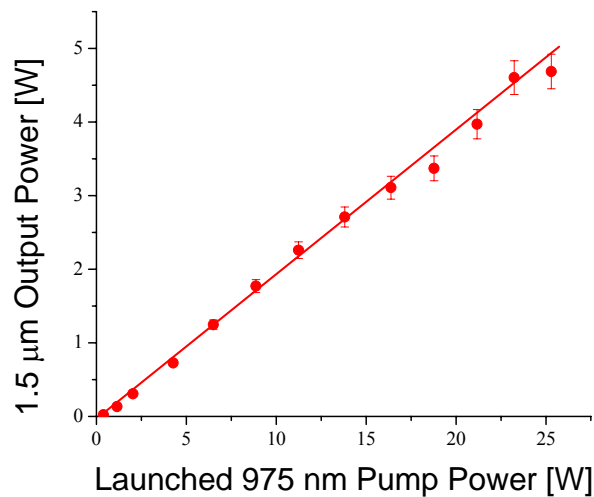


Fig. 5. Signal vs. launched pump power of a 3.5-cm phosphate microstructured fiber laser.

5.2. Watt-level Single-Frequency Fiber Lasers

The generation of high-power narrow-linewidth coherent radiation near 1550 nm from a compact fiber laser source is of great interest because of its applications in telecommunications, interferometers, and sensing instruments. Since the first demonstration of single longitudinal-mode fiber lasers, many successful single-frequency operations with fiber lengths of a few centimeters and powers in the mW-range were reported by several groups of scientists. Because of the lack of powerful single-mode pump diodes and small core sizes, these core-pumped single-frequency fiber lasers are not able to generate W-level powers. Although the use of multistage amplifiers can boost the single-frequency output power to the several-hundred-watts, it is still a challenging task to obtain watt-level single-frequency output, which can preserve a high signal-to-noise ratio, directly from fiber oscillators.

One of the key elements of a single-longitudinal mode fiber laser is a single-mode Er–Yb doped phosphate fiber. Heavily Er/Yb co-doped phosphate glass fibers have been successfully used in high-gain short-length amplifiers and lasers, as reported previously. Compared with other common host materials, e.g., silica glass, phosphate glass has a much higher solubility of rare-earth ions and low clustering effects, which allow the ion doping level to be increased without significantly enhancing the detrimental fluorescence-quenching process. In addition, phosphate glass has bigger phonon energy, leading to a higher transfer rate of energy from Yb to Er ions. Some glasses of our single-frequency fiber lasers were provided by NP Photonics, Inc.

End-pumped Single Frequency Fiber Laser

Within this project last we reported on two different linear cavity end-pumped single-frequency fiber lasers. The first device demonstration utilized an optimized, yet conventional step-index gain fiber, while the most recent device is based on a large core microstructured gain fiber. In both gain fibers high doping levels enabled sufficient absorption of multi-mode pump light launched into the cladding. The layout of our single-frequency lasers is shown in figure 6. The pump light is coupled into the gain fiber cladding through a dielectric mirror that is transparent for the 975 nm pump wavelength and highly reflective (broadband) at wavelengths around 1.5 microns. Narrow-band FBGs (fabricated in-house at the College of Optical Sciences in Arizona) at the output end of the fiber laser enabled the selection of a single longitudinal laser mode.

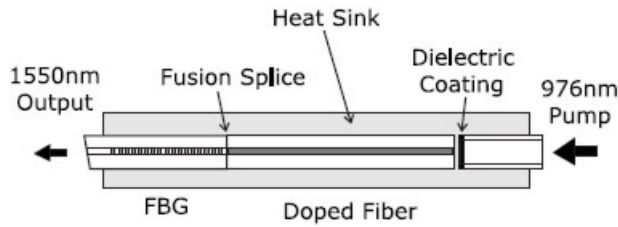


Fig. 6. Schematic of the single-frequency fiber laser.

With the conventional gain fiber we already achieved more than 1 W of single frequency output as shown in figure 7. The figure also demonstrates that we could approximately double the single-frequency output utilizing a microstructured fiber with a larger doped core. Utilizing the microstructured fiber provides another inherent advantage: the noncircular symmetry of the core results in polarization mode discrimination while in step-index fibers special polarization maintaining fiber has to be used to break the polarization degeneracy. Our new concept enabled for the first time the utilization of readily available, high-power, multimode laser diodes to pump single-frequency fiber lasers and boost their output power to the level of several Watts.

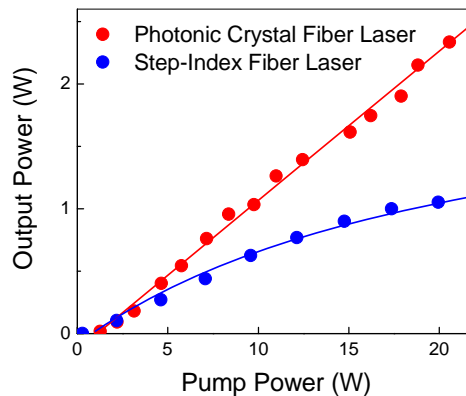


Fig. 7. Signal output vs. pump power of two single-frequency laser using 3.8 cm of active microstructured fiber (red circles) and 4 cm of active step-index fiber (blue circles), respectively.

Side pumping scheme for short, heavily doped phosphate-glass fibers

In order to make fiber lasers based on heavily doped phosphate-glass fibers robust, alignment-free and potentially low-cost we have devised a scalable side-pumping scheme for these fibers. The approach is schematically shown in Figure 17. In this scheme, the active fiber is surrounded by several passive pump delivery fibers, and the bundle is held together by a thin tube made of a low-refractive index polymer. The walls of the tube are as thin as $35\mu\text{m}$. The heat generated in the bundle during operation of the laser, is efficiently dissipated by placing the bundle on an aluminum heat sink.

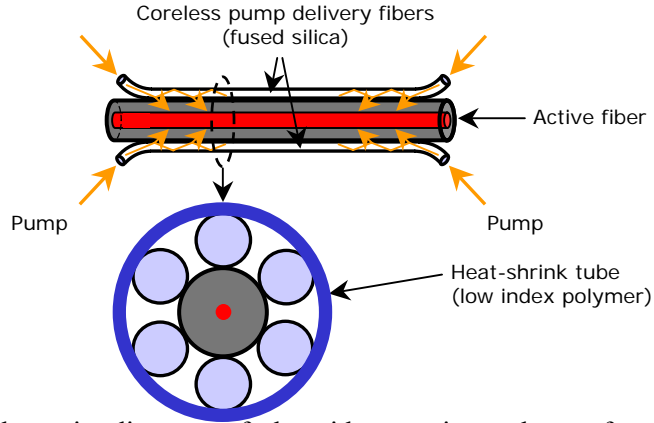


Fig. 17. Schematic diagram of the side-pumping scheme for short, heavily doped phosphate-glass fibers. The estimated pump absorption in 10 to 15cm-long bundle is 50%.

To demonstrate the viability of this pumping method, we built a simple and short multi-mode fiber laser operating at $1.5\mu\text{m}$. A single 12cm-long strand of a doped phosphate-glass fiber acts as an active medium of the laser. The diameters of the core and the cladding of the active fiber are $18\mu\text{m}$ and $125\mu\text{m}$, respectively, and the core is co-doped with 1% Er_2O_3 and 8% of Yb_2O_3 (by weight). The active fiber has $\text{NA}=0.2$, and thus supports multiple spatial modes for the laser light. The active fiber is surrounded by six coreless silica fibers creating twelve independent entrance points for the pump light. The laser resonator is formed by the 4% Fresnel reflections at the two cleaved ends of the active fiber.

The laser threshold occurs at 1.6W of combined pump power. As the pumping is increased, the output power reaches 5W, and the optical-to-optical slope efficiency of this laser is 24%, which is close to the theoretical maximum with respect to the estimated absorbed pump.

Single-frequency (SF) fiber laser oscillators based on side-pumped phosphate active fibers

Using our side-pumping scheme, we have demonstrated Watts-level, fully integrated SF fiber-laser oscillators at $1.5\mu\text{m}$. A SF fiber laser with direct output in the Watts range has various applications in nonlinear optics, remote sensing and free-space communications. In addition, if used as a master oscillator in a high-power Master-Oscillator-Power-Amplifier (MOPA) system instead of a mW-level DFB fiber laser, the Watt-level MO will allow for eliminating several low-power amplification stages. Furthermore, compared to an amplified SF laser system, a stand-alone laser oscillator offers a superior ASE-noise performance that can be critical in some applications.

All of our SF CW fiber lasers utilize a same type of active phosphate fiber. The fiber has $14\mu\text{m}$ core, $125\mu\text{m}$ cladding, and the core of the fiber is uniformly doped with 1% of Er_2O_3 and 8% of Yb_2O_3 . In order to integrate the phosphate fibers with conventional silica fibers, we have developed a process for reliable fusion-splicing between thermally dissimilar fibers. Photographs of two such splices are shown in Figure 18. One of the splices is performed on the fibers cleaved at an angle, thus eliminating the back-reflection off the splice point.

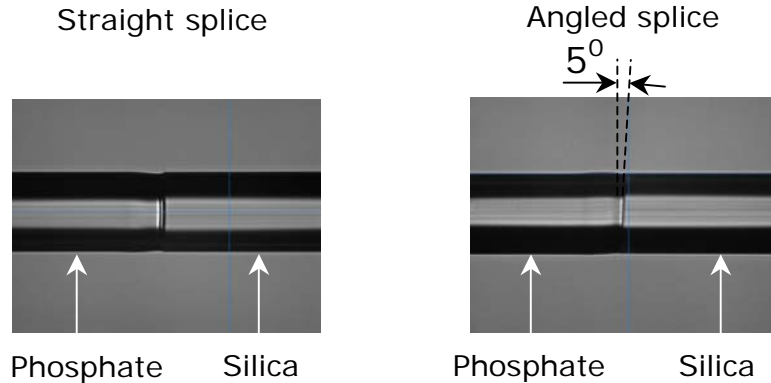


Fig. 18. Fusion splice between phosphate and silica fibers. The typical splice strength is half of that between two silica fibers, and the splice loss is consistent with the mode mismatch between the fibers. (~ 0.5 dB in this particular case)

In general, the output power of a SF laser oscillator with a standing-wave cavity is limited by the spatial hole-burning effect. In operation of a standing-wave cavity laser, the gain medium is under-saturated in the nodes of the standing-wave pattern. As a result, a second longitudinal mode, which has the least overlap with primary oscillating mode, will overcome threshold and make the laser multimode, at a particular finite level of pumping.

The natural approach of combating the spatial gain hole-burning effect is by making the oscillator cavity shorter. However, this approach has its limitations: Under practical conditions, the laser cavity has to be as short as ~ 3 to 5cm in order for the laser to remain single-frequency at ten times above threshold, which is a somewhat typical operation point.

Two alternative ways of eliminating spatial gain hole-burning are known: Lasers that utilize unidirectional ring cavity and the so-called twisted-mode cavity are free from this effect, as there is no standing-wave field pattern formed in the active medium. We have implemented both of these approaches in all-fiber format, and generated 1W and 2W of average power with SF ring-cavity and twisted-mode cavity oscillators, respectively, at $1.5\mu\text{m}$ wavelength.

Single-frequency ring fiber laser with 1W output power at $1.5\mu\text{m}$

The laser is shown schematically in Figure 19. The length of the active phosphate fiber in the oscillator cavity is 11cm, and the total cavity length is 50cm. In order to introduce an additional discrimination between the longitudinal modes of the oscillator, a sequence of two fiber-Bragg gratings is used as an output coupler. The two gratings act as a low-finesse Fabry-Perot etalon and modulate the amount of feedback in the frequency domain. A short piece of polarizing fiber is spliced into the laser cavity, and the unidirectional operation of the oscillator is enforced by the non-reciprocal optical circulator.

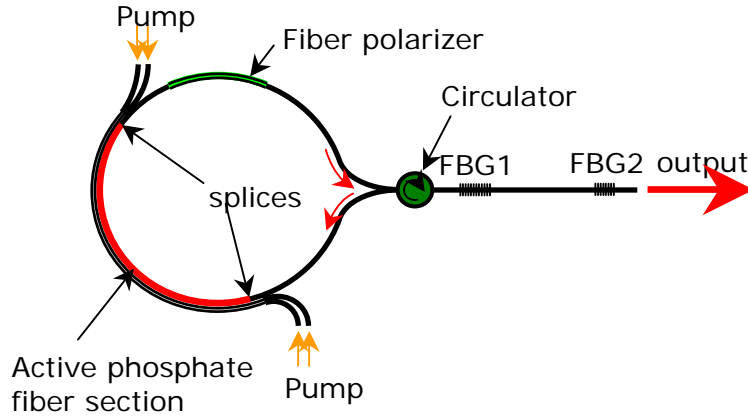


Fig. 19. Schematic diagram of the ring SF fiber oscillator based on phosphate active fiber. A sequence of two fiber-Bragg gratings provides additional wavelength selectivity.

The output power of this laser exceeds 1W at 19W of combined pump power, which corresponds to ~5% slope efficiency. The single-frequency operation is monitored by using the optical heterodyne technique, in which the attenuated output of the ring laser is mixed with the output of a stable single-frequency, tunable laboratory laser source, using a fiber coupler. Using this technique, the single-frequency operation of the ring oscillator was confirmed throughout the entire range of the output power. Figure 20 shows a typical RF heterodyne signal recorded in our experiments.

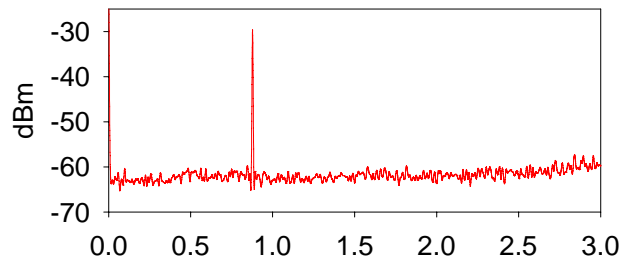


Fig. 20. RF spectrum of the beat signal between the ring fiber oscillator and a tunable single-frequency laboratory laser. The single peak corresponds to the single-frequency operation of the test source.

Single-frequency twisted-mode-cavity fiber laser with 2W output power at 1.5 μ m

In this approach, the spatial gain hole-burning effect is eliminated by using a fiber oscillator in the twisted-mode cavity configuration. The setup is shown schematically in Figure 21. The optical feedback in the laser is provided by Bragg gratings spliced into the cavity. One of the gratings is written into a PM-fiber; it has a bandwidth of 0.05nm and a peak reflection of 20%. Due to the refractive index difference for the two linearly polarized eigenmodes of the PM fiber, the reflection peaks for the two polarizations are separated by 0.4nm, in the wavelength domain. An 80% reflective, single-mode Bragg reflector at the other end of the cavity is fabricated such that its reflection band overlaps with that of the PM grating for only one polarization. Thus the laser cavity naturally acts as a linear polarizer. The total cavity length of the laser is 20cm, which corresponds to the longitudinal mode spacing of 500MHz, twelve times narrower than the 3dB bandwidth of the PM fiber grating. Two short pieces of a standard PM Panda fiber are spliced at either end of the active fiber. The length of the PM fiber segments is chosen equal to one quarter of the polarization beat-length in the fiber, thus these segments act as ultra-compact and robust

quarter-waveplates. At the splice point between the PM fiber grating and the adjacent waveplate, the birefringent axes of the two have been aligned at 45° with respect to each other. The waveplates manipulate the polarization state of the oscillating cavity mode. As a result, the two counter-propagating waves inside the cavity have circular polarizations which are orthogonal to each other. Thus there is no standing-wave intensity pattern formed in the active fiber, and the spatial gain hole-burning is eliminated.

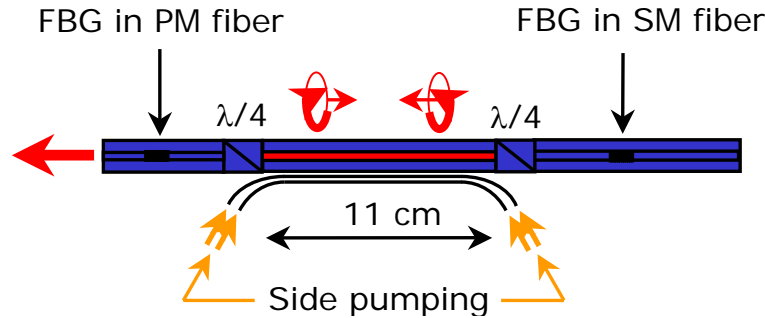


Fig. 21. Schematic diagram of the all-fiber twisted-mode cavity oscillator. Two short pieces of PM fiber at the either end of the active fiber act as ultra-compact quarter-waveplates.

As with the ring laser, the single-frequency operation throughout the full range of output power was confirmed using the optical heterodyne technique. At the maximum power level, the laser generates 2W of output power at 20W of total applied pump at 975nm. This power performance is record-high among all single-frequency fiber laser oscillators reported to-date. An additional advantage of this device is in the fact that the output light from the laser is linearly polarized and delivered through the polarization-maintaining fiber pigtail.

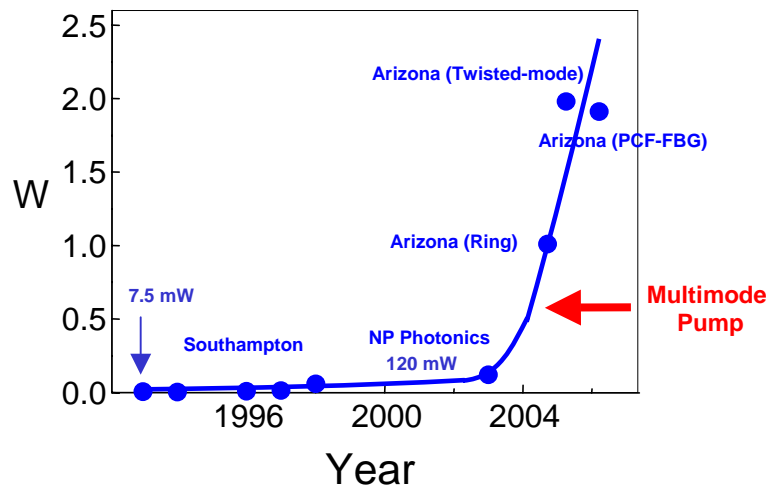


Fig. 8. Signal output of selected single frequency fiber lasers and the year when they have been demonstrated. The introduction of cladding pumped single frequency lasers advanced their output power by more than one order of magnitude.

In figure 8 the advancement of the output power of selected single frequency fiber lasers is shown. Conventional core pumped lasers have been limited to output levels of about 100 mW. Our introduction of cladding pumped single frequency fiber lasers enabled an increase in output power of

more than an order of magnitude. Such high power single frequency lasers will find applications in remote sensing, advanced interferometry, and coherent beam combination through phase-locking schemes.

5.3 Spin-off Compact Phosphate Fiber Laser Development

This section details an important series of spin-off applications that take advantage of the compact, highly-doped phosphate fibers developed under this project.

Gain-guided Yb-doped phosphate-fiber lasers

Due to the smaller quantum defect, Ytterbium-doped fibers emitting at $1\mu\text{m}$ are typically more efficient than their Erbium-doped counterparts with the emission at $1.5\mu\text{m}$. Furthermore, the solubility of Ytterbium oxide in phosphate glasses is by an order of magnitude higher compared to that of Erbium oxide. That allows for fabrication of Ytterbium-doped phosphate fibers with truly massive doping concentrations of up to 20% and beyond. Experiments with Ytterbium-doped phosphate fibers were generally beyond the scope of this program which was mainly focused on development of eye-safe lasers. We however have fabricated several types of Ytterbium-doped phosphate fibers and experimentally found that these fibers can be very promising in construction of compact fiber lasers based on gain guiding.

In our experiments, we used three types of phosphate Yb-doped fibers fabricated by drawing from rod-in-a-tube fiber preforms. The fiber parameters such as doping concentrations, core/cladding dimensions, and numerical apertures (NA) are summarized in Table I. An important circumstance is that the fiber NA is calculated from the values of refractive indices of the core and the cladding which are measured in the absence of optical pumping. The value of NA can change dramatically if the fiber is optically pumped, causing switching between index guiding, index anti-guiding, and gain guiding, at various levels of applied pump power.

	Yb ₂ O ₃	Core	Clad.	NA	MFD
Fiber 1	20 wt. %	12.5 μm	125 μm	0.085	11.6 μm
Fiber 2	12 wt. %	12.5 μm	125 μm	0.09	11.2 μm
Fiber 3	6 wt. %	10 μm	125 μm	0.07	12.0 μm

Table I. Parameters of the three Ytterbium-doped phosphate fibers used in the experiments on gain guiding.

In order to demonstrate the potential of generating high optical power at around $1\mu\text{m}$ wavelength with heavily Yb-doped fibers, we have constructed simple fiber-laser oscillators utilizing 15cm-long pieces of the three fibers from Table I. The optical feedback was provided by Fresnel reflections off the cleaved end-facets of the fibers. Thus the power output from the laser oscillators was evenly divided between the two ends of the active fiber. The fibers were pumped using the side-pumping technique described above. The combined output power for the three laser samples, versus total applied pump power at 975nm is shown in Fig. 22. We estimate that $\sim 50\%$ fraction of the pump light has actually penetrated into the cladding of the active fiber in our side-pumping scheme, resulting in the estimated slope efficiencies of 85%, 50% and 35%, for the doping concentrations of 20%, 12% and 6%, respectively. As expected, the oscillator utilizing active fiber with 20% doping yielded the highest output power, and the slope efficiency with this fiber was close to the theoretical maximum. In addition to substantially lower slope

efficiency, the device based on the 6% fiber exhibited a power roll-off at the pump power level of ~ 10 W. The roll-off limited the maximum output power attainable from a 15cm-long strand of such fiber by 2W.

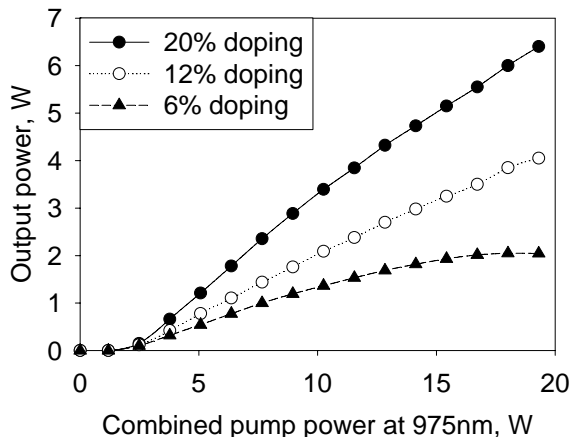


Figure 22. Combined output power from 15cm-long side-pumped fiber-laser samples with three different doping concentrations.

The undesirable feature that severely limits the use of the efficient fiber-laser oscillator with 20% Ytterbium-doped fiber is an extreme multimode nature of the spatial emission pattern and the associated low brightness. Even though in the un-pumped state the fiber has a low value of NA and the fiber V-number at $1.05\mu\text{m}$ wavelength is 3.179, close to the value of 2.405 required for the single-mode operation, the laser based on that fiber is highly multi-mode. Extremely large divergence of light emitted by the fiber indicates that the light in the fiber laser is predominantly guided by the cladding, and not by the core.

In order to quantify the dependence of the waveguiding properties in the three fibers on the level of pump power, we have used the following simple experimental setup in which a seed light from a broadband pigtailed LED at $1.05\mu\text{m}$ is amplified in 4cm-long amplifiers that utilize three different Yb-doped phosphate fiber samples with parameters summarized in the Table I. In these experiments, the amplifiers operate in the linear regime as 1mW of power emitted by the seed LED is not nearly enough for saturating the amplifiers. At the highest level of pumping, the amplifiers produce several dBs of gain.

The experimental results for the measured mode-field diameter (MFD) as a function of the pumping level in the three fiber samples are shown in Fig. 23. Systematic size variations of the guided fiber mode with pumping are evident in all three fibers. The initial growth of the MFD with pumping level is consistent with the decreasing refractive-index step between the core and the cladding. When the level of pumping is further increased, the fiber may become gain-guiding. In that case the MFD of the guided fiber mode is decreased. Both of these guiding regimes can be clearly identified in the case of the 20% doping. With the 12% fiber, the weakening of the index guiding with pumping level is clear, although the onset of gain-guidance is less pronounced.

Even with the lowest doping concentration of 6%, the change of the MFD induced by pumping is considerable and needs to be accounted for when a practical single-mode fiber with such concentration of doping is designed and integrated into a fiber-laser system. These results demonstrate the potential of the heavily Ytterbium-doped fibers in short fiber oscillators based on gain guiding. The massive doping concentrations that are attainable in phosphate fibers make this approach to power scaling extremely promising.

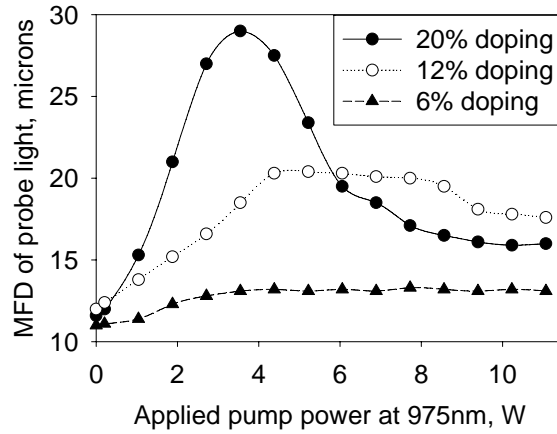


Figure 23. Mode-field diameter of the output beam for short Ytterbium-doped fiber amplifiers with different concentration of doping.

Modelocked fiber-laser oscillators with high average power and high repetition rates

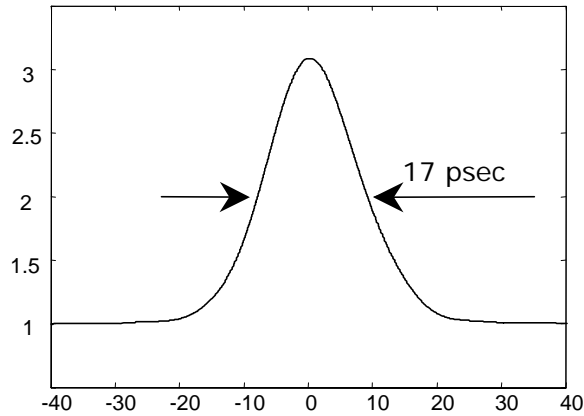
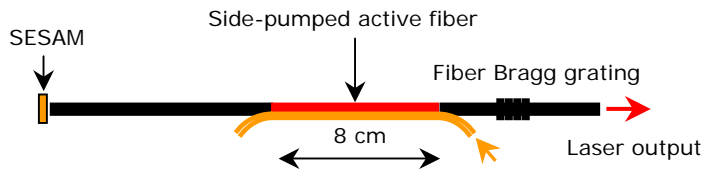


Figure 24. Top: Schematic diagram of the short fiber-laser oscillator modelocked with a semiconductor saturable-absorber mirror (SESAM). The fundamental pulse repetition rate of the oscillator is 550MHz. Bottom: Autocorrelation trace of the transform-limited pulse generated by the source.

Ultrafast lasers find applications in diverse areas of science and technology such as material processing, free-space communications, nonlinear optics, spectroscopy, optical frequency metrology, etc. Fiber-based sources of ultrashort pulses can be an attractive replacement for their counterparts based on bulk optics. In certain applications such as communications and optical frequency metrology, the high pulse repetition rate is an important attribute of the laser source. Since the fundamental repetition rate of a passively modelocked laser oscillator is inversely proportional to the laser cavity length, fiber-laser sources based on short and heavily doped phosphate fibers have advantages compared to lasers based on conventional meters-long doped fibers made of fused silica.

As a spin-off project of this MRI, we have developed various modelocked fiber-laser oscillators based on Er:Yb co-doped phosphate-glass fibers. In particular, using a carbon nanotube-based saturable absorber and active fiber only 1cm-long, we have demonstrated an oscillator with the fundamental pulse repetition rate of 10GHz and average power of 30mW. Using a more conventional semiconductor saturable absorber mirror (SESAM) modelocker, we have demonstrated a simple oscillator with 550MHz pulse repetition rate and 775mW of average power. The device is shown schematically in Figure 24, together with the autocorrelation trace of the generated transform-limited pulse.

Even higher average power levels can be attained by adjusting the spot size on the SESAM via adiabatic tapering the single-mode fiber which is butt-coupled to the absorber. Using this approach, we have demonstrated a picosecond fiber-laser oscillator with 100MHz repetition rate and 2.4W of average power at 1.5 μ m.

An alternative way of generating ultrashort pulses at high repetition rates is by using the so-called harmonic modelocking, when multiple pulses simultaneously co-exist in the fiber-laser cavity. Using a 20cm-long segment of a side-pumped, heavily-doped phosphate-glass fiber inside a 2m-long unidirectional ring-cavity oscillator, we have demonstrated a Watt-level emission of soliton pulses at repetition rates adjustable between 1.5GHz and 7.2GHz which is the 75th harmonic of the fundamental cavity frequency. The schematic diagram of this fiber laser is shown in Figure 25, together with the autocorrelation trace of the shortest pulse attainable from this laser source. The pulses are perfect transform-limited hyperbolic secants with FWHM pulse width of 300fs. (Corresponding FWHM of the autocorrelator is 450fs.)

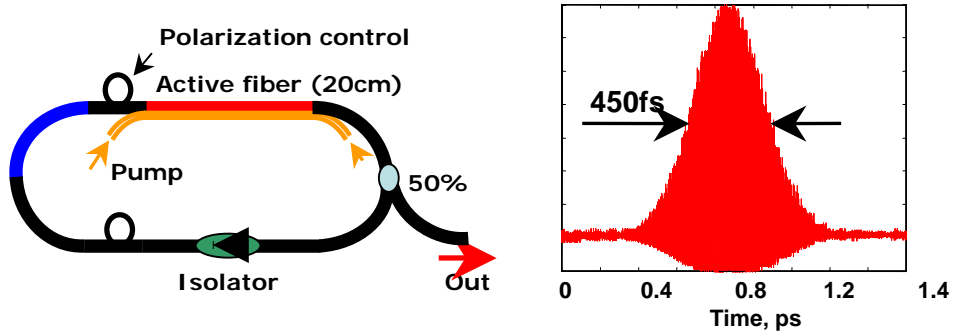


Figure 25. Left: Schematic diagram of the harmonically modelocked ring fiber-laser oscillator with the repetition rate adjustable via intra-cavity polarization control. Right: Autocorrelation trace of the shortest pulse attainable from the oscillator.

Distortion-free amplification of ultrashort pulses in short phosphate-fiber amplifiers

Amplification of ultrashort (picosecond or shorter) pulses in doped fibers is limited by the onset of nonlinear processes in the fiber amplifier such as self-phase modulation and stimulated Raman scattering. As an example, a practical limit on peak power directly attainable by amplification of multi-nJ pulses at 1.5 μ m in a standard 1m-long single-mode doped fiber with 10 μ m core is about 1kW. Beyond

this level, the pulses become broken into soliton sub-pulses with low energy, and the peak power cease to grow with further amplification.

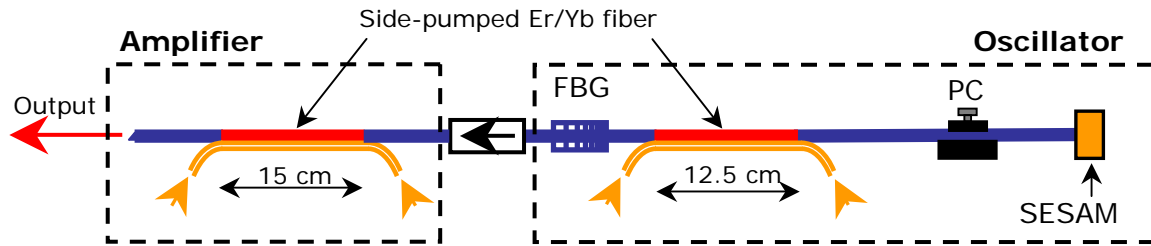


Figure 26. Single-stage MOPA system based on heavily Er:Yb co-doped active fiber.

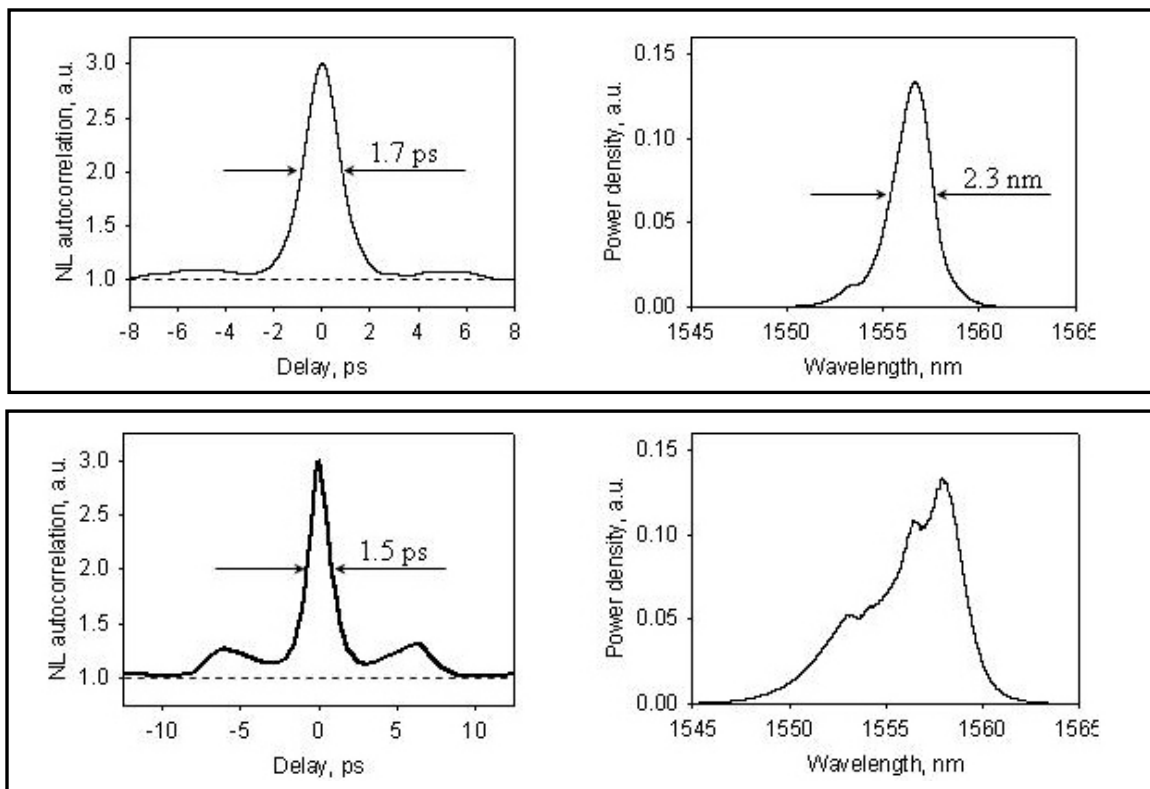


Figure 27. Autocorrelation trace and optical spectrum of the picosecond pulses before (top) and after (bottom) amplification. The three-peaked feature in the bottom spectrum is indicative of a moderate spectral broadening due to the self-phase modulation in the short fiber amplifier.

Several methods of mitigating the detrimental effects on nonlinearities have been developed. Most of them rely on compression of amplified pulses in touchy setups using free-space diffraction-gratings. The addition of bulk optics essentially eliminates the main advantages brought about by the fiber format of the source, such as robustness and immunity to misalignments.

Heavily-doped phosphate fibers offer a unique medium for amplification of ultrashort pulses. Since the doping concentration and the corresponding gain per unit fiber length in these fibers can be by about two orders of magnitude higher than that in conventional silica fibers, the length of the fiber

amplifier can be reduced in proportion. Then the amplification of pulses occurs so rapidly that no appreciable pulse distortion develops in either spectral or temporal domain.

We have demonstrated the validity of this approach by amplifying picosecond pulses at $1.5\mu\text{m}$ to the peak power level of 17kW. The schematic of the setup is shown in Figure 26. Both the oscillator and the amplifier in the single-stage MOPA system are based on heavily doped phosphate-glass fiber. The amplifier fiber is only 15 centimeters long. As a result, the distortion in the amplified pulses although noticeable, is minor. The power density in the fiber core at the output of the amplifier is over $20\text{GW}/\text{cm}^2$, which is the highest power density ever reported with directly fiber-amplified ultrashort pulses. There is a clear potential for further peak-power scaling with the core size of the active fiber.

Efficient frequency conversion of infrared picosecond sources into the visible in cascaded PPLNs at room temperature

Clean picosecond pulses produced by the phosphate-fiber MOPAs are ideally suited for nonlinear frequency conversion. An essential ingredient for viable wavelength conversion of pulsed infrared fiber lasers into the visible came with recent developments in the periodically-poled Lithium Niobate (PPLN) technology in M. Fejer's group at Stanford that we collaborate with. Until recently, operating PPLN devices at high levels of average power required heating the crystals by $\sim 100^\circ\text{C}$ in order to avoid the detrimental photorefractive effects. Combination of MgO doping with near-stoichiometric composition of LiNbO_3 allows for superior high-power performance at room temperature.

We have recently demonstrated a viable laser transmitter for undersea optical communications (OCOMM) using an efficient two-step nonlinear conversion of a picosecond fiber-laser system at $1.5\mu\text{m}$. Operation in the spectral window from 350nm to 580nm is essential for this application because shallow to mid-depth seawater has an absorption minimum in the blue-green. In principle, green light could be produced by second-harmonic generation of an Yb-doped fiber-laser source operating at $1\mu\text{m}$. However, using third-harmonic generation of a $1.5\mu\text{m}$ source has two practically important added benefits: First, a multitude of reliable and inexpensive fiber-optic components developed for telecom can be utilized in construction of the fiber-laser source. Second, $1.5\mu\text{m}$ light is eye-safe, thus the modulated fiber laser itself, prior to the wavelength conversion, can be used as a backup eye-safe OCOMM transmitter for communications above water.

In our demonstration, high-power picosecond pulses at $1.5\mu\text{m}$ were produced by amplification of a passively modelocked fiber-laser oscillator in 15cm-long heavily Er-Yb co-doped phosphate-glass fiber. The system generates clean, transform-limited pulses with 3ps duration, 0.9nm bandwidth and 5kW peak power. The average power of the generated infrared light is 1W. Digital information is encoded onto the fundamental modelocked pulse train by pulse picking with a commercial fiber-pigtailed electro-optic intensity modulator (EOM). The EOM is spliced between the oscillator and the amplifier, where the average power level is low.

The efficient nonlinear wavelength conversion takes place in two consecutive PPLN crystals. Both crystals are MgO-doped and operate at room temperature. The first 1mm-long PPLN doubles the frequency of the incoming infrared light. The second crystal is 3mm-long, and it has a period chosen for first-order quasi phase-matching of sum-frequency mixing of the generated second harmonic with the leftover fundamental at $1.5\mu\text{m}$. Since the nonlinear conversion occurs in a single pass, the system is virtually alignment-free.

In the demonstration, neither PPLN crystals nor focusing lenses were AR-coated. The conversion efficiency from $1.5\mu\text{m}$ into green is 14%, and it can be straightforwardly increased three-fold by using AR-coated optics in the setup. Furthermore, considerably higher pulse repetition frequencies than the demonstrated 65MHz can be achieved by using a faster modelocked master oscillator in the MOPA system.

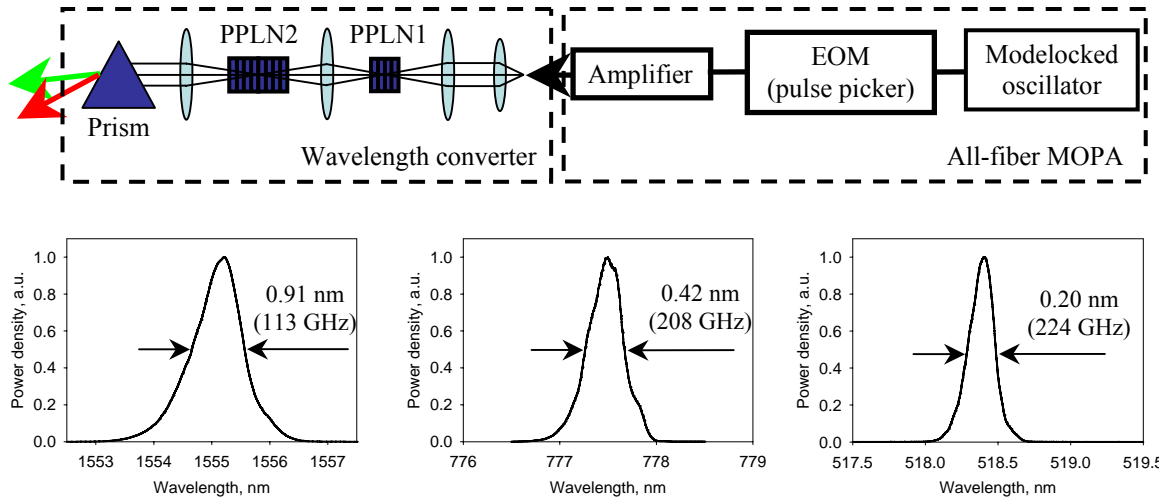


Figure 28. Top: Setup for the two-step nonlinear conversion of a picosecond fiber MOPA system at 1.5 μ m into the blue-green. Bottom: Optical spectra of the fundamental and the generated second and third harmonic signals, on linear scale.

Efficient energy storage in highly-doped phosphate fibers for applications in fiber CPA systems and amplification of nanosecond pulses

Another exciting development leading to new applications of phosphate-glass fibers in pulse amplification is the recent demonstration of efficient energy storage in these fibers. In these experiments, sub-20 nanosecond pulses at 1.5 μ m wavelength produced by an actively Q-switched all-fiber oscillator are amplified in 15cm-long, side-pumped phosphate fibers doped with 1 wt.% of Er₂O₃ and 8 wt.% of Yb₂O₃. Two different active fibers are used in the experiments, with the core diameters of 14 μ m and 25 μ m (The values of the fiber NA in these two cases are 0.08 and 0.2, respectively, thus the fiber with the larger core is highly multimode.) The energy levels achieved with these fibers are 105 μ J and 215 μ J, respectively, at a repetition rate of 605Hz. Because of the short length of the amplifiers, the amplified pulses have close to diffraction-limited beam quality even in the case of the highly multimode active fiber with 25 μ m core.

The experimental setup is shown in Figure 29. The oscillator in the MOPA is actively Q-switched by a fiber-pigtailed acousto-optic modulator (AOM). The oscillator produces nanosecond pulses at a variable pulse-repetition frequency, and the pulses are subsequently amplified in a short phosphate-fiber amplifier. The pulse energy versus pulse repetition rate and the temporal pulse trace at the highest energy level are shown in Figure 30.

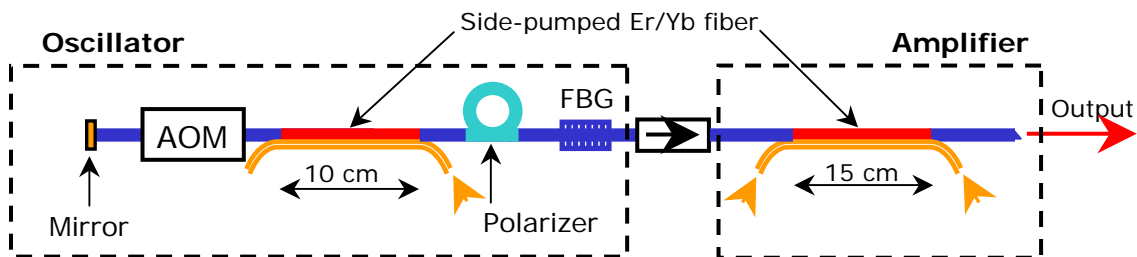


Figure 29. Diagram of the nanosecond MOPA system based on short phosphate-fiber amplifier.

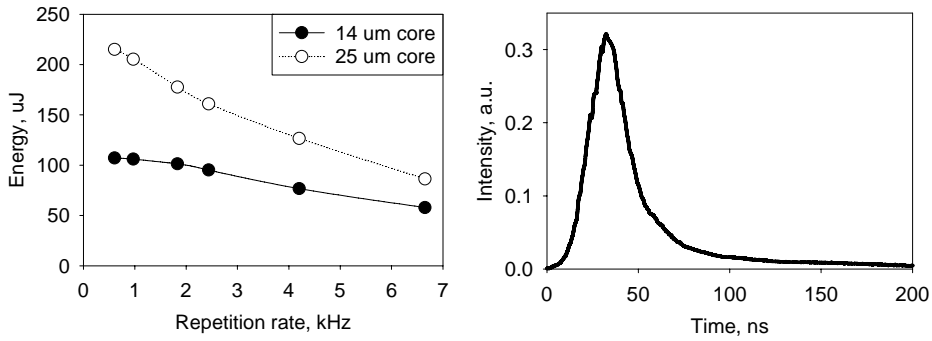


Figure 30. Left: Pulse energy versus pulse repetition rate, for two 15cm-long fiber phosphate-fiber amplifiers with different core sizes. Right: Temporal trace of the 20ns pulse with 215µJ pulse energy.

The excellent beam quality from the multimode-fiber amplifier indicates a potential for further energy scaling with the core size without sacrificing the beam quality performance. Using short fiber amplifiers based on heavily-doped phosphate fibers will be instrumental in mitigating the detrimental nonlinear effects in high-energy pulsed fiber-laser sources including fiber-based ultrafast CPA systems. Our preliminary demonstration is an important milestone towards this goal.

5.4. Phase Locking in Monolithic Multicore Fiber Laser

The flexibility of microstructured fiber fabrication enables another approach to improve fiber laser performances, namely incorporating several active cores into the same cladding. Figure 4 shows several examples of multicore fiber (MOF) fabricated at the College of Optical Sciences, The University of Arizona. To study the feasibility intrafiber coherent beam combining we made fibers containing up to 36 active cores.

Utilizing fibers with multiple active cores, we demonstrated a novel monolithic all fiber scheme to coherently combine the emission from all active cores into a single high power laser beam. This approach can provide a convenient and promising power-scaling solution to compact high-power fiber laser devices. By splitting the gain medium into discrete positions inside the cladding, instead of concentrating all active ions into an oversized core, optical damage and thermal management problems of high power single core lasers can be solved. It is therefore a complementary approach to large core fibers that can bring specific advantages while pushing the limits of achievable active core area which remains

the crucial factor in determining both the efficiency of multimode pump light absorption and the maximum output power per unit of fiber length.

There is a central challenge to effectively obtain high-brightness output beams from MCF, an essential feature to make this design advantageous compared with conventional single-core fiber. Usually, in a MCF with a 2-D isometric array, if each core is single-mode and neighboring cores are optically coupled, the MCF supports a number of non-degenerated supermodes that is equal to the number of cores. Among all supermodes, only the in-phase mode (all cores emit in phase) has the preferential far-field intensity distribution (Gaussian-like).

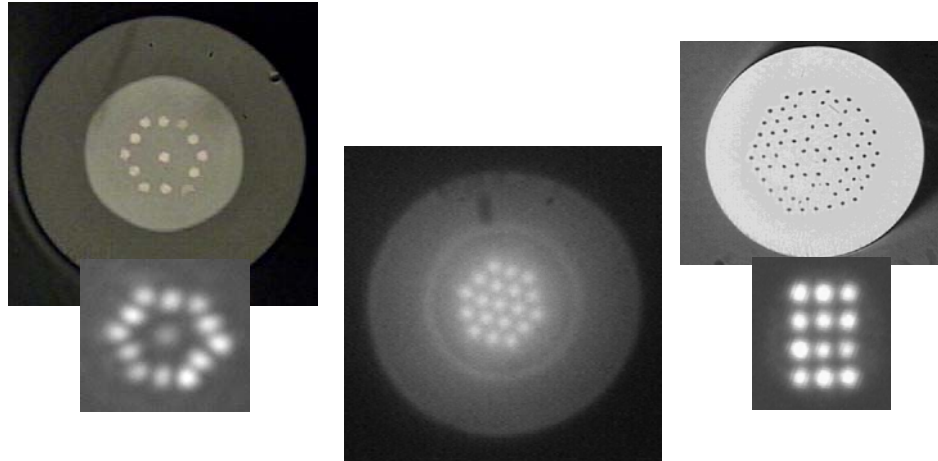


Fig. 9. Selected multi-core phosphate fibers made at the College of Optical Sciences and their near field emission patterns.

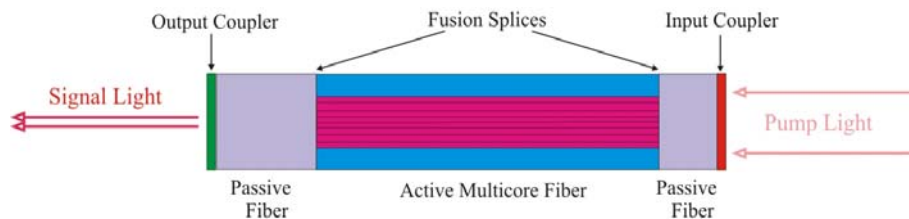
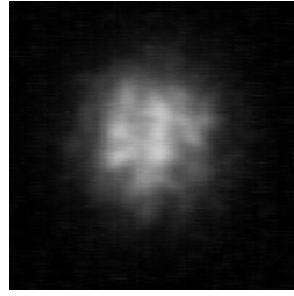
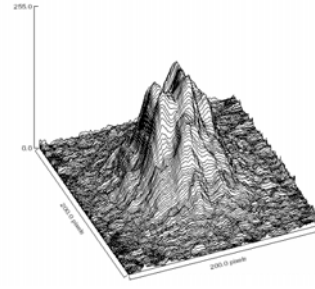


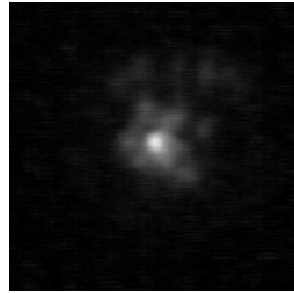
Fig. 10. Illustration of the multicore fiber laser device: both ends of the multicore fiber are spliced to passive fibers that are coated with dielectric mirrors (length not to scale).



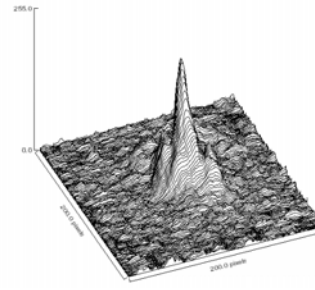
(a)



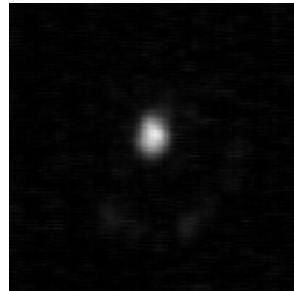
(b)



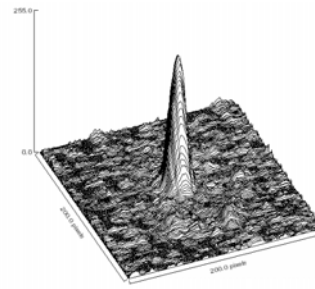
(c)



(d)



(e)



(f)

Fig. 11. Far-field intensity distributions of MC19 laser emissions: bare MC19 (a,b); one end spliced with passive fiber (c,d); both ends spliced with passive fibers (e,f). Pictures (b), (d) and (f) are 3-D views of (a), (c) and (e), respectively. All photos are taken at ~ 200 mW of output power.

To solve this problem and selectively establish the in-phase mode oscillation the laser resonator needs to be especially designed. Several coherent beam combining techniques currently exist to phase lock multiple emitters in fibers, including Talbot-cavity, structured mirror, collimating lens with high reflector and self-Fourier transform resonator. All these approaches involve free-space optics, i.e., air spacing and bulk optics, as part of the laser cavity. The inclusion of free-space optics not only increases the device size and alignment complexity substantially, but also decreases the laser efficiency owing to the additional cavity losses. More importantly, it also causes serious stability problems during high power laser operation because of its susceptibility to environmental and thermal disturbances accompanied with increased power level. To take full advantage of fiber laser device characteristics, i.e., the compact size as well as the robustness against external disturbances, the phase locking operation should ideally take place inside a confined waveguide. We notice that while there have been all-fiber approaches preferring out-of-

phase supermode lasing with ring-distributed MCFs and in-phase supermode amplification (seeded by a pulsed Gaussian beam) with isometric-distributed MCFs, there are lack of reports on in-phase mode oscillation through monolithic fiber device.

Within this project we developed and experimentally demonstrated an all-fiber approach that effectively selects the fundamental in-phase supermode of MCF lasers. By combining Talbot and diffraction effects, we show that the preferable supermode can be selected by dual pieces of passive optical fibers, of appropriate lengths, fusion spliced to both ends of a piece of active MCF (Fig. 10).

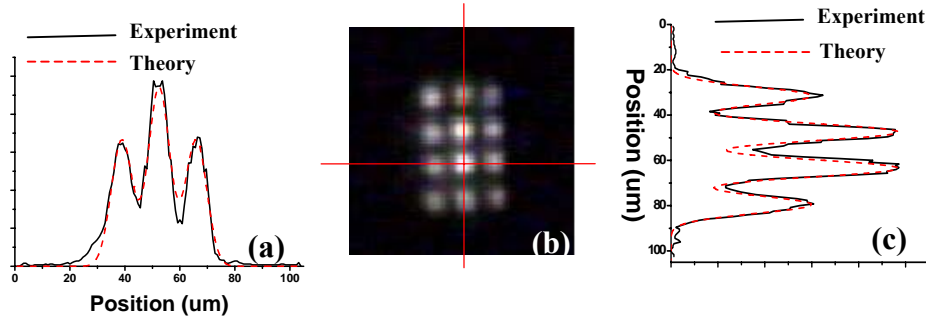


Fig. 12. Near-field distribution of the phase-locked 12-core microstructured Er/Yb co-doped phosphate fiber laser. (a) Profile along the x direction, (b) near-field image, (c) profile along the y direction.

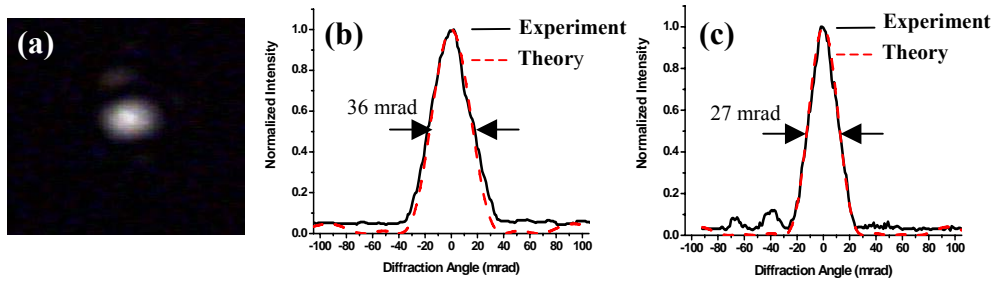


Fig. 13. Far-field intensity distribution of the phase-locked 12 core microstructured Er/Yb co-doped phosphate fiber laser. (a) Far-field pattern. (b) diffraction profile along x

Based on a 19-core MCF, such an all-fiber device has been fabricated and the laser emission properties have been studied. As demonstrated in Fig. 11 the phase-locked laser emission has been observed as a clean high-brightness on-axis spot in the far field, which is in sharp contrast to the messy pattern observed from the same MCF laser without mode selecting measures. All components of this phase-locked fiber laser can be incorporated into a single piece of fiber and the whole system is alignment-free during operation. This all-fiber design is robust against environmental and thermal disturbances at all power levels and can be conveniently integrated into compact photonics systems.

Furthermore, we demonstrated that similar all-fiber resonators can be applied to a large variety of multicore arrangements, including the 12 core fiber shown on the right in figure 9. Figure 12 and 13 show almost perfect agreement between experiment and theory for the near and far field characteristics of the 12 core fiber laser operating exclusively in the fundamental supermode. This core arrangement is special in so far that we succeeded, for the first time, to measure birefringent in-phase operation of a phase-locked multicore fiber laser. The in-phase operation of our 12-core rectangular-array microstructured fiber laser was confirmed by the near-field distribution, the far-field diffraction pattern, and the optical spectrum. The birefringence of the fundamental supermode in propagation constant $\Delta\gamma$ was measured as $\sim 4 \times 10^{-6} 1/\mu\text{m}$ from the beating of the two polarization modes shown in the RF spectrum in figure 14. The

break of the polarization degeneracy indicates the possibility of single polarization operation of phase-locked multicore fiber lasers and amplifiers.

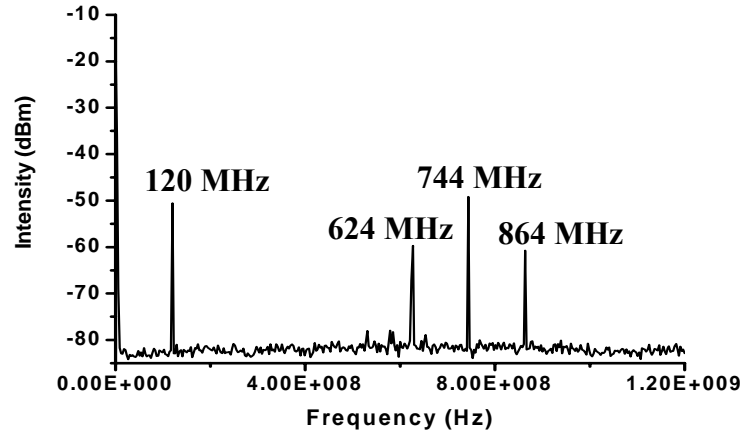


Figure 14 RF spectrum of the self-beat signal showing two non-degenerated, polarized in-phase supermodes emitted by the 12-core microstructured Er/Yb phosphate fiber laser.

5.5. UV-Written Bragg Gratings in Phosphate Glass Fiber

One of the major difficulties in building our ultra compact, Watt-level single frequency lasers is the fact that in these devices fiber Bragg gratings (FBGs) written in silica fibers are being used for selecting wavelength and narrowing the emission bandwidth while the gain fiber is made from phosphate glass. The combination of different glasses within one device constitutes a significant challenge, in particular since the thermal properties of phosphate and silica glasses are quite different - typical fiber drawing temperatures for phosphate and silica fibers are ~ 800 °C and ~ 2000 °C, respectively. Considering this difference, the fabrication of splices between phosphate and silica fibers exhibiting low optical loss and reasonable mechanical strength requires special techniques. In addition there is a large difference in the coefficients of linear thermal expansion for phosphate and silica glasses that are typically $\sim 100 \times 10^{-7}/^{\circ}\text{C}$ and $\sim 5 \times 10^{-7}/^{\circ}\text{C}$, respectively. This induces thermal stress at splicing joints that can also modify the index distribution of spliced fibers and lower the mechanical strength of the splices.

The main reason for the necessity of hybrid phosphate-silicate laser devices is the lack of photosensitivity of phosphate glasses that has prohibited direct writing of gratings into phosphate glass fibers. To solve this problem we fabricated a series of Ge-doped phosphate glasses and examined the photosensitivity of to 244 nm cw light from a frequency doubled Ar^+ ion laser. The glass samples were made by conventional melt and quench in air using high purity chemicals. Writing gratings into these glasses through a phase mask and analyzing the grating diffraction we studied the UV-induced index changes created in these phosphate glasses. As shown in figure 15 we observed index changes of up to $\sim 3.5 \times 10^{-5}$ in a glass doped with 30wt% GeO_2 (Ge30) indicating that this glass is suitable for the fabrication of UV written FBGs.

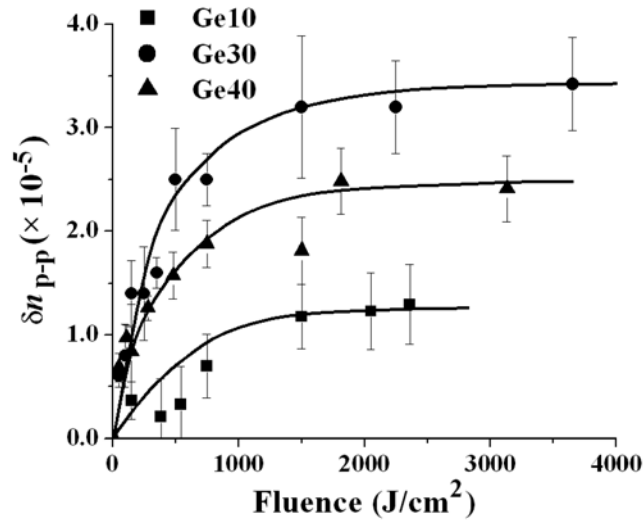


Fig. 15. Index modulation (δn_{p-p}) of Ge-doped phosphate glass as a function of fluence. Each data point represents several measurements of the diffraction from different 244 nm written gratings. Lines are drawn to guide the eye and the error bars show the standard deviation.

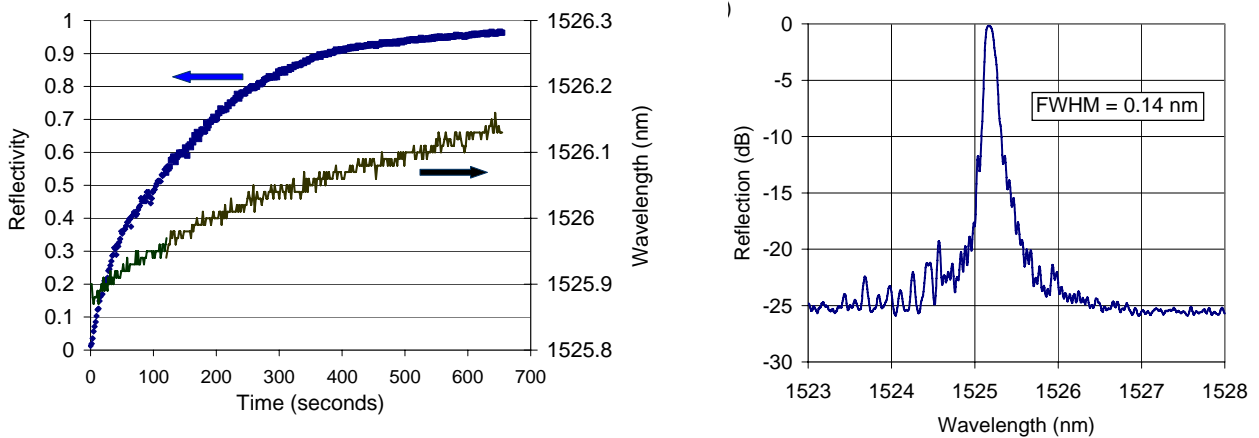


Figure 16 (a) Reflectivity and Bragg wavelength evolution during fabrication of a 14 mm long grating with 10 193 nm pulses per second and $200 \text{ mJ/cm}^2/\text{pulse}$. (b) Final reflection spectrum of FBG 1 ($R_{\text{max}}=96\%$).

5.6 Tapered fiber bundles for combining pump lasers used in fiber lasers/amplifiers

Multi-mode (MM) fiber bundles as well as tapered fiber bundles have found application as combiners of high-power laser diodes and laser-diode arrays. These bundles are ideal for pumping of solid-state lasers and cladding-pumped fibers due to their efficiency, ease of fabrication, and reliability. It has also been demonstrated that these bundles can accommodate at their core a single-mode fiber for applications involving the pumping of single-mode (active) fibers. A major drawback of bundled fibers is their relatively low brightness. For example, the radiance of a broad-stripe semiconductor emitter coupled to a multimode step index fiber with a $100\mu\text{m}$ -diameter core and 0.22 numerical aperture (NA) is about

30 times lower than the radiance of the laser diode itself. Improving the coupling efficiency and brightness of MM fiber couplers/combiners is thus highly desirable.

It must be recognized in such applications that the MM fiber is generally operated under restricted mode launch condition, that is, only a small fraction of the fiber's modal capacity is generally utilized. However, many coupler designs have traditionally required étendue invariance, namely,

$$[\sum_{i=1}^n A_i (NA_i)^2]_{in} = A_{out} NA_{out}^2. \quad (1)$$

Here NA is the numerical aperture and A the cross-sectional area of input and output fibers. This is a necessary condition for maintaining low-loss transmission under the over-filled mode launch condition, where the modal content of the input source(s) is greater than or equal to the modal capacity of individual fibers. (Transmission properties of tapered MM optical-fibers have been investigated, using ray-trace simulations, for a Lambertian source, which is a case of over-filled mode launch conditions.) To the best of our knowledge, no data has been published on the throughput of tapered MM fibers and fiber bundles under restricted-mode launch conditions.

In this report we explore different beam combining strategies based on tapered fiber bundles, aiming to increase the brightness of pump sources for double-clad fiber lasers and amplifiers. We consider single-stage $N \times 1$ combiners using tapering and fusing of a conventional multi-mode (MM) fiber bundle as well as multi-stage cascades of such $N \times 1$ combiners. Our approach to brightness enhancement does not contradict the so-called radiance theorem, because the laser diode sources used in conjunction with our scheme operate in a restricted-mode condition, whereby they occupy only a fraction of the input fiber's modal capacity. We present throughput measurements of step-index MM fibers of differing taper ratios under (low-order) restricted-mode launch conditions. The results are compared with throughputs of the same (tapered) fibers under conditions that approach over-filled mode launch conditions, where high-order spatial modes dominate the modal content of the input light source.

Experimental conditions. Tapered fibers were fabricated using a modified pipette puller (*Narishige Scientific Instruments PD-5* stage) that employs an oxygen-hydrogen torch as a heater, a gravitational force mechanism, CCD camera, microscope, and a side illuminator. Although the puller allows tapers with a maximum length of 32 mm, the most reproducible tapers were found to be in the range of 10-16 mm.

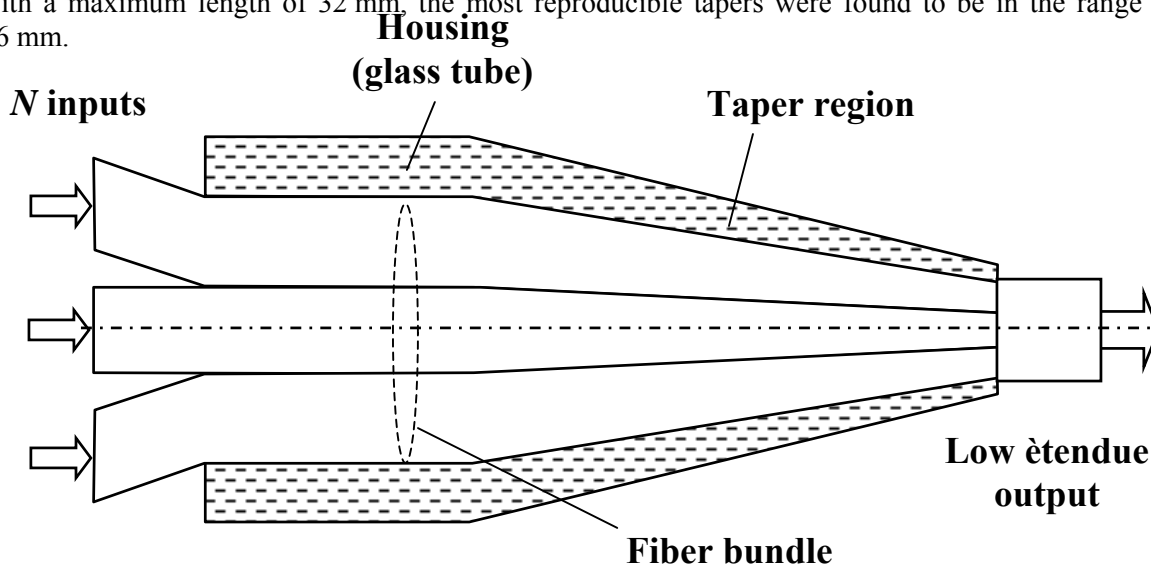


Figure 1. Diagram of an $N \times 1$ combiner, fabricated by fusing and tapering a fiber bundle. The beams of N laser diodes (either separate diodes or diodes from an array) enter from the left-hand side. The combined high-brightness beam emerges from the right.

A standard *Thorlabs* multi-mode fiber (AFS 105/125Y, 105 μm fused silica core, 125 μm fluorine-doped cladding, NA = 0.22) was the “raw material” in our experiments. With reference to Fig. 1, a fiber bundle consisting of 3, 4, 7, or 19 MM fibers was put through a quartz tube (*Polymicro Technologies, LLC*), then fused together by inertially collapsing the tube softened by the torch. (The quartz tubes had different diameters to accommodate the desired number of fibers in each bundle.) In the first stage of preparation only tight bundling was achieved. The taper was then pulled with simultaneous waist control while visually inspecting the taper through the microscope. The pulling stopped when the tapered end of the bundle matched the diameter of a standard MM fiber with reasonable tolerances. The fiber bundle was then cleaved at the tapered end.

Figure 2 shows cross-sectional photographs of typical tapered bundles thus obtained. The fused, tapered, and cleaved bundle was subsequently fusion-spliced to a length of standard MM fiber; see Fig. 3. All tapers were adiabatic, and the taper ratio $R = D'/D$, which is the ratio of the fiber diameter D' at the end of the taper to the original fiber diameter, $D = 125\mu\text{m}$, ranged from slightly below 0.2 to just under 0.5. This range allows the fabrication of a number of fused and tapered fiber bundles [each bundle containing three ($R = 0.49$), four ($R = 0.42$), seven ($R = 0.317$) or nineteen ($R = 0.193$) fibers] that matched the $\sim 105\mu\text{m}$ core diameter of a standard MM fiber. Since our fabrication method yields a nearly constant taper angle of $\Omega \sim 0.35^\circ$, different R values were achieved by varying the length of the taper.

Three light sources were used in our experiments; these were fiber-coupled semiconductor laser diodes ($\lambda = 980\text{ nm}$) exhibiting different angular distributions of their emissions. Source 1 was a single-mode laser diode with a (single-mode) 0.11NA fiber pigtail. The pigtail was fusion spliced to a 1 meter long piece of standard MM fiber (AFS105/125Y). The Gaussian-like far field pattern of this source had a full-width divergence angle of $\sim 12.6^\circ$. Source 2 utilized a *SpectraPhysics* BJ 234 laser diode (multi-mode), collimated to better than 1° in its fast axis with a short length of optical fiber (acting as a cylindrical lens), and butt-coupled to a standard MM fiber. Like Source 1, the far field distribution of this source was Gaussian-like, with a full-width diameter of $\sim 12.6^\circ$. The third light source, also based on a BJ 234 multi-mode laser diode, was prism-coupled into a double-clad silica glass fiber through a polished and flattened window on one side of the fiber; this fiber was then spliced into a 1 m-long MM fiber. Source 3 exhibits a donut-shaped far field pattern with a full-width diameter of $\sim 25^\circ$. Our restricted-mode launches were conducted with either Source 1 or 2. As will be seen below, the output of Source 3 approaches that of a source which satisfies over-filled mode launch conditions.

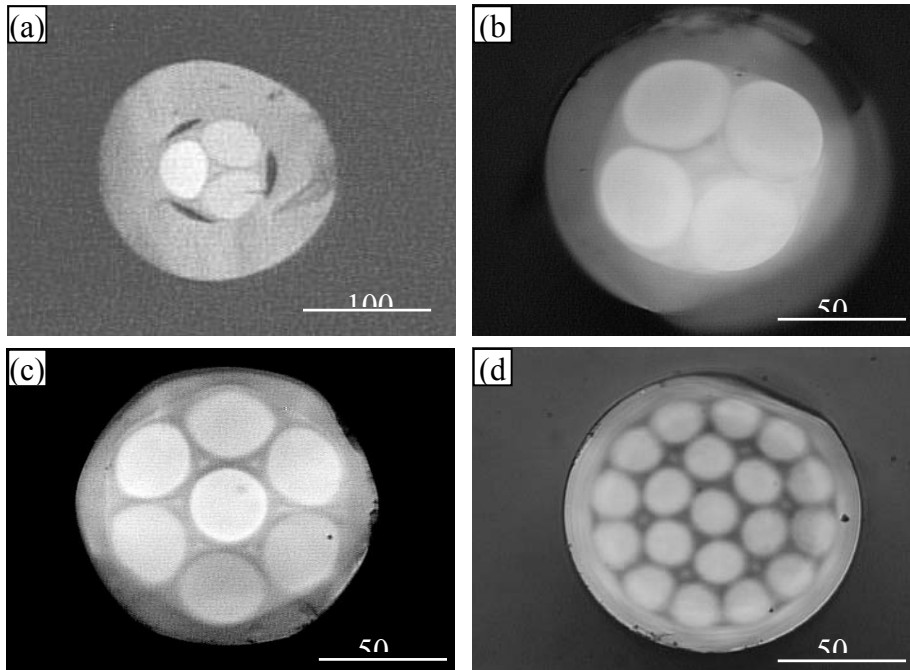


Figure 2. Cross-sectional photographs of fused, tapered, and cleaved MM fiber bundles. (a) 3×1 combiner; (b) 4×1 combiner; (c) 7×1 combiner, (d) 19×1 combiner. Note that the empty spaces between adjacent fibers have been filled. The different gray levels of individual fibers within the bundle are caused by random illumination of their opposite ends.

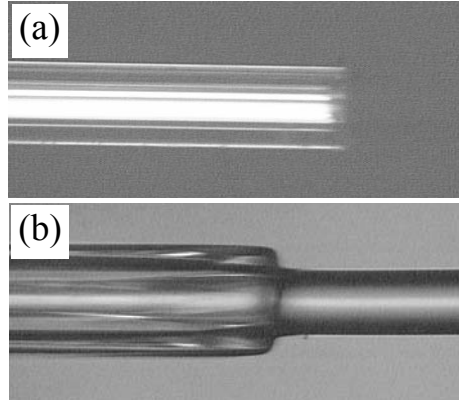


Figure 3. (a) Side view of the tapered end of the fused, tapered, and cleaved 4×1 MM fiber bundle of Fig. 2(b). (b) The cleaved facet of the tapered bundle in (a) is shown fusion-spliced to a MM fiber.

Beam-combiner characteristics. To study the feasibility of beam combining via fused and tapered MM fibers, we prepared several $N \times 1$ combiners – shown in Fig. 2 – and measured their transmission efficiency η_T . For maximum efficiency only adiabatic tapers were used. Our 3×1 combiner, connected to either Source 1 or 2, showed an efficiency $\eta_T \sim 83\%$ per input, thus confirming the feasibility of combining several high-power laser diode beams into a bright spot of $\sim 100\mu\text{m}$ diameter. Inter-channel differences of only 1-2% indicate the high quality of these combiners. The transmission efficiency of our 19×1 combiners, again measured with Sources 1 and 2, was $\eta_T \sim 30\%$ (per input). With 3.0W laser diodes placed at its 19 input terminals, for example, we expect a total optical power of $\sim 17.0\text{W}$ at the output facet (diameter $\sim 100\mu\text{m}$) of this combiner.

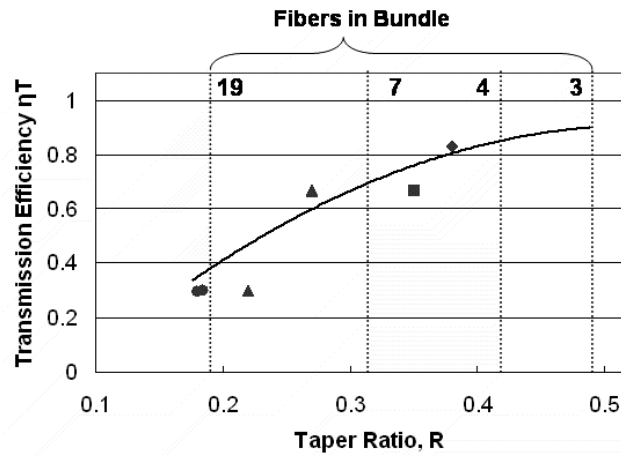


Figure 4. Transmission efficiency η_T versus taper ratio R for several $N \times 1$ combiners. (●) $N = 19$; (▲) $N = 7$; (■) $N = 4$. Some of the bundles were over-pulled, resulting in a leftward shift of the corresponding data point on this plot.

Figure 4 shows the measured transmission efficiency (per input) as function of the taper ratio R for several fabricated combiners. In the case of the 19×1 combiners (●) the taper ratio was about right,

but the two 7×1 combiners (\blacktriangle) and the 4×1 combiner (\blacksquare) were over-pulled, resulting in a smaller bundle (at the tapered end) than the core of the standard MM fiber. Despite this over-pulling, the measured efficiencies, when plotted against the taper ratio R , are seen to exhibit the expected behavior indicated by the solid curve (see the following sections for an explanation of the solid curve, which is the same as the upper curve of Fig. 8).

Cascaded tapered fibers. We devised a simple method of analyzing the performance of $N \times 1$ combiners and cascades of such combiners. With reference to Fig. 5, we fabricated several nearly identical tapered fibers having the same taper ratio R , then measured the transmission efficiency η_T of a chain of such fibers in which each tapered fiber was fusion-spliced to the next fiber at the center of its entrance facet (i.e., the unaltered facet). All tapers were adiabatic, with the taper ratio R covering the range corresponding to combiners with 3, 4, 7, or 19 fibers in a bundle. To ensure that the results were not unduly influenced by propagation inside the cladding, we passed a loop of the output fiber through index-matching fluid before measuring its output at the photo detector.

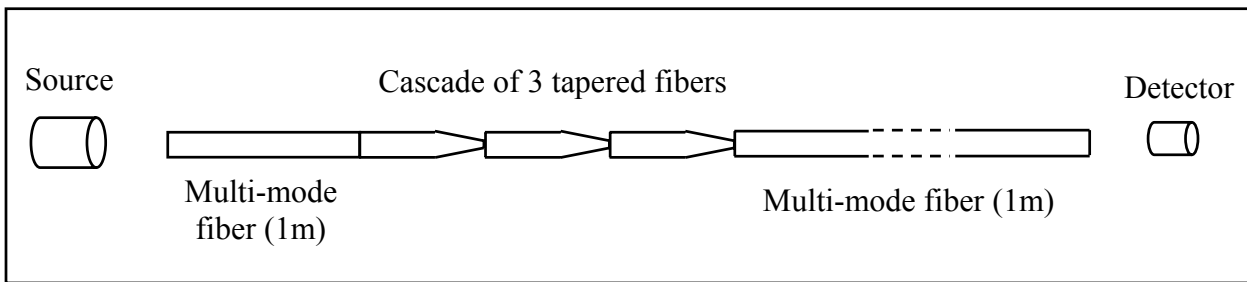


Figure 5. Cascade of tapered fibers, all having the same taper ratio R , fusion spliced to each other and to 1 meter-long pieces of the standard MM fiber on the input and output sides. The light beam is launched into the 1 meter-long input fiber. At the output side, a loop of the 1 meter-long fiber is passed through index-matching fluid to remove any light that might be coupled into its cladding. The transmitted light is measured by the photo detector at the end of the output fiber. Although three tapered fibers are shown cascaded in this figure, the actual number in our experiments could be anywhere from one to four.

Figure 6 shows cascade efficiencies for chains of 1, 2, 3, and 4 fibers (all having the same taper ratio $R = 0.26$), measured with Source 1. Although there is loss at every stage, the first stage's loss is relatively small. The large efficiency, $\eta_T = 47\%$, obtained in the first stage of this cascade is due to the fact that the input beam has a limited modal content. After passing through the first tapered fiber, the beam divergence increases, causing the efficiency of transmission through the second stage to drop to $\sim 18\%$. The rise in the modal content continues with passage through successive stages, resulting in $\eta_T = 13\%$ for the third stage and $\eta_T = 8\%$ for the fourth stage. For this last stage of the cascade, the input beam has approached a more or less Lambertian source, which leads to the correspondingly low transmission efficiency. Any brightness enhancement, therefore, must occur in the earlier stages.

For the above measurements to be relevant to our fused and tapered bundles, we must demonstrate that shifting the tapered (output) end of one fiber over the entrance facet of the succeeding fiber (as occurs for all but the central fiber in a cascaded bundle) does not seriously affect the throughput of the cascade pair. To this end, Fig. 7 shows the results of an experiment in which the tapered end of one fiber ($R = 0.23$) was scanned across the entrance facet of an adjacent fiber. The two sets of measurements in Fig. 7 show the effect of core offset in the case of a tapered fiber displaced from the center of an output fiber (configuration A), and, in the case of a two-fiber cascade (configuration B), the effect of the first fiber's core offset from the center of the second fiber. Accordingly, the coupling efficiency is seen to be fairly independent of the core offset, as long as the tapered fiber's core remains within the core area of the fiber that follows. In configuration A, the slight enhancement of efficiency near the edge of the fiber (i.e.,

when the tapered fiber's displacement from the center of the MM fiber is $\sim \pm 40\mu\text{m}$) is not presently understood.

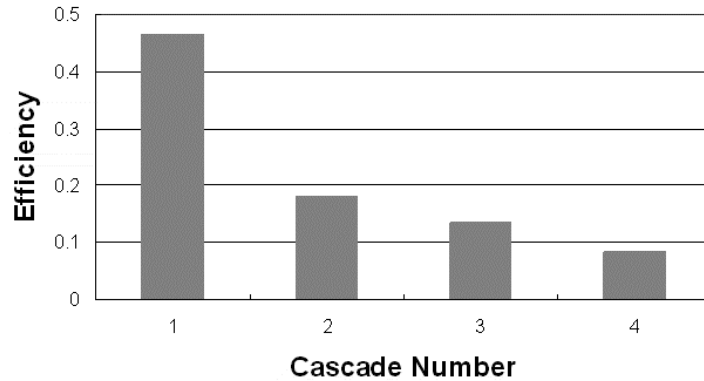


Figure 6. Transmission efficiencies in a cascade of four tapered fibers. The taper ratio for all four fibers is $R = 0.26$. The light source is a single-mode laser coupled to a 1 meter-long MM fiber (Source 1). The transmission efficiency of the first stage is $\eta_T \sim 47\%$; the remaining stages show progressively smaller efficiencies.

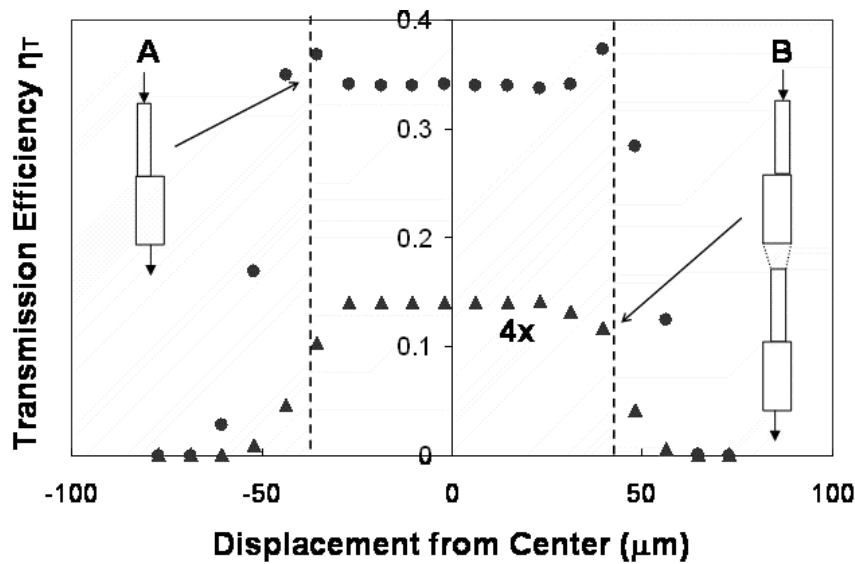


Figure 7. Effect of core offset between the tapered end of one fiber and the untapered entrance facet of the next fiber in the cascade. In configuration A the transmission efficiency η_T is measured for a single taper, offset from the center of the 1 meter-long output fiber, as a function of the displacement between the two cores. In configuration B, efficiency is measured for a cascade of two tapered fibers as a function of the core displacement of the first tapered fiber relative to the center of the second. In both cases the taper ratio was $R = 0.23$. The second curve is magnified by a factor of 4 to aid better visualization.

Fused and tapered $N \times 1$ combiners under restricted (low-order) mode launch condition. To predict the coupling efficiency of $N \times 1$ combiners we thus measured the efficiency η_T for several values of the taper ratio R in the system of Fig. 5 (using a single tapered fiber between the 1 meter-long fibers); the results obtained appear in Fig. 8. The behavior of η_T versus R is seen to be nearly the same for Sources 1 (\blacktriangle) and 2 (\blacksquare), but substantially different for Source 3 (\bullet), indicating that the source's angular spectrum (which is related to its spatial coherence) is of importance in this regard. The numbers at the top of the figure indicate the number of fibers that can be combined in a fused and tapered bundle for a given value

of R . Thus, under the restricted-mode launch conditions, it should be possible to combine the beams of several high-power, multi-mode lasers into one bright spot. A 19×1 combiner of this type, for example, should yield the equivalent power of six lasers at its output facet in an approximately $100\mu\text{m}$ -diameter spot. We thus predict that low-divergence sources (e.g., $\text{NA} \leq 0.075$), when launched into a fused and tapered MM fiber combiner, will result in ~ 8 dB increase in irradiance for a 19×1 combiner. (Note that the output étendue is $1/19$ that of the input bundle). In contrast, the radiance theorem predicts that over-filled mode launch condition will result in no such brightness enhancement.

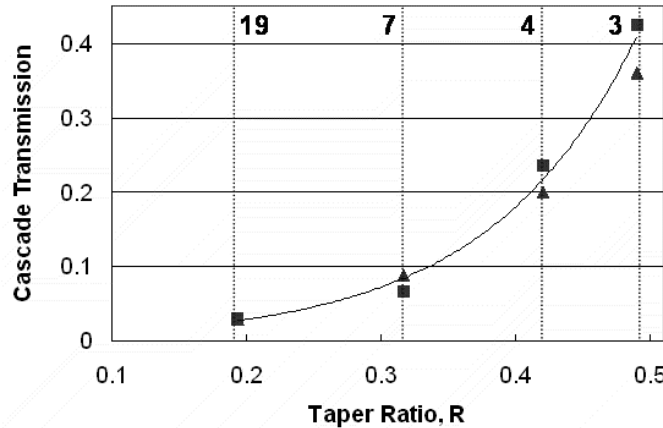


Figure 8. Measured values of η_T versus the taper ratio R for a single tapered fiber in the system of Fig. 5. Light sources 1 (▲) and 2 (■) yield nearly identical patterns of behavior. The measured efficiency for Source 3 (●) is substantially below that of the other sources. Shown at the top of the figure is the number of tapered fibers that can be bundled and fused together to create an output beam equal in diameter to that of a single, standard MM fiber.

High-order mode launch condition. Figure 8 also shows a plot of the measured transmission efficiency η_T of a single fiber versus the taper ratio R , when Source 3 is used to provide the input beam in the system of Fig. 5 (again, with a single tapered fiber between the 1 meter-long fibers). The high-spatial-mode content of the light source in this instance results in a substantial reduction of η_T over that achieved under restricted-mode launch conditions. For instance, at $R = 0.193$ (corresponding to a 19×1 fused and tapered combiner) the measured value of $\eta_T \sim 0.06$ per laser indicates the absence of any meaningful brightness enhancement in the combined beam. This limitation, typical of over-filled mode-launch condition, follows from the radiance theorem and the principle of conservation of energy.

Multi-stage beam combining using a cascade of $N \times 1$ fused and tapered bundles. To extend the preceding results obtained under restricted-mode launch conditions to a cascade of $N \times 1$ combiners, we measured the transmission efficiency η_T versus taper ratio R for a string of two tapered MM fibers in the fusion-spliced chain of Fig. 5; the results obtained with Sources 1(▲) and 2 (■) are shown in Fig. 9. These results indicate that essentially all the gain in brightness is obtained in the first stage of the cascade combiner, with the second stage acting primarily in the high-order mode launch condition. Consequently, not much brightness enhancement should be expected from the second stage of the cascade configuration.

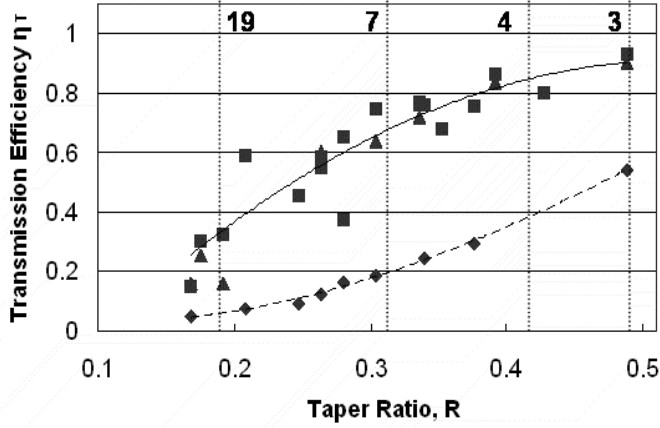


Figure 9. Overall transmission efficiency versus taper ratio R for a cascade of two tapered fibers in the fusion-spliced chain of Fig. 5. Shown at the top of the figure is the number N of fused and tapered fibers that can be bundled together to create the $N \times 1$ combiners needed in a cascade configuration such as that shown in Fig. 10.

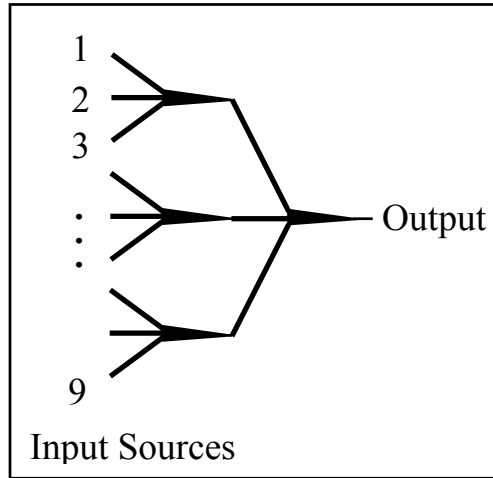


Figure 10. Two-stage 9×1 combiner, composed of four identical 3×1 combiners.

Transmission measurements on a fusion-spliced cascade of two identical 3×1 combiners (depicted schematically in Fig. 10) showed a 22% total efficiency, namely, from each source to the output of the second stage. Although a value of $R \sim 0.5$ is generally sufficient for 3×1 combiners, the particular combiners used in this experiment were over-pulled, resulting in a reduced taper ratio of $R \sim 0.4$. The measured value of $\eta_T = 0.22$ is thus in agreement with the results depicted in Fig. 9. This means that placing nine identical lasers at the input ports of the system of Fig. 10 yields a combined output power equal to that of two lasers ($9 \times 0.22 \sim 2$). Although this particular two-stage cascade of 3×1 combiners has poor efficiency, according to the data in Fig 9, one should be able to build a two-stage cascade of 3×1 combiners (using $R \sim 0.5$ tapers) with an efficiency of $\sim 40\%$ per laser. Combination of nine identical lasers with such a device should then yield, at the output terminal, the equivalent power of 3.6 lasers.

Conclusion. We have demonstrated that beam combining with fused and tapered fiber bundles results in brightness increase under restricted-mode launch conditions (mode-filling parameter ~ 0.285) for 3×1 , 4×1 , 7×1 , and 19×1 combiners. The measured values of the coupling efficiency varied about 1-2% among the various fibers in each bundle, thus confirming the high quality of the fabricated devices. To analyze the performance of $N \times 1$ combiners and cascades of such combiners, we devised a simple

method employing a concatenated chain of tapered fibers in which every tapered fiber was fusion-spliced to the next fiber's unaltered facet. Good agreement between the tapered bundle efficiency estimates obtained by this method and the actual (fabricated) combiner efficiencies confirmed the validity of our approach.

For cascaded tapers with a shifted core geometry, a slight efficiency enhancement near the edge of the fiber was observed. This effect is not presently understood and requires more experimental efforts. For cascades of tapered fiber bundles, we achieved brightness enhancement only in the early stages of the cascade. We focused mainly on the dependence of the coupling efficiency on the mode-filling properties of the source. This enabled us to develop practical combiners in the form of fused and tapered fiber bundles and cascades of such bundles. Further experiments with controlled degrees of mode-filling are left for future research. The dependence of the taper transmission efficiency on the modal content of the launched beam may be viewed from the opposite direction, namely, the degree of mode-filling in MM fibers can be estimated by measuring the corresponding taper transmissions. This also requires detailed taper efficiency measurements under varying mode launch conditions.

6. Technical Report: VECSEL Project

6.1 First Principles Quantum Design Approach for Semiconductor Epitaxial Growth

A critical underpinning for this aspect of the project was the development of a comprehensive theoretical understanding of the physics of light matter interaction with semiconductor material systems. Once this key breakthrough was made, we could move on to design optimized semiconductor QW active structures and fast track to an end laser device without going through costly, time-consuming and inefficient semiconductor wafer growth, packaging, testing and re-growth cycles. While such a predictive theory would impact all semiconductor amplifier and laser devices, the intrinsic complexity of design of VECSEL sub-cavities makes it indispensable. This section outlines the key breakthroughs made in our theoretical understanding of this phenomenon and discusses how this predictive approach impacted our own VECSEL program.

6.2 High-Power High-Brightness VECSELS

The extraction of high power with high beam quality from semiconductor lasers has long been a goal of semiconductor laser research. Optically pumped vertical-external-cavity surface-emitting lasers (VECSELS) have already shown the potential for their high power, high brightness operation. In addition, the external cavity arrangement in these lasers makes intracavity nonlinear frequency conversion quite convenient. High-power high-brightness VECSELS with wavelength flexibility further extends their application space.

One of the objectives of the project was to investigate high-power high-brightness VECSELS. High power high, brightness operation is a fundamental aspect of VECSEL applications. In this section, we focus on high power, high brightness operation of VECSELS, including the design of VECSEL wafers, the fabrication of the devices, characterization of the wafer and device, demonstration of high power high brightness VECSELS.

We use periodic stacks of compressively-strained InGaAs/GaAs quantum wells (resonant periodic gain RPG) as active region of the device. The active region is grown on an AlGaAs/AlAs high index contrast multilayer reflector that acts as a Bragg mirror. These are grown on a GaAs substrate and the VECSEL is designed and optimized to emit at 975-980 nm.

Two VECSEL structures operating around 975 nm were designed by above state-of-the-art modeling tool. They are referred to “single-well” resonant periodic gain structure (SW-RPG) and “double-well” resonant periodic gain structure (DW-RPG), respectively. Figure 1 shows the details of each design. In the single SW-RPG, each 8-nm-thick compressively strained InGaAs quantum well is aligned at the antinodes of the semiconductor sub-cavity standing wave. In the DW-RPG, the active region consists of nine double-wells, each comprised of two 4-nm compressively strained InGaAs quantum wells separated by a 6-nm-thick GaAsP strain compensating layer. Each double-well is aligned at an anti-node of the sub-cavity standing wave. Both structures are grown as bottom emitters on undoped GaAs substrate by MOCVD.

Compared with the design using the 8-nm-wide single-well RPG (SW-RPG) structure, this DW-RPG structure has several apparent advantages. For a given carrier density and temperature, the material gain for a 4-nm-wide quantum well is approximately twice the value that one gets for an 8-nm-wide quantum well. In fact, the thinner well results in a larger density of states for each sub-band and larger sub-band separation, thus a higher percentage of carriers occupies the lowest sub-band, leading to a large inversion ($1 - f_e - f_h$) and higher gain. Thus, the modal gain for a double-well with 4-nm-wide wells is larger than for a single-well with an 8-nm-wide well. Since the gain material of a double-well is spread out over a larger region (14 nm total), the geometry increases the tolerance to the growth variation and process control. This geometry can also compensate for any temperature gradient between various wells and the

heat sink, and thermally induced shift of the antinodes of the lasing modes. The relative confinement factor of a VECSEL with 4-nm-wide DW-RPG structure is more tolerant to the shift of the antinodes of the cavity standing wave than that of a VECSEL with 8-nm-wide SW-RPG structure. Furthermore, the DW-RPG configuration can support more quantum wells while maintaining a thinner active region, which can aid in more efficient heat dissipation. The above logic is based on the raw material gain itself. However, our ability to calculate rigorously the gain and recombination losses, led us to predict that the recombination losses offset the gain advantage and, in fact, the SW-RPG lasing threshold is approximately half of the DW-RPG VECSEL. This is confirmed in Figure 3 below, where the SQW threshold is lower.

Growth			Growth		
Repeats	Thickness [nm]	Material	Repeats	Thickness [nm]	Material
1	250	GaAs	1	250	GaAs
1	200	Al(0.85)Ga(0.15)As	1	200	Al(0.85)Ga(0.15)As
1	20	GaAs	1	20	GaAs
1	140 (75)	Al(0.98)Ga(0.02)As (Al(0.85)Ga(0.15)As)	1	140 (75)	Al(0.98)Ga(0.02)As (Al(0.85)Ga(0.15)As)
1	432.1	Al(0.3)Ga(0.7)As	1	432.1	Al(0.3)Ga(0.7)As
1	137.4 (136.0)	Al(0.06)Ga(0.94)As	1	117.7 (115.2)	Al(0.06)Ga(0.94)As
14	ML (~0.28nm) 8.0 ML 31.6 99.8 (100.2)	GaAs In(0.143)Ga(0.857)As GaAs GaAs(0.927)P(0.073) Al(0.06)Ga(0.94)As	9	18.6 ML (~0.28nm) 4.0 ML 6.0 ML 4.0 ML 18.6 86.7 (88.8)	GaAs(0.927)P(0.073) GaAs In(0.196)Ga(0.804)As GaAs GaAs(0.927)P(0.073) GaAs In(0.196)Ga(0.804)As GaAs GaAs(0.927)P(0.073) Al(0.06)Ga(0.94)As
1	8	Al(x)Ga(1-x)As Rampe	1	30.2 (23.1)	Al(0.06)Ga(0.94)As
1	65.1	AlAs	1	8	Al(x)Ga(1-x)As Rampe
25	16 56.3 16 65.1	Al(x)Ga(1-x)As Rampe Al(0.2)Ga(0.8)As Al(x)Ga(1-x)As Rampe AlAs	1	65.1	AlAs
1	8	Al(x)Ga(1-x)As Rampe	25	16 56.3 16 65.1	Al(x)Ga(1-x)As Rampe Al(0.2)Ga(0.8)As Al(x)Ga(1-x)As Rampe AlAs
1	10.0	GaAs	1	8	Al(x)Ga(1-x)As Rampe
			1	10.0	GaAs

Etch stop layers

Active region

DBR

(a)
(b)

FIGURE 1. Two VECSEL structures grown by MOCVD: (a) SW-RPG structure and (b) DW-RPG structure.

The fabrication of VECSEL structures is critical to laser performance. Since VECSELs are low gain lasers, the VECSEL should have high surface quality to minimize scattering/diffraction losses. Moreover efficient heat extraction from the active region is necessary to avoid thermal rollover. To achieve this goal, high thermal conductivity ($>18\text{Wcm}^{-1}\text{K}^{-1}$) chemical vapor deposition (CVD) diamond with high surface quality (peak to valley height $<100\text{ nm}$) is used as the submount/heat spreader. The fabrication process includes sample mounting and substrate removal. First, the epitaxial side of a $2\text{ mm} \times 2\text{ mm}$ VECSEL wafer and CVD diamond are metallized with titanium and gold. Since indium has highest thermal conductivity ($0.83\text{ Wcm}^{-1}\text{K}^{-1}$) and can reduce thermal stress at the semiconductor/submount interface, the wafer is mounted on CVD diamond by soft indium solder with flux. The substrate is first etched to a thickness of about $50\text{ }\mu\text{m}$ by a fast non-selective wet chemical etching using $\text{H}_2\text{SO}_4:\text{H}_2\text{O}:\text{H}_2\text{O}_2$ 1:1:8. The remaining GaAs substrate is subsequently removed by selective wet chemical etching using $50\%\text{C}_6\text{H}_8\text{O}_7:30\%\text{H}_2\text{O}_2$ 4:1. After the substrate removal, a diluted hydrofluoric acid is used to remove the AlGaAs etch-stop layer (5 % HF for $\text{Al}_{0.85}\text{Ga}_{0.15}\text{As}$ and 1.5 % HF for $\text{Al}_{0.98}\text{Ga}_{0.02}\text{As}$). After substrate removal the remaining semiconductor is only $6.5\text{ }\mu\text{m}$ thick, allowing efficient heat dissipation at high pumping energy. The surface quality of the VECSEL sample is then characterized by the interferometer, WYKO NT-2000, and a peak to valley height of less than 40 nm in an area of $0.5\text{ mm} \times 0.5\text{ mm}$ can be achieved. This optically smooth surface makes the scattering/diffraction loss negligible and results in high slope efficiency and high beam quality. After etching, a single layer Si_3N_4 low reflecting coating is deposited on the surface of chip.

Void-free solder bonding is very critical to the performance of VECSELs. Voids in the solder layer cause huge thermal impedance and poor heat dissipation during high power operation of the VECSEL. To investigate the solder bonding quality, we used focus ion etch technique to cut a processed VECSEL sample (GaAs substrate and etch-stop layers removed), and then took an SEM photograph of the cross section. In the focus ion etching processing, the focus ion beam removes all of material from the surface of the processed VECSEL chip to the surface of CVD diamond.

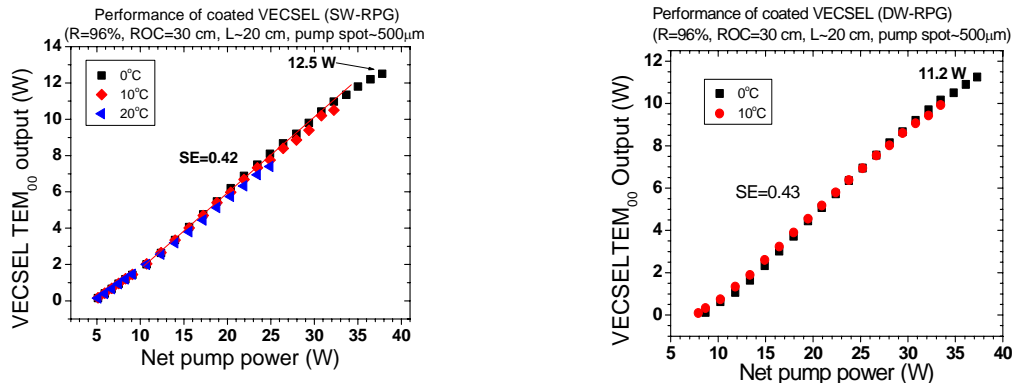
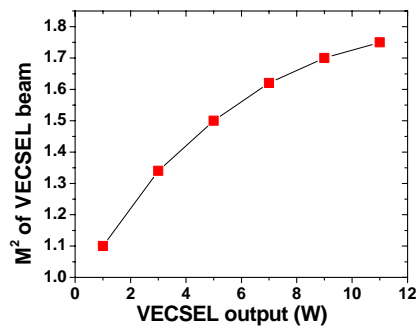


FIGURE 3. VECSEL TEM_{00} output vs. net pump power: SW-RPG VECSEL (left) and DW-RPG VECSEL (right).



$M^2=1.75$ and Ellipticity=1.02 at 11 W output

FIGURE 4. Beam quality of high-power optically pumped VECSEL (SW-RPG and DW-RPG)

The processed VECSEL sample is mounted on a copper heatsink whose temperature is controlled by a chiller. Between the CVD diamond submount and copper heatsink is a 50- μm -thick indium foil. The lasing experiment is conducted by using a fiber coupled multi-mode 808 nm diode laser pump source. The pump light from the fiber with 200 μm core fiber diameter and 0.22 numerical aperture (NA) is imaged onto the sample by a collimator and a condenser at an incident angle of $25^\circ\sim 30^\circ$. The focal length of the collimator is 18 mm. The pump spot size on the VECSEL chip, as estimated from the photoluminescence image, is adjusted by the focal lengths of the condenser. A single layer Si_3N_4 ($n=1.78$) quarter wave LR coating is deposited on the surface of VECSEL chip, which provides a reflectivity less than 1% at the signal wavelength and a reflectivity around 3% for oblique 808 nm pump light. The external cavity is formed using a concave mirror with certain radius of curvature and reflectivity. In the following measurement. The cavity parameters are: the reflectivity of output coupler $R=96\%$, the radius of curvature of the output coupler $\text{ROC}=30\text{ cm}$, cavity length $=21\text{ cm}$ and pump spot size = 500 μm diameter.

High power, high brightness operation of the VECSEL is demonstrated. Over 11 W and 12 W output power with high slope efficiency are demonstrated from the DW-RPG and SW-RPG VECSEL, respectively (see Figure 3). The M^2 factor slowly increases to 1.75 when the VECSEL output power reaches 11 W (see Figure 4).

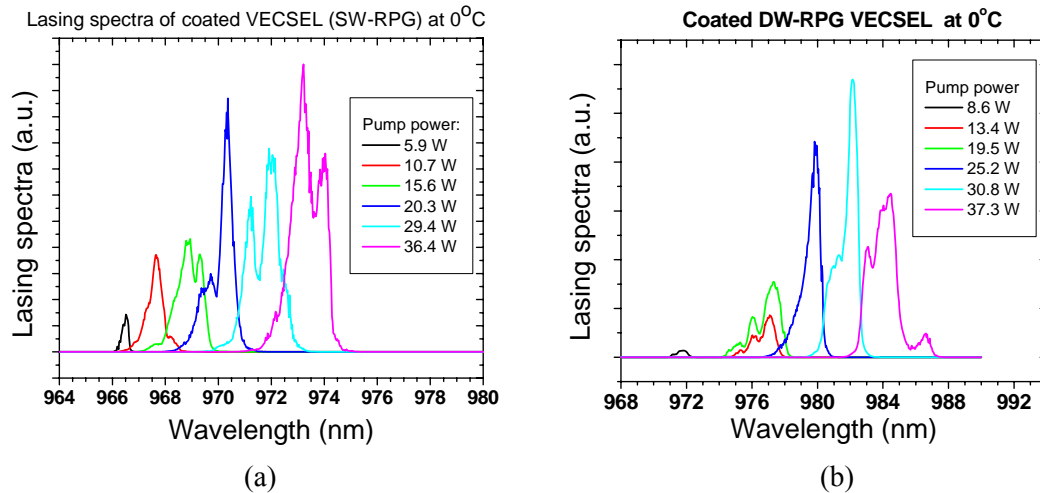


FIGURE 5. Lasing spectra of VECSEL at different pump power: (a) SW-RPG VECSEL and (b) SW-RPG VECSEL.

In summary, the quantum design and demonstration of a SW-RPG and DW-RPG VECSEL are presented. The on-wafer characterization shows the growth of SW-RPG is uniform and very close to the designed structure. After the fabrication of the VECSEL chip, a good indium solder bonding and a high surface quality of the chip are achieved. High power, high brightness operation of the VECSEL is demonstrated, with over 11 W and 12 W output power with high slope efficiency from DW-RPG and SW-RPG VECSEL, respectively. An M^2 factor of 1.75 is achieved when the VECSEL output power reaches 11 W.

A thermal-induced lasing wavelength red-shift and poor spectral impurity are evident in the lasing spectra. These are significant drawbacks of VECSEL's, potentially limited their applicability. A scheme and experimental demonstration to solve these problems is presented in the next section.

6.2. Tunable High-Power Linearly Polarized VECSELS with a Narrow Linewidth

Optically pumped VECSELS have demonstrated multi-Watt high power output and excellent beam quality. However, a thermally induced wavelength shift and broad spectral linewidth are drawbacks for applications where laser wavelength stability is required. Tunable high-power, high-brightness VECSELS would overcome these drawbacks and significantly enlarge the application space for VECSELS.

The challenges in developing tunable high-power VECSELS are (1) they are low-gain lasers and (2) microcavity resonance clamps the lasing wavelength of VECSELS. To achieve a wide tunability for the laser, the laser must have a broad accessible gain bandwidth. Since semiconductor gain media have a broad gain bandwidth, VECSELS have the potential to achieve a large wavelength tuning range. To tune the lasing wavelength, a spectral filter or wavelength-selective element has to be employed in the laser cavity. Since VECSELS exhibit low-gain, low loss filters that can be tuned over broad wavelength are suitable candidates. Birefringent filters were intensely studied several decades ago as devices to control the wavelength of dye lasers. In its simplest form, a birefringent filter is simply a waveplate inserted into the resonator at the Brewster's angle and acts as an extremely low loss wavelength-selective element for the laser. This is the reason why we choose the birefringent filter.

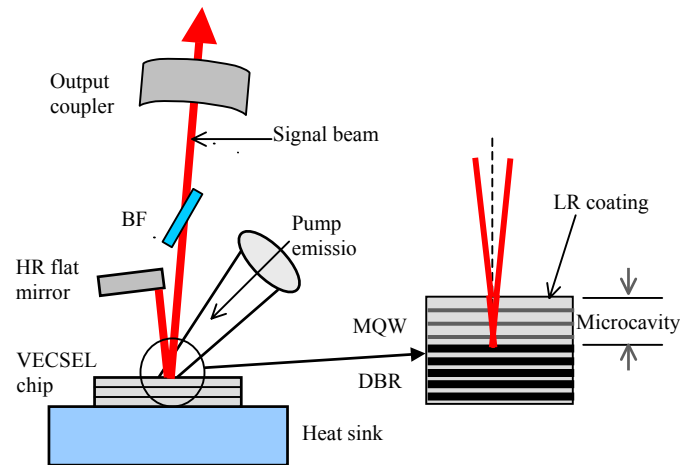


FIGURE 6. Schematic diagram of the tunable VECSEL with the V-shaped cavity and a BF.

To achieve a tunable high power VECSEL with a wide tuning range, we use a V-shaped cavity in conjunction with a birefringent filter (BF) shown in Figure 6. In this cavity, the VECSEL chip (active mirror) is placed at the fold, a high reflectivity ($R > 99.9\%$) flat mirror and a spherical output coupler on the two ends. Since the lasing eigenmode (signal beam) of the V-shaped cavity is incident on the VECSEL chip with a small incident angle, the propagation direction of the signal beam in the semiconductor microcavity, formed by DBR and semiconductor/air interface, is not perpendicular to the surface of the VECSEL chip and DBR mirror. As a result, the cavity eigenmode no longer experiences the microcavity resonance, which influences the lasing wavelength. In this way, the effect of microcavity resonance is completely eliminated. A birefringent filter is inserted in the V-shaped cavity to tune over the modal gain spectrum of the VECSEL to achieve wide tunability.

By “unfolding” the V-shaped cavity about the DBR mirror, we see that we may interpret the VECSEL chip as a tilted intra-cavity etalon within a linear cavity. However, in order to maintain the

antinodes of the cavity standing wave in the VECSEL chip at the quantum wells, the cavity angle between two arms of the cavity must be kept as small as possible. To eliminate walk-off losses in the etalon, a low reflectivity coating must be applied on the surface of the VECSEL chip. In a round trip, the cavity mode passes through the active region four times in the V-shaped cavity and two times in the linear cavity, thus the V-shaped cavity provides higher round trip gain for a given carrier density than the linear cavity. This higher round trip gain not only compensates walk-off losses and surface scattering loss, but also enlarges the tunability range.

To achieve tuning, the birefringent filter (BF) is inserted in one arm of the V-shaped cavity at Brewster's angle. The BF with this special orientation is equivalent to a waveplate sandwiched between two parallel polarizers. The transmission of the BF is given by $T = \cos^2(\Delta\phi/2)$, where $\Delta\phi = 2\pi(n_e - n_o)L_e/\lambda$, n_o and n_e are refractive indices for ordinary and extraordinary ray, λ is vacuum wavelength and L_e is the plate thickness along the beam direction within the plate. At $2\pi(n_e - n_o)L_e/\lambda = 2m\pi$ with $m = \text{integer}$, the transmission of the BF is equal to 1, and the laser signal beam at the wavelength λ in the cavity suffers no loss passing through the plate. Rotating the BF about its surface normal changes n_e , thus tunes the wavelength to the maximum transmission of the filter ($T=1$). Since the cavity mode no longer sees the microcavity, by rotating the BF, we can tune across the modal gain spectrum (proportional to $\Gamma_r(\lambda)g(\lambda)$), where $\Gamma_r(\lambda)$ is the relative confinement factor and $g(\lambda)$ is quantum well gain spectrum, and achieve a large continuous wavelength tuning range.

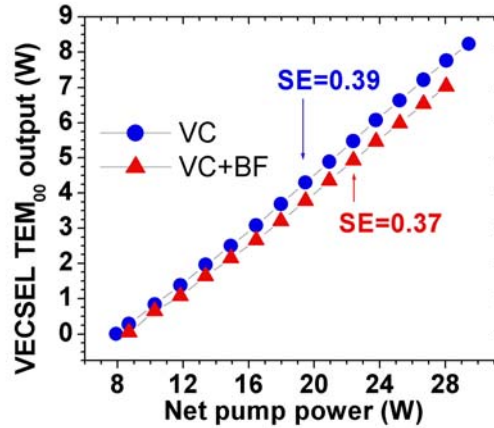


FIGURE 7. TEM₀₀ output power from the VECSEL with V-shaped cavity (VC) vs. net pump power (blue dot) and maximum TEM₀₀ output power from the VECSEL with V-shaped cavity and BF (VC+BF) vs. net pump power (red triangle).

Figure 7 shows the VECSEL TEM₀₀ output power at 10°C as a function of net pump power for two cases: V-shaped cavity (VC) and V-shaped cavity with birefringent filter (VCBF). Before the BF is inserted into the cavity, the slope efficiency is 0.39. After the BF is introduced into the cavity at the Brewster angle, the linearly polarized VECSEL is tuned to achieve the maximum TEM₀₀ output at each pump level. In this case, the laser threshold slightly increases and the slope efficiency decreases by 2% since a small amount of loss is inevitably introduced into the cavity by the BF.

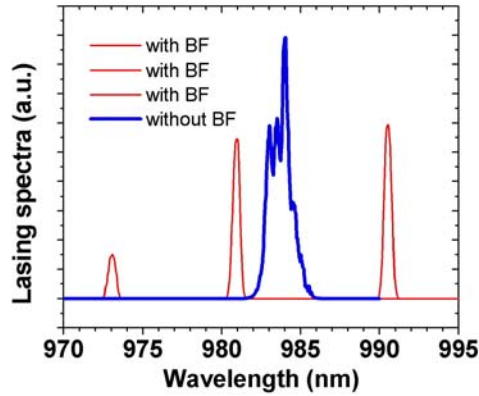


FIGURE 8. Comparison of the lasing spectra with/without birefringent filter in the V-shaped cavity.

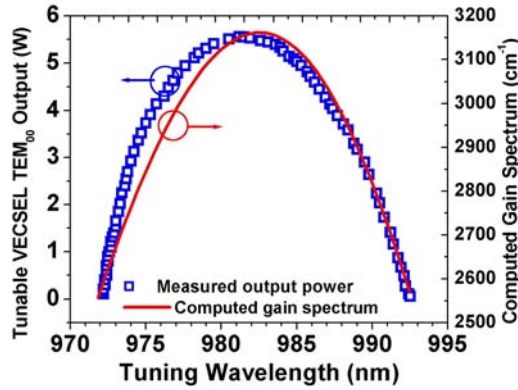


FIGURE 9. High power, linear polarized TEM₀₀ VECSEL output with 20 nm tuning range and computed quantum well gain spectrum.

Figure 8 is a comparison of the several tuned laser spectra (with BF) and un-tuned lasing spectrum (without BF) in the V-shaped cavity. In this case, the untuned lasing wavelength is located at the peak wavelength of modal gain spectrum. Since the cavity mode no longer experiences the effect of the micro-cavity resonance and the top of the modal gain spectrum is relatively flat in a range of 15~20 nm, the tuned laser wavelength is within this range and is determined by the wavelength at which the maximum transmission of the BF occurs. The tuned lasing spectra achieved with a BF are far more uniform and narrower than those achieved without a BF and exhibit a nominal linewidth of 1 nm as measured with an optical spectrum analyzer with a resolution of 1 Å. This is a consequence of longitudinal mode discrimination afforded by the BF and the absence of competing spectral filtering due to the micro-cavity resonance.

The tuning range of the VECSEL with the V-shaped cavity and birefringent filter is shown in Figure 9. In the measurement, the pump power (24 W) and the temperature of heat sink (10°C) are fixed. Multi-watt cw linearly polarized TEM₀₀ output with a 20 nm tuning range is demonstrated. In order to get an insight into the observed tuning range, a computed quantum well gain spectrum at the expected operating carrier sheet density around $5 \times 10^{12} \text{ cm}^{-2}$ and temperature around 360 K is also shown in Figure 9. We can observe that the tuning range is defined by the bandwidth of the gain spectrum. Figure 10 shows the

lasing spectra of the VECSEL at several points along the tuning range. Within a 20 nm wavelength tunable range, the envelope of the lasing spectra can be continuously tuned with narrow linewidth.

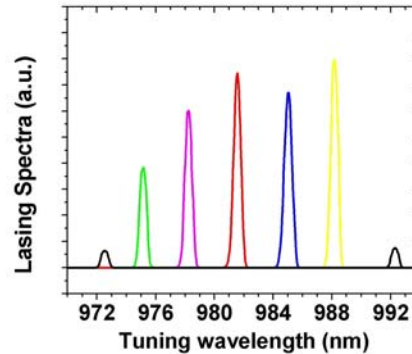


FIGURE 10. Several lasing spectra within 20 nm tuning range.

In conclusion, we developed and demonstrated a tunable high-power high-brightness linearly polarized VECSEL with a V-shaped cavity and intra-cavity birefringent filter. Multi-watt high-power cw linearly polarized TEM₀₀ output with a 20~30 nm tuning range and narrow linewidth is demonstrated near room temperature. Combining with temperature tuning or using a higher reflectance output coupler, the tunability of the laser is even larger. In short, high-power high-brightness linearly polarized tunable VECSEL with a wide tunability and narrow linewidth will significantly enlarge the application range of VECSELs.

6.3. Tunable Watt-Level Blue-Green VECSEL

Intracavity second-harmonic generation (SHG) is an efficient way to extract significant visible light from VECSELs. Combining intra-cavity frequency doubling with a multi-watt tunable VECSEL operating around 976 nm can provide wavelength-tunable laser operation around 488 nm. This tunable blue-green laser is tremendously important since it is difficult to generate tunable laser output in this spectral region by other lasers. With a few nanometers wavelength tuning range, this laser provides the desirable wavelength range for biomedical fluorochromes excitation, flow cytometry and some spectroscopic applications.

A Z-shaped cavity as illustrated in Figure 11 is designed for tunable intra-cavity SHG. In this cavity, the anti-reflection (AR) coated VECSEL chip serves as an active folding mirror to provide high round trip gain and a large tunability for the fundamental beam. In order to take the advantage of RPG structure, the folding angle at the VECSEL chip must be kept as small as possible. By “unfolding” the Z-shaped cavity about the VECSEL DBR mirror, we interpret the VECSEL active region as a tilted intra-cavity etalon. To weaken the resonance of this tilted etalon and eliminate its walk-off losses, a low reflectivity coating must be applied on the surface of the VECSEL chip. A birefringent filter (BF) is inserted in the cavity at Brewster’s angle. For the fundamental signal, the functions of the BF are three-fold: an extremely low-loss wavelength tuning component, a Brewster window to select polarization, and a filter introducing longitudinal mode discrimination. The linear polarization and narrow linewidth of the fundamental beam are extremely important for the SHG phase-matching condition. In this cavity there exist two beam waists on flat mirror 1 and on flat mirror 2 respectively. Since the beam waist at flat mirror 2 is much smaller than that at flat mirror 1, the LBO crystal is inserted close to flat mirror 2 such that the highest fundamental beam intensity is in the crystal. To build a high Q cavity for the high-power circulating fundamental beam, all of cavity mirrors must be highly reflective around 976 nm. Since the VECSEL

chip is highly absorbing for the SHG signal, the output coupler should be transparent for the SHG signal around 488 nm. The tilted concaved spherical output coupler results in a difference between the tangential and sagittal focal lengths, making the fundamental beam and SHG beam asymmetric. To neglect this asymmetry, the folding angle at the output coupler must be kept as small as possible.

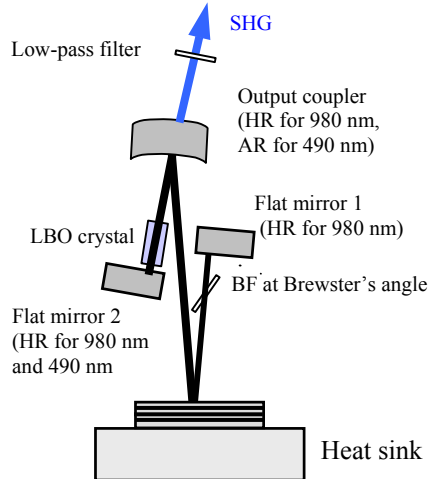


FIGURE 10. Schematic diagram of a tunable blue-green VECSEL with a Z-shaped cavity and a birefringent filter by intra-cavity SHG. Relative dimensions not to scale.

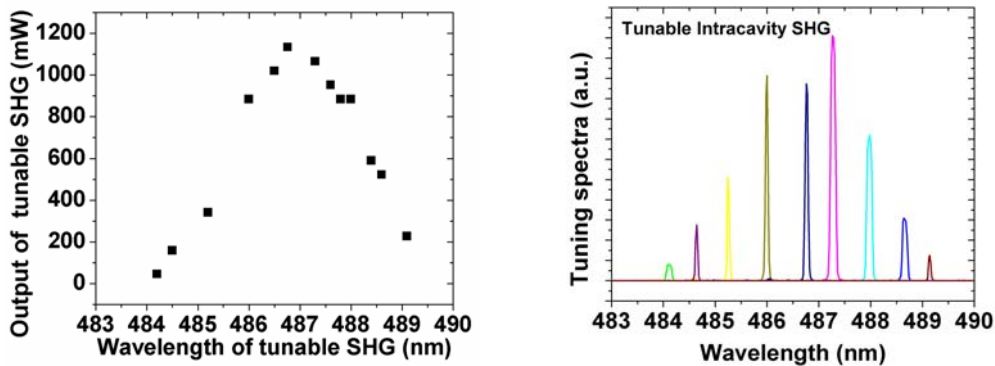


FIGURE 11. Tuning curve of tunable blue-green VECSEL (left) and several spectra of intracavity SHG within 5 nm tuning range (right).

The LBO crystal (3 mm×3 mm×10 mm) is cut to satisfy Type-I angle phase-matching condition and both facets are AR coated for the fundamental and SHG wavelengths. When the wavelength of fundamental beam is tuned in the range of 980 ± 10 nm, the phase matching condition can be maintained by tilting ϕ angle. In the experiment, both the fundament beam and the SHG beam pass through the central area of the LBO crystal facets, and there is no thermoelectric cooler for temperature control of the crystal. When the tuning of the intra-cavity SHG is investigated, the VECSEL chip is mounted on 10°C heatsink and about 35 W 808-nm pump power is launched into the chip. Figure 11 shows the tuning curve of Watt-level blue-green VECSEL and several spectra of the intracavity SHG signal over a 5 nm tuning range. The FWHM of fundamental signal is around 0.4 nm and the total optical length of cavity is about 24 cm, suggesting that there are more than 200 longitudinal modes in the spectral envelope. This extreme multi-mode operation prevents the “green problem” of intracavity SHG.

6.4. Spectral Beam Combining of VECSELs

There has been considerable interest in ways to power scale while maintaining the brightness of the laser output beam. One of the approaches that we adopted was to combine the output of multiple VECSEL laser elements. Spectral beam combination requires spectrally narrow individual lasers. Compared to an alternative approach, namely a single laser giving diffraction-limited output with kilowatts of output power, such combination scheme can operate in soft-failure-mode, allowing the whole system to continue to work when some of the laser elements fail. Further, the heat dissipation requirement can be relieved as the sources of the heat can be distributed. Unlike spatial beam combination, spectral beam combination allows for relative preservation of the source laser beam qualities

For spectral combination schemes, a highly wavelength-dependent combination device and tunable laser sources are necessary. Volume Bragg gratings (VBG) in photo-thermo-refractive (PTR) glass have narrow diffraction bandwidth combined with high diffraction efficiency, low losses and tolerance to high power laser radiation. These gratings were effectively used for spectral radiation combination of high power fiber lasers where efficient combination of two 100-W beams exceeded 90%. Compared to conventional surface diffraction gratings, VBG allows the diffraction angle and wavelength to be independently tailored, giving flexibility in configuration when cascading multiple elements to increase the number of channels. In this report, we demonstrate spectral beam combination of 2 tunable VECSELs, using a VBG made of PTR glass and discuss the scaling of combined power based on the results.

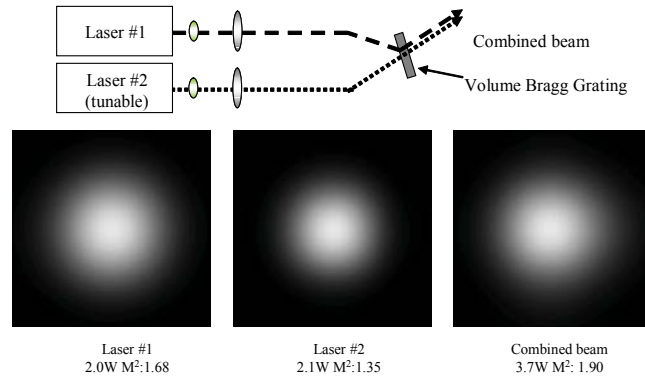


FIGURE 12. Experimental schematic and far field beam profile of the beams.

Beam combination was performed using two similar tunable VECSELs, one of which (Laser #1) was operating at a fixed wavelength of 982 nm and an output power of 2 W. The other laser (Laser #2) was operated at 2.1 W and was tuned to 975 nm. The output beams from the two lasers were individually collimated to approximately 5-mm diameter, and directed to the VBG. The angle of incidence onto the VBG was adjusted so that the 982-nm beam was diffracted, and we adjusted the wavelength of the other laser for maximum transmission. With the total 4.1-W of incident power onto the VBG device, 3.7 W was combined in a single beam, representing 90% combination efficiency. The loss was mainly due to the reflection loss of the VBG that was not AR coated. The M^2 value of the 982-nm laser was 1.68, and that of 975-nm laser was 1.35. We measured the M^2 of the combined beam to be 1.9. Slight increase in the M^2 value for VECSELs could be attributed to the small mismatch of collimation of the two input beams. The beam patterns of the individual lasers and the combined beam are shown in Figure 12.

6.5. MultiChip VECSELS: A Coherent Power Scaling Scheme

Laser beam combining is an effective way to achieve power scaling. Spectral beam combining (SBC) of VECSELS by using volume Bragg grating can maintain near-diffraction-limited beam quality, but the combined output is an incoherent multi-wavelength beam. The most sophisticated approach is coherent beam combining (CBC), where the lasers are artificially phase locked with each other, and the electromagnetic fields of their beams combine coherently. While this approach sounds good in theory, in practice it requires complex phase-locking loops that can be extremely difficult to implement and maintain.

We proposed an alternative effective coherent power-scaling approach; the multi-chip VECSEL. Compared to the single chip VECSEL, this multi-chip VECSEL has several potential advantages: (1) The heat generation and management is distributed across multiple VECSEL chips instead of a single chip. Consequently thermal rollover is delayed since less pump power on each chip will be needed to extract high power. (2) The multi-chip VECSEL has a much higher round trip small signal gain than a single chip VECSEL. As a result, we can use an output coupler with low reflectance to increase the slope efficiency of the laser. (3) The output of a multi-chip VECSEL is a stable coherent beam with good beam quality that is easily controlled by the folded cavity. In this subsection we present the development and demonstration of a two-chip VECSEL operating around 970 nm to prove the concept of the multi-chip VECSEL.

To prove the concept, we put two VECSEL chips together in the W-shaped cavity (Figure 13). The chips served as the cavity folding mirrors, reflecting more than 99.9 percent of the incident radiation from the 25 pairs of AlGaAs/AlAs that formed a distributed Bragg reflector behind the quantum wells. The InGaAs compressively strained quantum wells themselves (14 of them on one chip and 10 in the other) were spaced so that each quantum well aligned with an anti-node of the cavity standing wave. Each chip had a quarter-wave anti-reflection coating (reflectivity less than one percent at the 970-nm laser wavelength, and less than three percent at the 808-nm pump wavelength) on its surface. Both chips were optically pumped with 808-nm light from diode bars. Because we had a limited budget, pumping of the two VECSEL chips was carried out with different power pump diode bars. We applied the same power density to both chips until they reached the maximum power (~20 W) of one of the pump lasers. Because the other pump laser could not go to higher power, we continued increasing the power of the second pump up to 40 W.

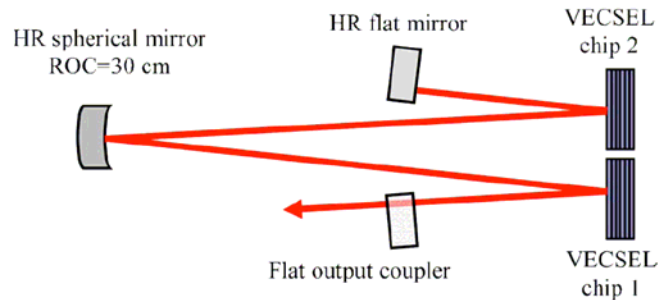


FIGURE 13. Schematic diagram of a two-chip VECSEL with a symmetric W-shaped cavity. (Relative dimensions not to scale).

For comparison purposes, we first characterized each of the VECSEL chips in its own, linear resonator. The two chips were then aligned in a common resonator, as indicated in Figure 13. The comparison showed that the two-chip resonator produced almost twice as much power as either individual chip did in its own resonator (Figure 14). The two-chip resonator showed a definite roll-over at the upper end, an indication of overheating one (or both) of the chips. We believe that only one chip – the one

pumped at 40 W overheated, and the roll-over could be avoided by pumping both chips with the same power.

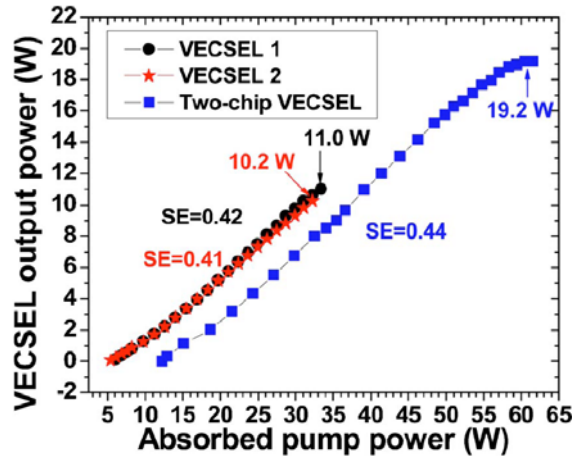


FIGURE 14. The output power of two single-chip VECSELS and two-chip VECSEL vs. total absorbed 808-nm pump power. The roll-over at the upper end of the two-chip trace could probably be avoided by pumping both chips at the same power.

The beam quality of the two-chip resonator was excellent. The measured M-square value was a perfect 1.0 at low pump powers, and increased to about 2.2 at the highest powers (Figure 15). At the highest powers, the beam profile started to show the two peaks of the TEM₀₁ mode.

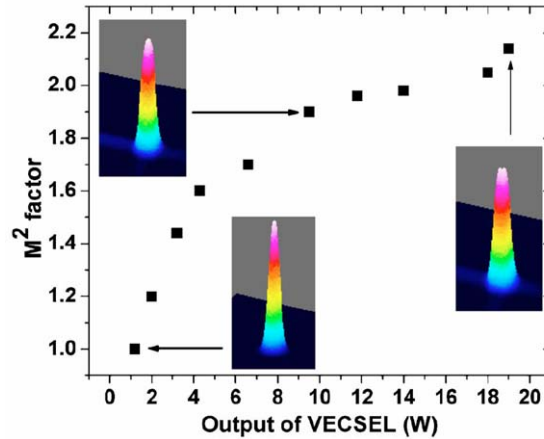


FIGURE 15. Beam quality factor (M^2 factor) vs. the output power of two-chip VECSEL.

The basic experimental demonstrations performed here with seed funding have established that the basic elements for power scaling VECSELS to kW levels are feasible. The initial challenge is to power scale an individual OPSL chip by improving wafer surface quality – significant power scaling by increasing the pump spot while maintaining the power density below the thermal rollover point. The next phase is to cascade a finite number of such OPSL chips in a common cavity. Finally, the latter high power modules can be spectrally beam combined as a final step towards a multi-kW OPSL laser source. The success of this project can be attributed mainly to our unique capability to calculate microscopically all of the critical semiconductor optical properties and consequently design the full VECSEL sub-cavity prior to wafer growth and processing.

7. MIT Final Report 1

Yoel Fink

Research Laboratory of Electronics, Massachusetts Institute of Technology, Cambridge, Massachusetts 02139, USA

Abstract: All fiber lasers to date emit radiation only along the fiber axis. Under this program a fiber that exhibits laser emission that is radially directed from its circumferential surface was demonstrated. A unique and controlled azimuthally anisotropic optical wave front results from the interplay between a cylindrical photonic bandgap fiber resonator, anisotropic organic dye gain, and a linearly polarized axial pump. Low threshold (86nJ) lasing at nine different wavelengths is demonstrated throughout the visible and near-infrared spectra. We also report the experimental realization of unprecedented layer thicknesses of 29.5 nm maintained throughout meter-long fibers.

7.1 Introduction

The great variety of optical cavities and their coupling to gain media has made lasers pervasive in science and technology. In particular, fiber lasers have recently been the focus of much interest [1-3]. A common feature of all fiber lasers is the emission along the fiber axis from an area that is small when compared to the total cavity surface and with nearly planar wave front. Here we report on the design, fabrication and characterization of a photonic band gap fiber laser that emits radiation in the plane transverse to the fiber axis from an extended surface area. Furthermore, the unique wave front is azimuthally anisotropic with a radiation pattern resembles an optical dipole. This is due to the interaction between a cylindrical resonator, anisotropic gain, and a linearly polarized axial pump beam. The cylindrical fiber-cavity structure consists of a hollow-core multilayer [4] photonic band gap fiber, and an organic dye gain medium that is introduced into the core. The complete photonic band gap provides the longitudinal confinement of the higher-frequency optical pump and at the same allows light to travel along the fiber at steep angles (with respect to the fiber axis) not afforded by conventional index-guiding fibers. Lasing at 9 different wavelengths is demonstrated throughout the visible and near-infrared spectra. We also report the experimental realization of unprecedented layer thicknesses of 29.5 nm maintained throughout meter-long fibers. Such a device may have interesting medical applications ranging from photodynamic therapy [5] to in vivo molecular imaging [6], as well as textile fabric displays [7].

7.2 Fiber Laser Structure

The surface-emitting fiber laser structure and pumping arrangement are shown schematically in Fig. 1. The structure comprises a gain medium in the core surrounded by a photonic band gap (PBG) structure [8-11] made of 58 layers of a wide mobility gap amorphous semiconductor, As_2S_3 , alternating with a high glass-transition temperature polymer, poly(etherimide) (PEI). A scanning electron microscope micrograph of the multilayer structure (Fig. 2a) demonstrates the uniformity of the layer thicknesses throughout the fiber. The individual layer thicknesses of As_2S_3 and PEI are 59 nm and 89 nm, respectively, and the structure is terminated by a 29.5-nm thick layer of As_2S_3 to eliminate surface modes. The gain medium is pumped axially while the resonant cavity provided by the PBG ensures laser emission in the radial direction. The PBG structure performs a dual role enabled by the characteristic shift of the band edges to higher frequencies with increase in wave vector as depicted in Fig. 2b. The normal-incidence band gap, defined for axial wave vector $k = 0$ (region A), provides the optical feedback necessary for emitting laser light from the whole surface area in the radial direction. Concurrently, the

blue-shifted band gap having axial wave vectors near the light line (region B) is responsible for guiding the pump frequency.

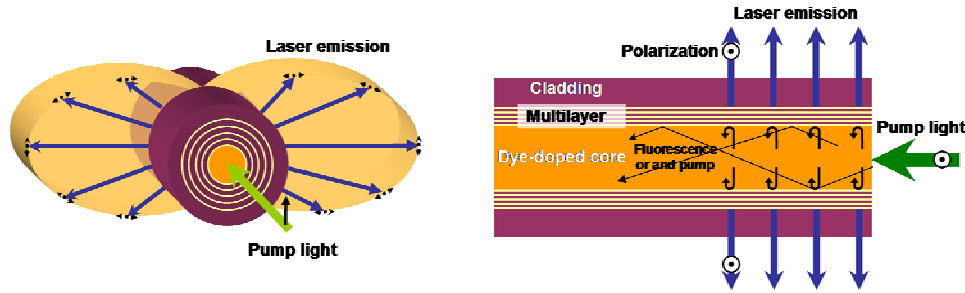


Figure 1 Photonic band gap fiber laser. The fiber laser emits light in the transverse direction (propagation and polarization vectors shown as solid arrows and dashed lines, respectively) having a dipole-like wave front from an extended length of the fiber.

While different types of gain media may be used in conjunction with the fiber, for convenience we chose an organic laser dye [12] incorporated into a copolymer matrix. The upper inset in Fig. 2a is a fluorescence micrograph of the fiber cross section (see Appendix A). An organic dye, LDS698, having a fluorescence peak at 645 nm was dispersed in a copolymer and inserted into the otherwise hollow core of a PBG fiber. Since the normal-incidence PBG is 26% of its centre-frequency, it encompasses the entire fluorescence spectrum as shown in Fig. 2c (see Appendix B). This same fiber supports the propagation of a pulsed optical pump at 532 nm traveling through the fiber core.

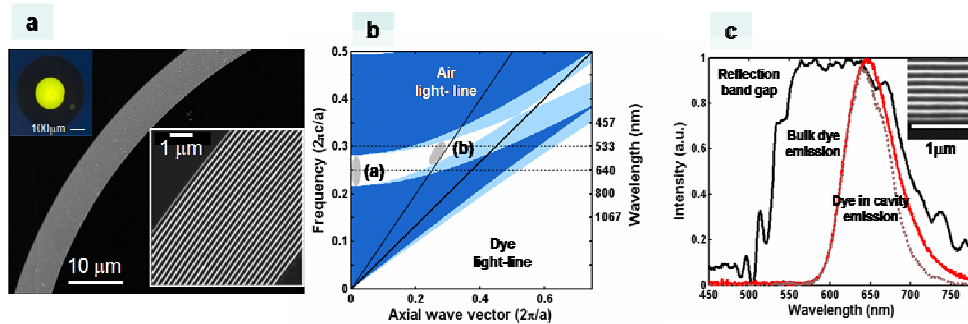


Figure 2 Structure of the fiber laser cavity. **a**, Cross-sectional SEM micrographs of the PBG multilayer structure at various magnifications. The PEI in the cladding and the layers appears black, and the As_2S_3 layers white. The PEI and As_2S_3 layers are 89 nm and 59 nm thick (except for the first and last As_2S_3 layers which are 29.5 nm thick; the first layer is not visible). The top left inset shows a cross-sectional fluorescence micrograph of the full cross-section of a PBG fiber with an R590 organic dye in the core and enveloped by a thick PEI protective cladding. **b**, Projected band structure of a one dimensional photonic crystal consisting of alternating layers of As_2S_3 and PEI. Transverse-electric (TE) and transverse-magnetic (TM) propagating modes are in dark and light blue, respectively; evanescent modes are in white. Light incident normally to the structure ($k=0$) and axially propagating modes through the hollow core are shown as regions A and B, respectively. **c**, Measured reflection band gap centered around 620nm (see ‘Optical characterization’ in methods) in black; fluorescence spectrum of LDS698 (500 ppm concentration) in red; and calculated dye-in-cavity emission obtained by multiplying the last two, dashed line.

7.3 Optical Properties

We observe broad fluorescence emission from the above described fiber laser at pump-pulse energies lower than the 86 nJ threshold, while radially directed lasing occurs with sharp peaks at 652 nm above threshold (Fig. 3a). To confirm that the emitted radiation is indeed laser light and not amplified spontaneous emission, we show in Fig. 3a the emission spectra of the fiber for three different pump

energies: below (A), near (B) and above (C) threshold. The lasing threshold occurs at pump energies of 86 nJ and 110 nJ for dye concentration of 500 ppm and 50ppm, respectively. The dependence of the emission bandwidth (Fig. 3a inset) and energy (Fig. 3b) on the pump energy for both 500 ppm and 50 ppm dye concentrations are shown. Both clearly demonstrate laser thresholds. The slope efficiencies are 37.5% and 16.5% for the 500 ppm and 50 ppm concentrations, respectively.

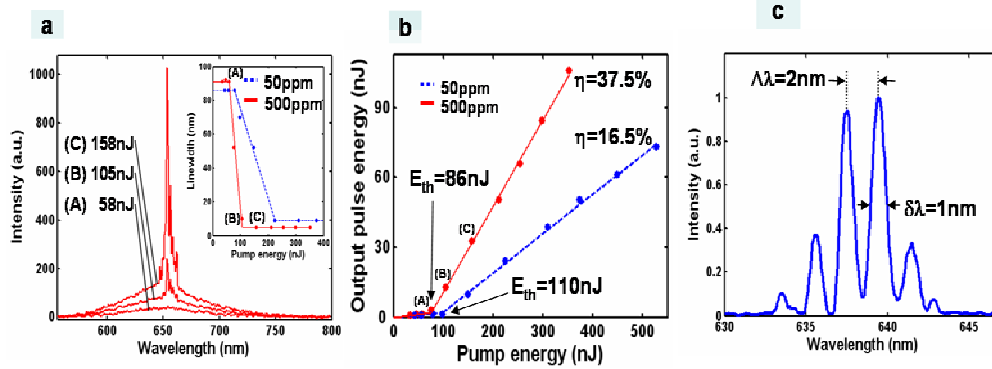


Figure 3 Lasing characteristics of an LDS698-doped PBG fiber. **a**, Emission spectra of the fiber laser for a dye concentration of 500 ppm and pump energy below threshold (A), $1.2E_{th}$ (B) and $1.8E_{th}$ (C), where E_{th} is the lasing threshold energy. Inset shows the spectral full-width at half-maximum as a function of input energy for 500 ppm (red line) and 50 ppm (dashed blue). **b**, Dependence of the laser energy on the pump energy showing threshold values of $E_{th} = 86$ nJ and $E_{th} = 110$ nJ for the 500 ppm and 50 ppm, respectively. **c**, High resolution spectral measurement reveals mode spacing of 2 nm and quality factor of 640.

The PBG fiber (core diameter $d_c = 70$ μm) supports many longitudinal cavity modes in the transverse plane having a free spectral range $\Delta\lambda \approx \lambda_0 / 2nd_c$, where n is the core refractive index and λ_0 is the lasing centre wavelength. The lasing spectrum was resolved into its modes, as shown in Fig. 3c, using an optical spectrum analyzer (ANDO AQ6317), and the 2-nm mode spacing (corresponding to a 68- μm core diameter) is in good agreement with the expected value. The measured quality factor $Q = \lambda_0 / \delta\lambda$ ($\delta\lambda$ is the spectral width of one mode) of 640 is lower than theoretically expected. Possible reasons for this discrepancy are the losses arising from an imperfect cavity structure and the limited spectral resolution of the measurement setup.

The optical wave front emanating from the fiber laser has several unique characteristics that stem from the combination of the emission properties of the dye and the resonant cavity design. First, the emitted laser wave front has a dipole-like radiation pattern, shown in Fig. 4a. This result was obtained in two different ways. First the orientation of the pump polarization at the input to the fiber was rotated while a probe recorded the emitted intensity in the x-polarization at a fixed location along the y-axis. The measurement was then corroborated by physically rotating the probe around the surface of the fiber laser while keeping the pump polarization fixed in the x-direction. Upon comparing the radiation pattern to that of a bulk dye-doped copolymer excited with the same pump, we find the dipole-like radiation pattern is not as pronounced as in the fiber laser. These results can be understood by noting that the polarization of the dye fluorescence is determined mainly by the pump polarization and the relative orientation of the transition moments in the dye molecule for the absorption and emission transitions [12]. The polarized dye molecules that are aligned with the pump polarization contribute the most to the fluorescence. This may be confirmed by analyzing the dye emission with a linear polarizer rotated in the x - z plane, normal to the direction of maximum emission (y -axis), with a fixed x-polarized pump, as shown in Fig. 4b (dotted line). The dipole radiation patterns of the dye molecules combine to result in the radiation pattern shown in Fig. 4a where the strongest radiation is in the direction orthogonal to the pump polarization and the fiber axis. Since fluorescence polarized parallel to the pump is stronger, cavity modes with this polarization have lower thresholds. Consequently, the fiber laser has an enhanced polarization component parallel to the pump as compared to that of the bulk dye emission (Fig. 4b, solid line) and a more

prominent dipole-like radiation pattern. These interesting results suggest that the direction of the laser beam can be controlled remotely just by rotating the pump polarization.

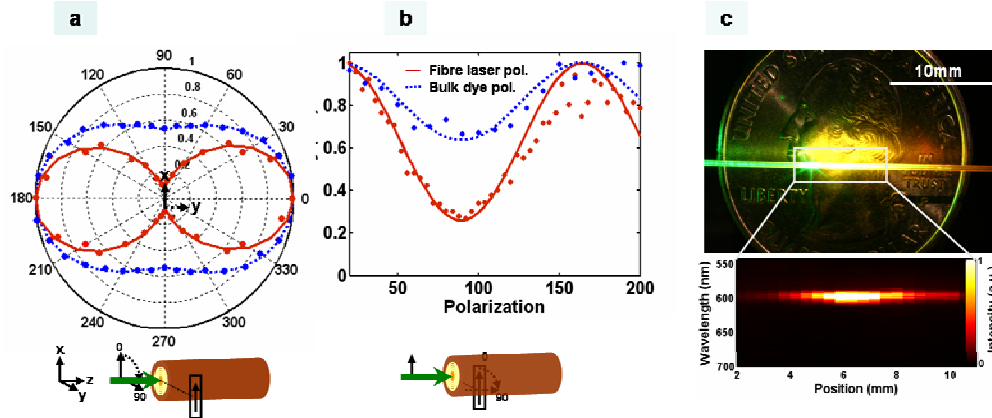


Figure 4 Geometric dependence of the emission for an LDS698-doped PBG fiber laser. **a**, Angular intensity pattern of the bulk dye and fiber laser emission at a fixed location along the y -axis measured by rotating the input polarization. This measurement is equivalent to fixing the pump polarization while measuring the emission intensity around the fiber. **b**, Polarization of light emitted from bulk dye (dashed blue) and dye in a fiber cavity (red line) having a ratio of intensities in the x - and y -directions of 0.22 and 0.6, respectively, measured by fixing the pump polarization in the x -direction and recording the intensity as a function of polarizer rotation about the direction of maximum emission (y -axis). **c**, Emission spectra from large core (200- μm) PBG fiber laser measured along the fiber axis at 10- μJ pump energy measured by scanning a probe fiber along the fiber side. The upper panel shows a photograph of the fiber showing laser light emitted from a spatially extended region along the fiber (~ 5 mm).

A second unique feature of this laser is that emission occurs over a spatially extended region by virtue of the extended surface area of the fiber resonator walls. This is in contrast to semiconductor [13,14] and polymer [15] planar annular resonators in which the resonator thickness is on the order of the emission wavelength. Figure 4c shows the emission spectrum as a function of position along a large-core ($d_c = 200 \mu\text{m}$) PBG fiber. By moving a probe along its axis we observed laser radiation extending along ~ 5 mm of the fiber (measured at full-width-half-maximum). The upper panel of Fig. 4c shows a photograph of this operating laser. One may further increase the surface area from which laser light is emitted by optimizing dye concentration, core size, and PBG structure.

The dual action of the PBG structure as both a transverse laser cavity and a transmission waveguide is highlighted in Fig. 5a. In this specific fiber, a short segment of Rhodamine 590 doped copolymer was introduced into a PBG fiber, leaving the rest of the core hollow. The photograph of the bent fiber displays both features: the hollow-core portion of the fiber transmits the pump light (green, $\lambda = 532$ nm, top of the photograph), and the dye-doped portion emits orange-colored laser light ($\lambda = 576$ nm).

Furthermore, the placement of dye-doped segments along a fiber can be carefully controlled. A demonstration that highlights the ability to finely tune segment size, location, and composition is shown in Fig. 5b. A lasing display projects the letters "MIT" in two colors. All the lasing fibers contain copolymer segments doped with DCM (orange). Additionally, the "i"-fiber contains both DCM and LDS698 (red) demonstrating that more than one gain medium can be precisely placed in the same fiber. This specific display contains 12 dye-filled fibers that are pumped from both ends. The large segments contain less than $0.5 \mu\text{l}$ of dye-doped polymer.

Finally, the use of dyes with fluorescence spectra that extend over the visible and near-IR wavelengths is made possible by simply scaling the PBG structure and hence shifting the band gap. Nine different dyes were inserted into separate fibers having band gaps matched to their emission peaks. The lasing spectra of these fibers are displayed in Fig. 5c, and photographs of three lasers are shown depicting bright blue, green and red laser light. Moreover, the fiber's photonic band gap is readily scalable from the UV [11] to the IR [8,10].

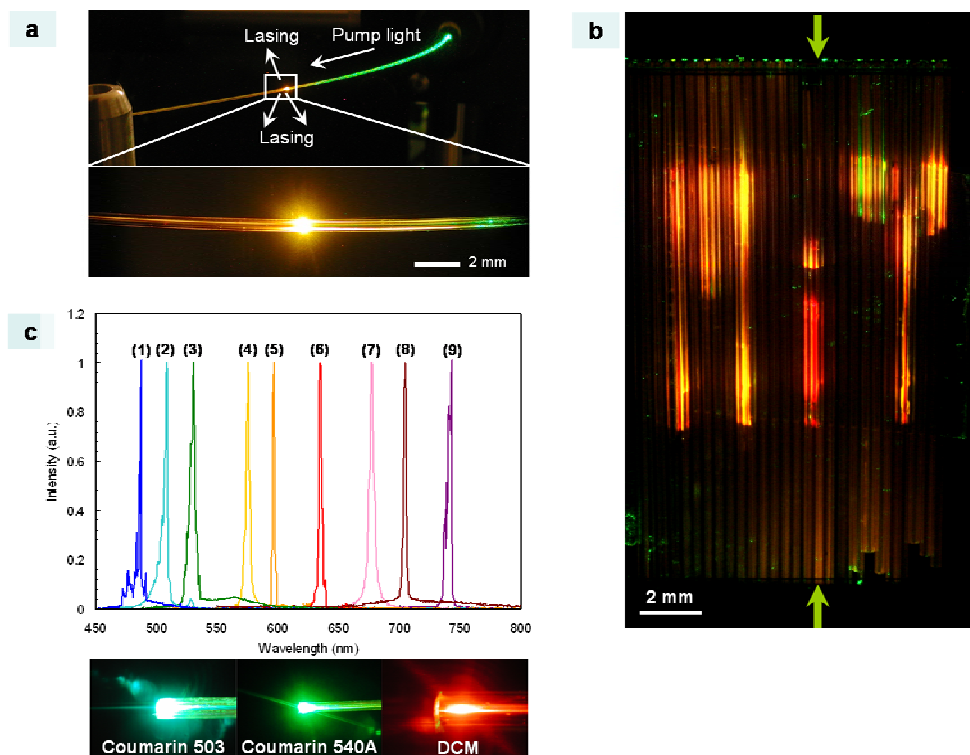


Figure 5 a, A photograph of an R590-doped PBG fiber showing the pump (532 nm, green) guided in the hollow-core PBG fiber. Lasing at 576 nm (orange) occurs in the R590-doped region. **b**, Lasing “MIT” made out of 12 PBG fibers doped with DCM (orange) and LDS698 (red) that are simultaneously pumped in both directions. This display design illustrates the ability to finely tune dye location, size, and concentration. **c**, Laser emission spectra from fibers doped with nine different dyes. The lasers producing emission spectra 1-3 are constructed using the same hollow-core PBG fibers having a fundamental reflection band gap at 500 nm, and were pumped at 355 nm. The fibers used to produce emission spectrum 4 has a fundamental reflection band gap at 600 nm, while those used for spectra 5-9 have a fundamental reflection band gap at 690nm, and all were pumped at 532 nm. Photographs of the organic dye-doped PBG fiber lasers showing the individual laser colors (blue, green and red) emitting from the fiber surface.

7.4 Conclusions

This new polymer surface-emitting fiber laser offers unique control over the direction and polarization of the lasing wave front, is inherently wavelength scalable, and can be used for the remote delivery of radial laser emission. The ability to control the gain medium location, spatial extent, and concentration coupled with the fiber’s mechanical flexibility paves the way for lasing textile fabrics or even 3D laser-light-emitting structures.

Appendix A: Fiber Preparation

The hollow-core PBG fiber preform was fabricated by thermal evaporation of an As₂S₃ layer (5 μm) on both sides of a free-standing 8-μm-thick PEI film and the subsequent rolling of the coated film into a hollow multilayer tube. This hollow macroscopic preform with a thick protective outer layer of PEI was consolidated by heating under vacuum at ~ 260 °C and was then drawn in a fiber draw tower into hundreds of meters of fiber at ~ 305 °C. The SEM samples were prepared with JEOL Cross Section Polisher (CP) SM-09010 and the micrographs produced with JEOL JSM 7000F.

Mixed solutions of methyl methacrylate (MMA) and 2-hydroxyethyl methacrylate (HEMA) monomers containing t-butyl peroxide (tBP) or azobisisobutyronitrile (AIBN), n-butyl mercaptan, and organic dyes (0.05-0.5 wt%) were prepared and inserted into the hollow core PBG fibers. The fibers were placed in an

oven at either 90 °C (tBP) or 60 °C (AIBN) for 20 hours for polymerization. All dyes were obtained from Exciton, Inc. The dyes used to produce the laser emissions shown in Fig. 5a are as follows: (1), 0.5 wt% coumarin 503; (2), 0.5 wt% coumarin 500; (3), 0.5 wt% coumarin 540A; (4), 0.1 wt% rhodamine 590; (5), 0.1 wt% DCM; (6), 0.1 wt% LD698; (7), oxazine 720; (8), 0.1 wt% LD700; (9), 0.1 wt% oxazine 725.

Appendix B: Optical Measurements

The reflection spectra of the hollow-core fibers were measured using a xenon lamp (Oriel 68840-M). The light was collimated using a 5-cm focal-length lens, directed through a beam splitter, and focused onto the fiber outer surface using a $\times 10$ microscope objective lens. The light reflected back from the multilayer structure was collimated by the objective lens and directed by the beam-splitter to a spectrometer (Ocean Optics HR2000CG-UV-NI) and then normalized with respect to the spectrum of the lamp.

The optical pump for the fiber lasers was a linearly polarized, pulsed Nd:YAG laser (Continuum Minilite II) with nominal pulse durations of 9 ns and repetition rate of 10 Hz. Both the second (532nm) and third (355nm) harmonics were utilized as pumps in accordance with the dye's fluorescence. The pump beam was spatially filtered by a 500- μm pinhole, a small percentage of the energy was directed away by a beam splitter to monitor the pump energy, a half-wavelength plate controlled the pump polarization, and a one-inch focal-length lens coupled the pump into the fiber core. The pump input energy was measured using an energy meter (Coherent PM1000, J4-09 and J3S-10). The energy of the resulting laser light emitted from the fiber laser was collected by an integrating sphere (Sphere Optics) and measured using the same energy meter with a high-pass filter mounted in front to eliminate any pump signal. The pump energy was adjusted using a variable optical attenuator. The emission spectra of the generated laser light were measured with the spectrometer after being collected by a 600- μm -diameter multimode fiber probe. The polarization measurements of both the bulk dye and the fiber were made using a linear sheet polarizer placed between the sample and the spectrometer.

References and Links

1. Dignonnet, M. J. F. Rare-Earth-Doped Fiber Lasers and Amplifiers (Marcel Dekker, Inc., Stanford, California, 1993).
2. Wadsworth, W. J., Knight, J. C., Reeves, W. H., Russell, P. S. and Arriaga, J. Yb³⁺-doped photonic crystal fiber laser. *Elect. Lett.* **36**, 1452-1454 (2000).
3. Argyros, A., Issa, N., Bassett, I. & van Eijkelenborg, M. A. Microstructured optical fiber for single-polarization air guidance. *Opt. Lett.* **29**, 20-22 (2004).
4. Yeh, P., Yariv, A. & Marom, E. Theory of Bragg fiber. *J. Opt. Soc. Am.* **68**, 1196-1201 (1978).
5. Verdaasdonk, R. M., and van Swol C. F. P. Laser light delivery systems for medical applications. *Phys. Med. Biol.* **42** 869-887 (1997).
6. Ntziachristos V, Bremer C., Weissleder R. Fluorescence imaging with near-infrared light: new technological advances that enable in vivo molecular imaging. *Eur. Radiol.* **13**, 195-208 (2003).
7. Koncar, V. Optical fiber fabric displays. *Optics & Photonics News* **16**(4), 40-44 (2005).
8. Temelkuran, B., Hart, S. D., Benoit, G., Joannopoulos, J. D. and Fink, Y. Wavelength-scalable hollow optical fibers with large photonic bandgaps for CO₂ laser transmission. *Nature* **420**, 650-653 (2002).
9. Hart, S. D., Maskaly, G. R., Temelkuran, B., Prideaux, P. H., Joannopoulos, J. D., and Fink, Y. External reflection from omnidirectional dielectric mirror fibers. *Science* **296**, 510-513 (2002).
10. Kuriki, K., Shapira, O., Hart, S. D., Benoit, G., Kuriki, Y., Viens, J. F., Bayindir, M., Joannopoulos, J. D., and Fink, Y. Hollow multilayer photonic bandgap fibers for NIR applications. *Opt. Express.* **12**, 1510-1517 (2004).

11. Kuriki, K. et al. in preparation.
12. Schafer, F. P. *Dye lasers* (Springer-Verlag, Berlin, 1989).
13. Erdogan, T., King, O., Wicks, G. W., Hall, D. G., Anderson, E. H., Rooks, M. J. Circularly Symmetrical Operation of a Concentric-circle-grating, surface-emitting, AlGaAs/GaAs quantum-well semiconductor-laser. *App. Phys. Lett.* **60**, 1921-1923 (1992).
14. Scheuer, J., Green W. M. J., and Yariv, A. Annular Bragg Resonators: Beyond the Limits of Total Internal Reflection. *Photonics Spectra*, May 2005.
15. Bauer, C., Giessen, H., Schnabel, B., Kley, E. -B., Schmitt, C., Scherf, U., and Mahrt, R. F. A surface-emitting circular grating polymer laser. *Adv. Mater.* **13**, 1161-1164 (2001).

8. MIT Final Report 2

Analytic and numerical calculations of the dispersion characteristics of two-dimensional dielectric photonic gap structures

[K. Samokhvalova, C. Chen and B.-L. Qian, *J. Appl. Phys.* **99**, 063104 (2006)]

Chiping Chen

Plasma Science and Fusion Center
Massachusetts Institute of Technology
Cambridge, Massachusetts 02139

We have derived an exact analytical dispersion relation for transverse-magnetic modes with $k_z = 0$ in a particular two-dimensional rectangular photonic band gap (PBG) structure. We have presented a method for solving the dispersion relation and determining the dispersion characteristics. We have compared analytical results with results from the Massachusetts Institute of Technology Photonic Band Gap Structure Simulator (PBGSS) code. We have established the error tolerance in the PBGSS code. Finally, we have computed analytically the attenuations of modes with frequencies in the global band gap.

We consider a 2D periodic PBG structure consisting of rectangular dielectric rods, as shown in Fig. 1. The structure is infinite in the z -direction. Applying the boundary conditions on the interface of the dielectric rods and the periodic boundary conditions on the boundaries of the elementary cell, we derive analytical dispersion relation for a special case in which the dielectric constants of the rods satisfy the algebraic condition

$$\varepsilon_1 + \varepsilon_3 = \varepsilon_2 + \varepsilon_4. \quad (1)$$

In this case, we can obtain the following analytical dispersion relation for the TM modes with $k_z = 0$:

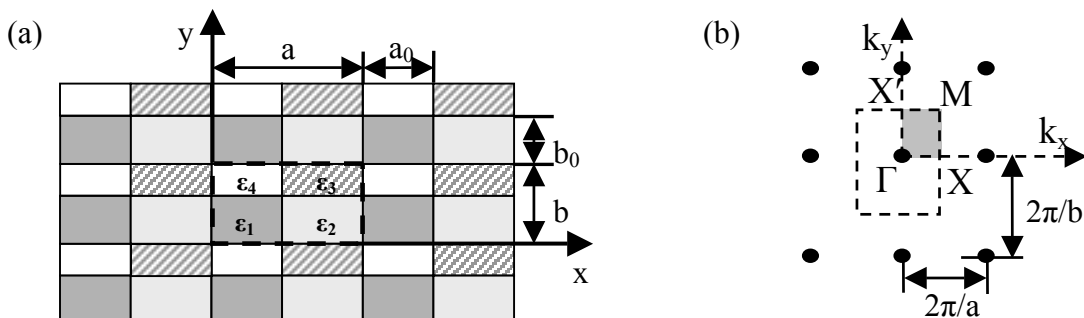


Fig. 1 Schematics of a 2D rectangular PBG structure representing (a) several cells of the structure, with an elementary cell inside the dashed box and (b) reciprocal lattice and a Brillouin zone with an irreducible Brillouin zone in the shaded region.

$$D(\omega, k_x, k_y) \equiv 2 \cos(k_x a) - 2 \cos(k_{1x} a_0) \cos[k_{2x}(a - a_0)] + \left(\frac{k_{1x}}{k_{2x}} + \frac{k_{2x}}{k_{1x}} \right) \sin(k_{1x} a_0) \sin[k_{2x}(a - a_0)] = 0, \quad (2)$$

where the functions $k_{1x} = k_{1x}(k_y, \omega)$ and $k_{2x} = k_{2x}(k_y, \omega)$ are implicitly defined by the relations

$$2 \cos(k_y b) - 2 \cos(k_{1y} b_0) \cos[k_{3y}(b - b_0)] + \left(\frac{k_{1y}}{k_{3y}} + \frac{k_{3y}}{k_{1y}} \right) \sin(k_{1y} b_0) \sin[k_{3y}(b - b_0)] = 0, \quad (3)$$

$$k_{1x}^2 + k_{1y}^2 = \frac{\varepsilon_1 \omega^2}{c^2}, \quad (4)$$

$$k_{2x}^2 + k_{1y}^2 = \frac{\varepsilon_2 \omega^2}{c^2}, \quad (5)$$

$$k_{2x}^2 + k_{3y}^2 = \frac{\varepsilon_3 \omega^2}{c^2}. \quad (6)$$

Results of the analytic and PBGSS calculations of the first six bands are presented in Fig. 2 for a square PBG structure with the following parameters: $a_0/a = 0.7$, $b_0/b = 0.7$, $a/b = 1.0$, $\varepsilon_1 = 1.0$, $\varepsilon_2 = \varepsilon_4 = 5.0$, and $\varepsilon_3 = 9.0$. In the PBGSS code, the fundamental unit cell is covered by square mesh with $(2N + 1) \times (2N + 1)$ mesh points. In our calculation, we use the value of $N = 8$. On the scale shown in Fig. 2, it is evident that the results of the PBGSS calculations agree well with the analytical calculations.

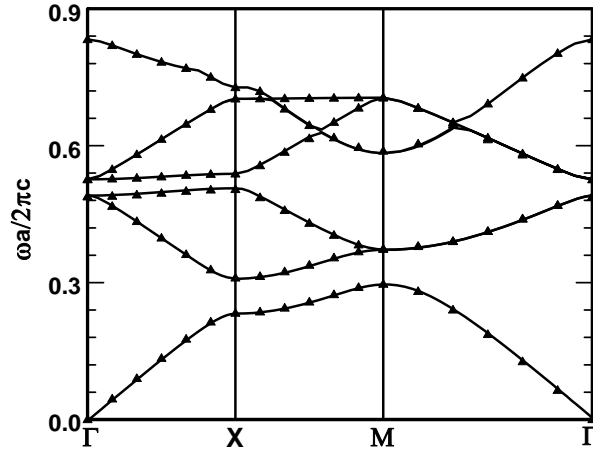


Fig. 2. Plot of the normalized frequency $\omega a / 2\pi c$ versus the wave vector \mathbf{k}_\perp for the first six bands of TM modes with $a_0/a = b_0/a = 0.7$, $b/a = 1.0$, $\varepsilon_1 = 1.0$, $\varepsilon_2 = \varepsilon_4 = 5.0$, and $\varepsilon_3 = 9.0$. Here, \mathbf{k}_\perp

varies from Γ to X , X to M , M to Γ [see Fig. 1(b)]. Solid curves are the analytical results, whereas the triangles are the results from the PBGSS calculations.

To understand the sensitivity and dependence of the PBGSS results to the mesh choice, e.g., the parameter N , one can analyze the error in frequency at any given wave vector \mathbf{k}_\perp . Because we are interested in the global band gaps, we have performed the error analysis at point M in the first band and point X in the second band. The results for point M in the first band are shown in Fig. 3. The frequency error is oscillating as N increases. Note that at $N = 8$, the error is less than 1%, which is consistent with the results shown in Fig. 2. The absolute value of the maximum error is found to scale approximately as $1/N$, as expected. At point X in the second band, results similar to those in Fig. 3 are obtained.

We make use of Eq. (2) to calculate the attenuation of the evanescent wave in the band gap as a function of angle of the wave vector with respect to $\Gamma-X$ direction in the irreducible Brillouin zone in Fig. 1(b). In Fig. 4, the results of the wave attenuation calculation are shown for a square PBG structure, for the same choice of system parameters as in Fig. 2. The frequency was chosen to be in the middle of the first global band gap, i.e., $\omega a / 2\pi c = 0.303$. The wave attenuation depends on the direction of propagation.

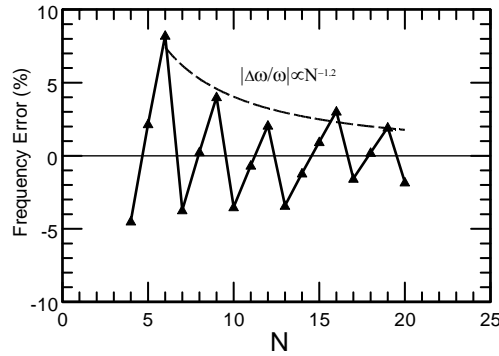


Fig. 3 Percentage error in normalized frequency $\omega a / 2\pi c$ as a function of N for first TM mode at point M . Dashed line represents the fit for the absolute value of the maximum errors.

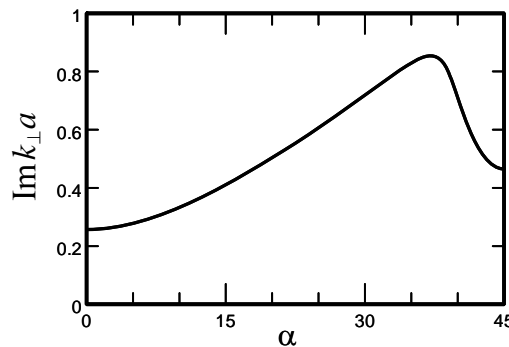


Fig. 4 Normalized imaginary part of \mathbf{k}_\perp for TM modes with frequency in the middle of the first global band gap as a function the angle of propagation with respect to the x -axis.

There are a number of useful applications of the analytical dispersion relation. First, it allows for benchmarking the existing numerical codes for PBG calculations. Second, it enables us to perform a rigorous error analysis and establish error tolerance in a PBG simulation code. Third, it allows for an

accurate determination of global band gaps, especially very narrow ones which are required in order to design an oversized PBG cavity or waveguide with a single transverse mode. Fourth, it allows us to study the attenuation of the mode which has a frequency in the global band gap and therefore it is trapped in the defect of the structure.